CRANFIELD UNIVERSITY

Gorka Martin Duñabeitia

Vortex Induced Aerodynamic Forces on a Flat Plate in Ground Proximity

School of Aerospace, Transport and Manufacturing (SATM)
Aerospace Dynamics

MSc Thesis
Academic Year: 2017 - 2018

Supervisor: Prof. Kevin Garry
September 2018

CRANFIELD UNIVERSITY

School of Aerospace, Transport and Manufacturing (SATM)
Aerospace Dynamics

MSc Thesis

Academic Year 2017 - 2018

Gorka Martín Duñabeitia

Vortex Induced Aerodynamic Forces on a Flat Plate in Ground Proximity

Supervisor: Prof. Kevin Garry
September 2018

This thesis is submitted in partial fulfilment of the requirements for the degree of Master of Science

ABSTRACT

A computational analysis of large-scale vortex generators in ground proximity was performed in order to predict the forces and flow structures induced underneath a flat plate model for a range of ride-heights. The investigation focused in two different set of experiments: assessment of the aerodynamic characteristics of different vortex generators shapes and the effect of the addition of side endplates. To effectively resolve the numerical turbulent flow RANS method with K- SST turbulence model was used.

Amongst all the shapes of the simulated vortex generators, it was observed that the rectangular VG was the most efficient design, being able to generate the highest aerodynamic loads and suction peaks. In turn, it was found the triangular VG produced the highest vorticity peak values in the early stages of vortex shedding.

The configuration of the endplates on the flat plate induced an additional dominant lower edge vortex that strongly contributed to the rate of change of the negative lift and drag gradients. It was observed that the downforce enhancement was directly related to the strengthening of the vortex and the change in the pressure distribution. From computational vorticity flow patterns was shown that the increase of vane spacing reduces the interaction of the vortices. Likewise, the increase of vane incidence angle from $\beta=10^{o}$ to $\beta=20^{o}$ indicated the appearance of the vortex burst as the ride-height of the model was reduced. A comparison of this model with the one without endplates showed the beneficial effects of using side plates. At the maximum downforce location ($h/c=0.02$) for $\beta=20^{o}$, a favourable difference of 48.5% can be obtained, generally improving the downforce coefficient from $C_L=0.35$ to $C_L=0.52$.

Keywords:

Computational Analysis, Side Endplates, Vortex Generators, Optimisation

ACKNOWLEDGEMENTS

I would like to express my very great appreciation to my supervisor, Professor Kevin Garry, for his valuable knowledge and encouragement provided throughout the thesis. I am particularly grateful for his generous guidance.

In addition, I would like to thank my family, because without the continuous and close support and encouragement throughout these years none of this would have been possible, especially to overcome the toughest moments.

Finally, but not least, I wish to thank my very close friends for their unconditional support.

TABLE OF CONTENTS

LIST OF FIGURES

LIST OF TABLES

LIST OF ABBREVIATIONS

AR	Aspect Ratio (AR=d/a)
a (mm)	Height of the vortex generators
c (mm)	Length of the flat plate
CFD	Computational Fluid Dynamics
CD [-]	Drag Coefficient
CL[-]	Lift or downforce (when negative) coefficient
CP[-]	Pressure Coefficient
d [mm]	Distance between the vortex generators
FIA	Federation Internationale De L´Automobile
h [mm]	Distance from the lower surface of the plate to the ground plane
HPC	High Performance Computing
k	Turbulent Kinetic Energy
LDA	Laser Doppler Anemometry
PIV	Particle Image Velocimetry
RANS	Reynolds-Averaged Navier-Stokes
SA	Spallart-Allmaras
SST	Shear Stress Transport
VG	Vortex Generator
β[°]	Incidence angle of the VG`s with respect to the flow direction
δ[°]	Angle of the trailing edge moveable flap
ω	Specific Dissipation rate

1 INTRODUCTION

Aerodynamic development plays a significant role to enhance continuous progress in vehicle performance, both in race and road vehicles. In single-seater race cars, such as Formula 1 and Formula E, the generation of negative lift through the use of ground proximity aerodynamics facilitates the increase in mechanical grip in tyres and, therefore, high-speed cornering and braking stability [1].

Aerodynamic appendages such as front and rear inverted wings and under-trays are used to improve the vehicle's dynamic performance. Most recently, the investigations of Katz et al. [2] and Garcia et al. [3] revealed that by adding vortex generators (VG) at the front of a vehicle´s underbody, region of low pressure will be induced and vertical aerodynamic load would be increased as ground clearance is reduced.

Adopting a similar approach, the main aim of this thesis is to investigate the flow physics of the vortices developed in the lowermost part of the vehicle in the proximity of the ground through a fully computational study. To achieve this goal, a simplified flat plate model (that simulates race car flat bottom) was used, based on previous studies carried out by Zaproudis [4], Byrne [5] and Arguelles [6]. However, in order to widen the perspective of induced vortices in ground effect the main aim was divided into two principal studies.

On the one hand, the project aimed to study the effect caused by different shapes of vortex generators on the aerodynamic performance and on the flow structures underneath the flat plate. For that purpose, the angle of incidence of the flow control devices respect to the freestream flow direction and the spacing between the vanes was varied.

On the other hand, the results in ground proximity obtained due to the addition of two endplates on both sides of a flat plate having a moveable trailing edge flap (simulating a rear diffuser) will be evaluated. Thereby, an extension of the previous work carried out by Arguelles [6] and a subsequent comparison will be performed. For this case, the design of lateral walls will not be investigated, but

the aerodynamic performance will be assessed. As part of this study, experimental tests performed by Arguelles [6], in Cranfield´s University 8'x6' Low-Speed wind tunnel, were used to validate the computational model designed in the present thesis.

1.1 Objectives

In order to comply with everything that has been established above, a series of more specific objectives has been created, which are the ones presented below:

- Validation of the computational model, based on the experimental data and the plate geometry designed by Arguelles [6].
- Design four different shapes of vortex generators.
- Adaptation of the computational model to each of the VG shapes designed.
- Evaluate the aerodynamic performance and flow structures underneath the plate for each VG design, in ground proximity.
- Adaptation of the computational model in order to obtain a final design with side endplates.
- Evaluate and compare the computational results to the data presented by Arguelles [6], in ground proximity.
- The project must present an adequate structure, in terms of the parameters studied and the results obtained, so that it can be used as a support for the development of a future experimental test programme.

2 LITERATURE REVIEW

2.1 Race Car Underbody

It is well known that the underbody region of race cars have undergone significant changes over the years, the main reason being the safety of the drivers. According to Katz [7], it was in the early 1970s when regulations limited the size and location of aerodynamic devices, giving way to extend the search for new aerodynamic designs to generate downforce. It was then that Lotus F1 engineers used an inverted wing underbody and sealed the side skirts, producing big flow accelerations underneath the vehicle (Figure 1). The effect achieved was called “ground effect”.

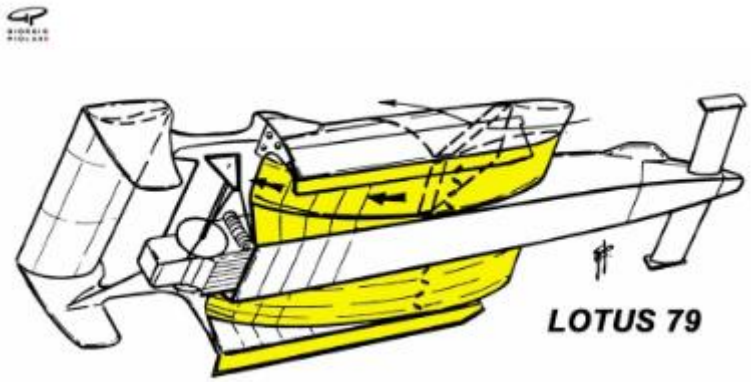

Figure 1: 1979 Lotus F1 car. Reproduced from [8]

2.1.1 Ground Proximity Aerodynamics

When an aircraft is flying close to the ground, the earth´s surface proximity modifies the flow motion around the wing, reducing the induced drag and increasing the lift [9]. As noted above, the idea of using an undertray is to take advantage of the performance enhancement it induces, significantly increasing the downforce generation with a low drag penalty.

Ground effect is effectively a Venturi-tunnel flow acceleration underneath the vehicle´s body, providing a downforce enhancement mechanism without adding weight to the vehicle. The Venturi-type effect, between the ground and the body, can be defined in terms of the equation of continuity and Bernoulli´s principle [9].

A simplify air motion of high and low pressure areas through the underbody of a car, in which the Venturi nozzle can be highlighted, is depicted in Figure 2.

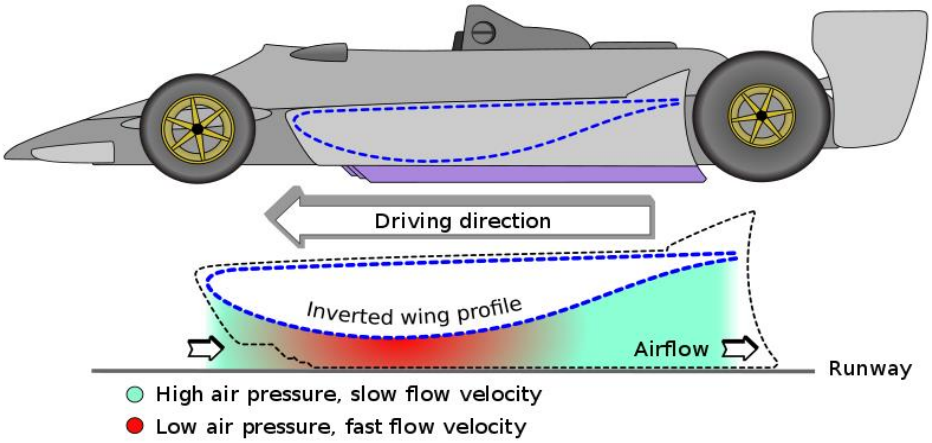

Figure 2: Representation of the Venturi nozzle on a racecar. Reproduced from [10]

A detailed study on the behaviour of the aerodynamic loads of a wing in ground effect was conducted by Zhang et al. [11]. Free-transition and fixed-transition cases were studied on a wing equipped with endplates (see Figure 3), obtaining the same tendency of the lift coefficient as the ground clearance was varied.

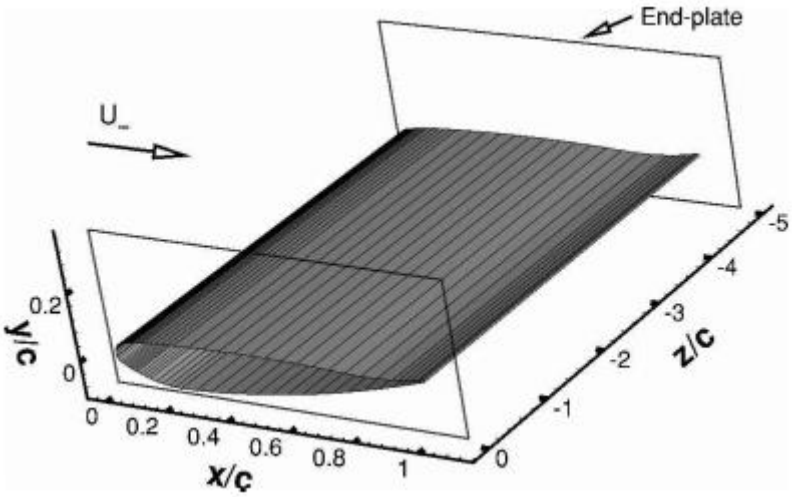

Figure 3: Schematic design of the wing model with endplates. Reproduced from [11]

A series of wind tunnel tests were carried out in order to obtain the forces acting over the wing, for a range of ride heights. A rapid increase of negative lift coefficient was observed, which enhances the downforce as the ground plane was approached. The amount of downforce yielded will be highly dependent on the distance between the body and the ground plane, being generally smaller as the ground clearance was increased.

Figure 4 shows the variation in lift coefficient for different riding-heights of the wing-model. Eventually, after the maximum value of force was reached at h/c=0.01 a sharp reduction of the lift coefficient was observed. The authors attributed this effect to the separation of the flow in the suction-surface of the body.

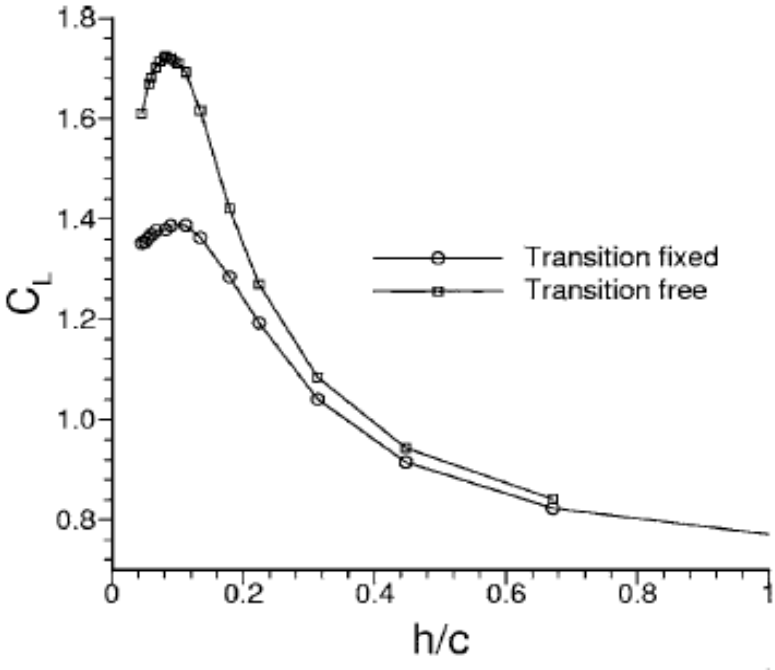

Figure 4: Lift coefficient against ground clearance. Reproduced from [11]

2.1.2 Underbody Diffuser and Undertray

Currently, open-wheel car underbody is very similar to a low-aspect ratio flat bottom, which includes a diffuser between rear wheels. The main objective of this streamlined aerodynamic device is to replicate the action that drives the Venturi effect and results in high aerodynamic efficiency. This way, the production of downforce (with a low drag penalty) will help pushing the car onto the track,

improving vehicle performance [9]. In a review by Agathangelou and Gascoyne [12], it was estimated that the underbody was responsible for generating 40% of the total downforce of the race car. Hence, an improvement in the design of the floor and the ability to control the flow beneath the car will bring beneficial effects in terms of vehicle stability and dynamic behaviour.

Cooper et al. [13] published a work centred in the understanding of flow physics in the underside of the car. The authors observed that the presence of the underbody affects the flow behaviour around the entire body and defined the pressure recovery as a fundamental parameter that drives the performance of flat-walled diffuser. It was surmised that there were three different methods of producing downforce: i) Ground Interaction: proximity to the track generated asymmetric flow field ii) Body Upsweep: the geometric characteristics act in favour of negative lift creation. iii) Diffuser Pumping: increase of the flow amount beneath the model.

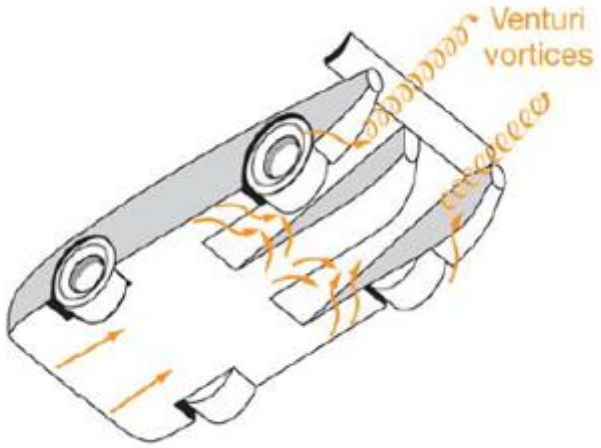

Figure 5: Illustration of Venturi vortices underneath a car. Reproduced from [14]

Senior and Zhang [15] studied the effects of the diffusers in ground proximity in order to understand the complexity of the flow dynamics underneath the vehicle. It was found that the vertical aerodynamic load was generated in four phases depending on ride height. At the same time, through the technique of flow visualisation, the authors demonstrated that a pair of counter rotating vortices is prone to appear in the region of force improvement (Figure 6), whose strength increases as the height to the ground decreases. However, a reduction of

downforce was revealed for low ground clearances and attributed to flow separation. It should be pointed out that the flow described a symmetrical behaviour around the centre line of the model.

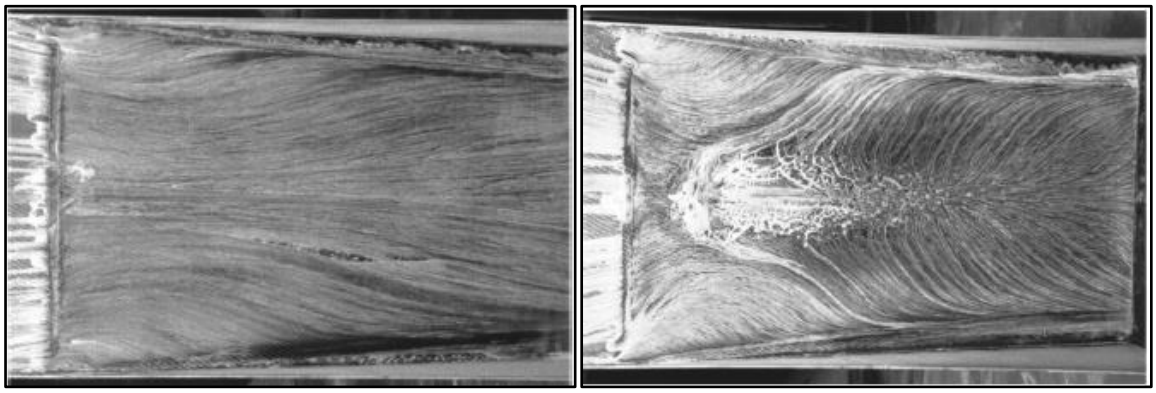

Figure 6: Surface flow visualisation in force enhancement region (left) and maximum force region (right). Reproduced from [15]**.**

Ruhrmann and Zhang [16] conducted an experiment for a wide range of diffuser angles in ground effect at different ride heights (Figure 7). The aim was to investigate the effect of the pressure forces over the flat underbody and extend the understanding of the flow behaviour in order to improve the design of flow control devices. The study indicated that the diffuser ramp leads to vortex flow development and flow separation. This was the main cause of producing a general force reduction. When the ride height varied to low values, the pressure experienced a drop that leads to the separation of the flow (Figure 8). At low angles, the aerodynamic behaviour was characterised by the burst of counter rotating vortices. However, as the angle increased the beginning of the flow separation merged with the growth of the vortex that produced the force reduction (Figure 9).

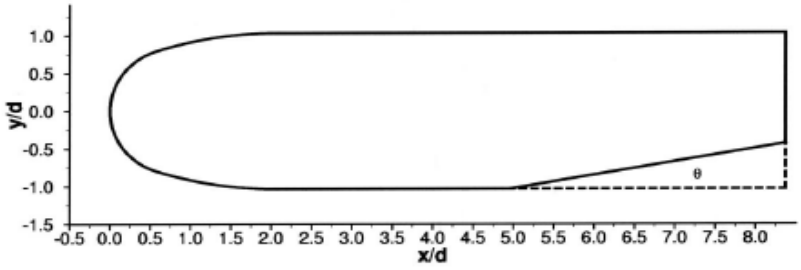

Figure 7: Schematic design of the experimental model. Reproduced from [16]

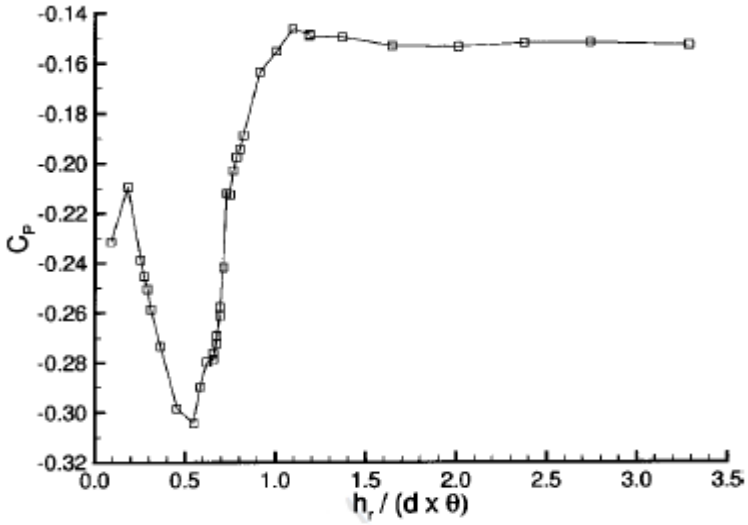

Figure 8: Pressure coefficient for diffuser ramp at 20 degrees. Reproduced from [16]

Figure 9: Flow visualisation of diffuser ramp at 20 degrees. Flow from left to right. Reproduced from [16]

2.2 Flow Control Devices. Vortex Generators

Conventional passive vortex generators have been used for aeronautical applications for a long time. Normally these take the form of thin plates that are mounted perpendicularly on the aircraft´s wing surface in order to generate a rotating flow that interacts with the boundary layer, retarding the separation at high angles of attack. It should be noted that in the vicinity of the rotating flow a low pressure area will be generated, enhancing the negative lift force [17].

Flow separation is caused on surfaces when a critical value of adverse pressure gradient is exceeded. In other words, introducing vortex generators before the separation point of the flow an increase in the momentum will be obtained. Thereby, one of the objectives of the vortex generators comes to energise the boundary layer.

Aeronautical VGs are usually known as sub-scale vortex generators or micro VGs, because of their size, which alternates between 10%-50% of the thickness of the boundary layer, avoiding as much as possible the drag penalty [18]. However, not only aerospace sector exploits this effect, the automotive sector, and especially motorsport, incorporate this type of flow control devices. In this case, they are large-scale vortex generators as they are in contact with the flow outside of the boundary layer in order to increase the downforce [19]. Figure 10 presents a schematic description of both types of vortex generators.

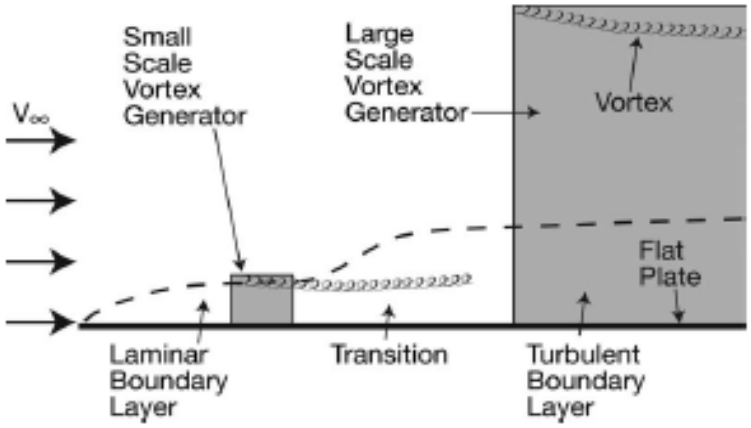

Figure 10: Schematic description of Small and Large-scale VGs. Reproduced from [19]

Figure 11 shows a large-scale turning vane upstream of a vehicle´s underbody, used by racecar designers to create streamwise vortices. This way, it is expected that trapped vortices influence the fluid motion generating a suction force that will produce a low-pressure region underneath the car, enhancing tyre mechanical grip and vehicle´s performance.

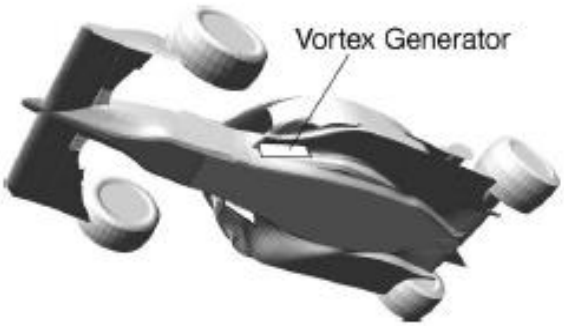

Figure 11: Vortex generator location on an open-wheel racecar. Reproduced from [19]

Several studies have been conducted with underbody rectangular VGs in order to characterise the magnitude of the aerodynamic loads.

Katz et al. [2] investigated the partial contributions of Indy-Car elements. Among others, the comparison of the aerodynamic behaviour between Indy Car prototype underbody and a flat plate with mounted vortex generators could be highlighted. The authors clearly demonstrated how a simplified geometry of a plate could characterise flow behaviour beneath the car. A general overview of the results reported that, as ground clearance was reduced the vortex strength increased and therefore, downforce and drag increased. At the same time, a reduction of the maximum downforce value in close proximity to the ground was observed, which was attributed to a possible vortex burst.

To date, a number of investigations have been conducted in order to understand the effects of the vortex breakdown phenomenon. Early investigations observed these effects over delta wings at high angle of attack. It was suggested that the vortex burst was related to wave propagation, flow stagnation and instability [20]. However, Benjamin [21], not in absolute agreement with these explanations, defined vortex breakdown as an axisymmetric swirling flow that undergo sudden changes in the structure, based on a supercritical to subcritical transition. More recently, extended studies revealed the existence of two different types of vortex breakdown: axisymmetric (bubble) and spiral flow [22].

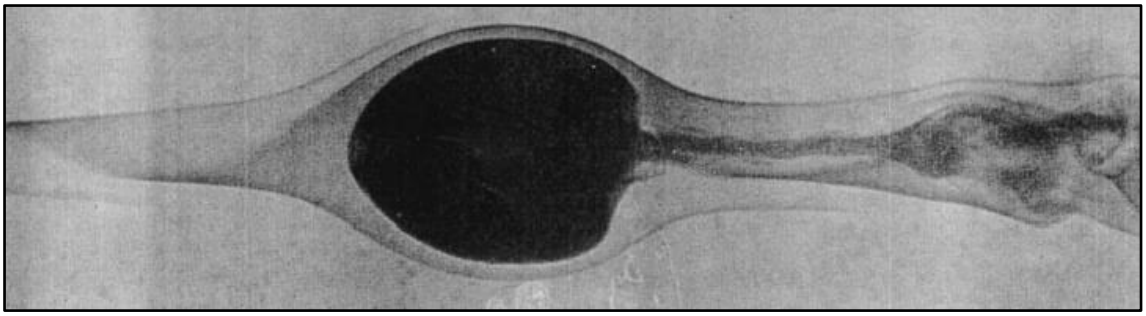

Figure 12: Bubble type vortex breakdown. Reproduced from [22]

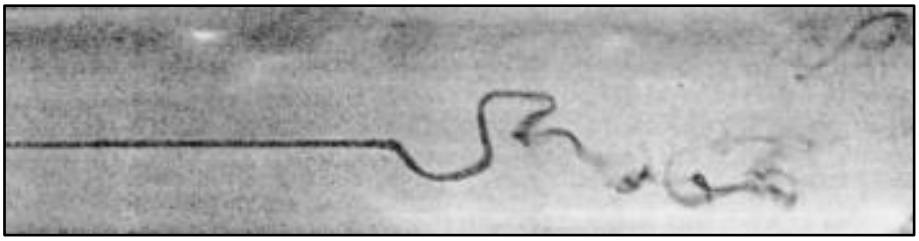

Figure 13: Spiral type vortex breakdown. Reproduced from [22]

Axisymmetric breakdown is characterised by the formation of a bubble-shape vortex around the central axis of the swirl. The spiral breakdown may be interpreted as a non-linear global mode characterised by an abrupt deceleration of the core [22].

Garcia et al. [3] carried out a systematic experimental study of an inverted flat plate equipped with two vortex generators at each side (Figure 14), simulating the lower surface of racecars. The experiment considered the main geometric characteristics respect to the ground clearance: local inclination angle (β) of the VGs and aspect ratio (VG lateral spacing/VG height).

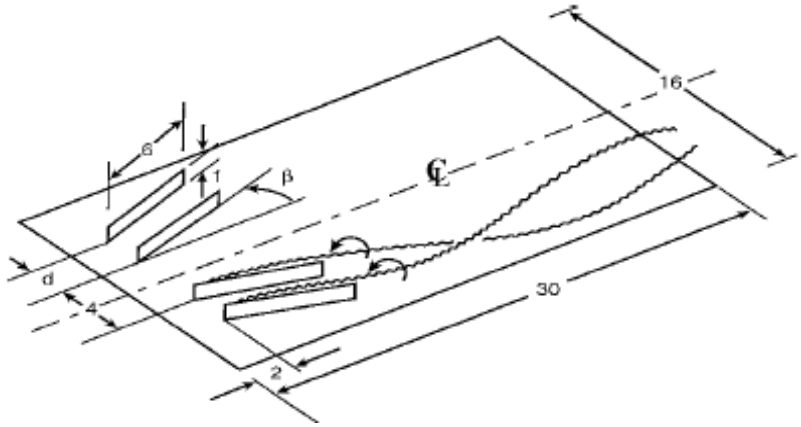

Figure 14: Flat plate equipped with VGs. Reproduced from [3]

The experimental data measured for different parallel VG incidences is represented in Figure 15. It was found that larger VG angles created a lift increment as the distance to the ground was reduced. Furthermore, flow visualisation showed that at large ground clearances vortices interacted with each other, while at low ride heights the untwisting of the vortices was observed. As stated above by Katz et al. [2], in this case the reduction of the maximum lift coefficient, at large angles and low heights, was related to the vortex breakdown.

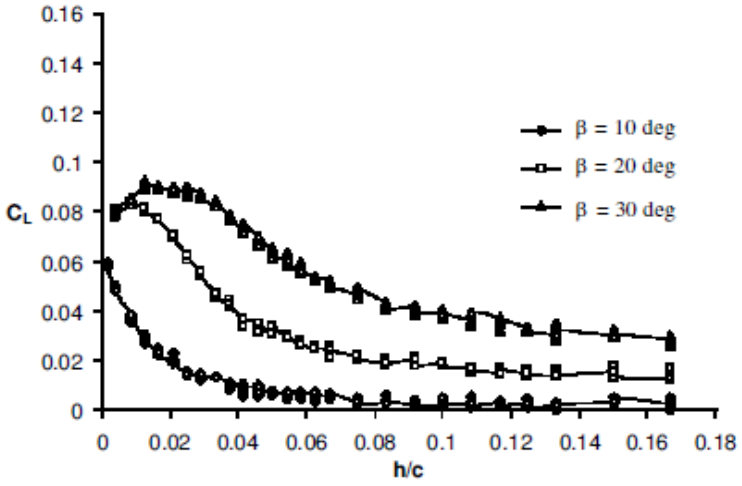

Figure 15: Lift coefficient for a range of VG incidence angles. Reproduced from [3]

The effectiveness of the aspect ratio was also assessed. Figure 16 shows the lift coefficient recorded for various lateral spacings. It can be clearly observed that as the distance with the ground was reduced and lateral spacing was augmented,

the lift coefficient increases. However, in a particular case, with the aim of testing the effect of a single vortex generator, aspect ratio was defined as infinity. It was effectively proved that the lift coefficient for a single turning vane could be comparable to that for two turning vanes in close proximity to each other (AR=0.5). The authors concluded there was no necessity of mounting two vortex generators to trap a vortex between the plate and the ground.

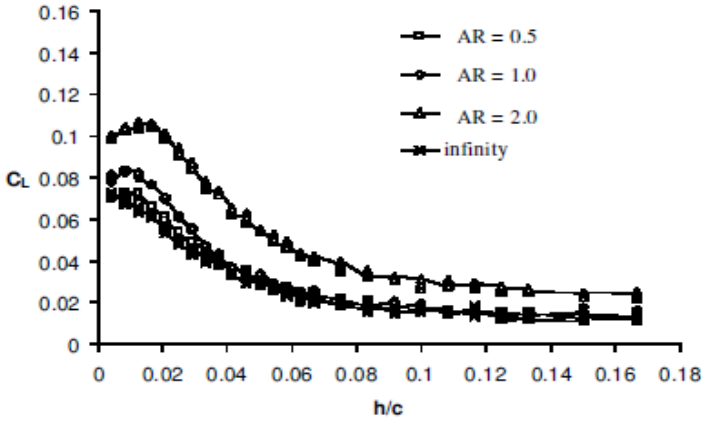

Figure 16: Lift coefficient for a range of VG spacings. Reproduced from [3]

In order to extend the studies on modelling vortex effects on simulated vehicle lower surfaces, Van de Wijdeven et al. [23] recorded the peaks of vortex suctions on a flat plate, through pressure distribution, and traced the vortex wake development behind the VGs.

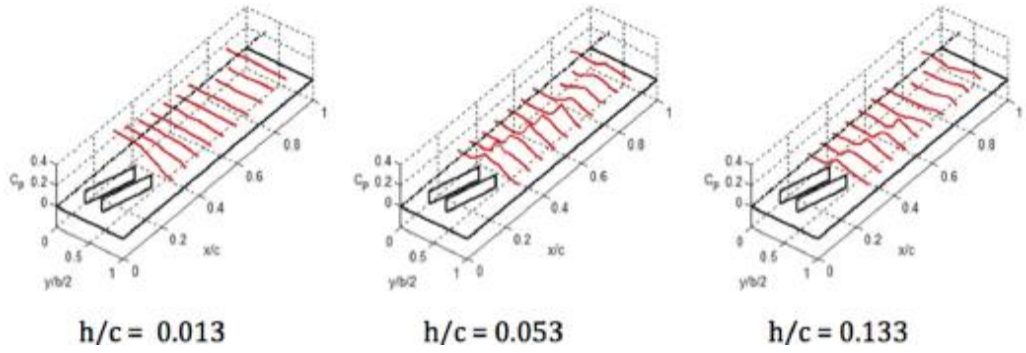

Figure 17: Vortex suction behind the VGs at different ground clearances Reproduced from [23]

The authors found that as the distance from the ground was increased the vortex trail definition behind the turning vanes was clarified. At the same time, the

tendency of the vortex core to move outwards emerged and was directly related to the vortex roll up. This implied a reduction in the pressure distribution for higher distances to the ground plane. Figure 18 shows the pressure distribution on a plane defined behind the flow control devices, in which the reduction in the suction and the displacement of the vortex was reported.

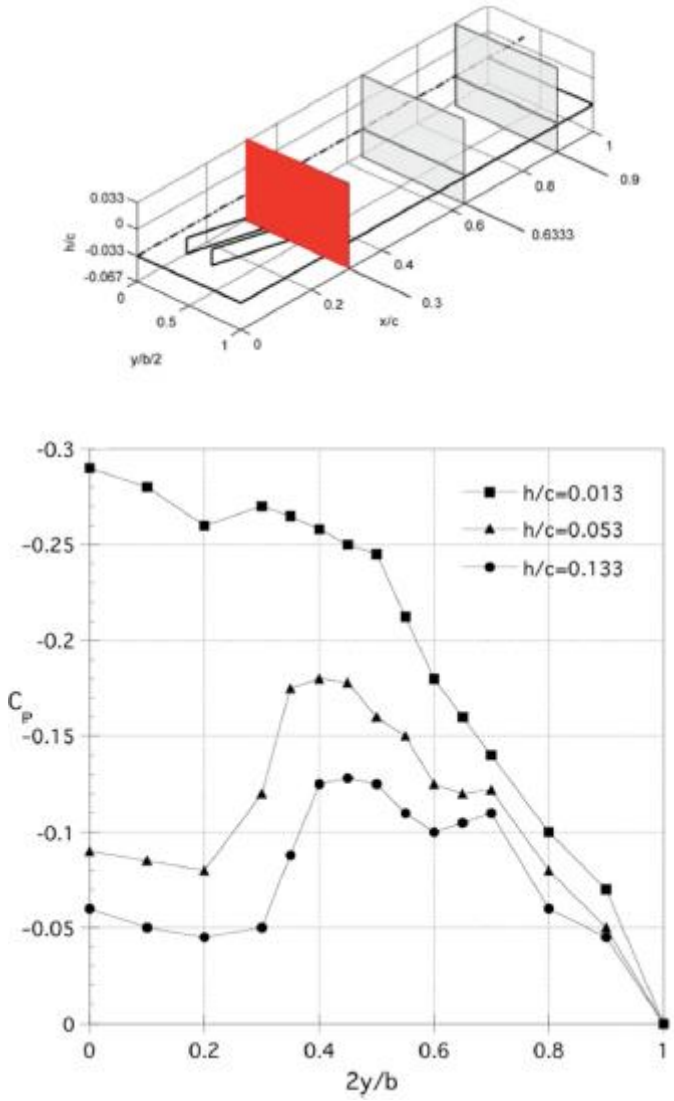

Figure 18: Vortex suction peaks at x/c=0.30. Reproduced from [23]

2.2.1 Vortex Generators Geometries

As previously discussed, this project aims to perform an optimisation of vortex generators, investigating and testing different shapes. Notice that earlier studies

on flat plates used mainly rectangular vortex generators. As a result, there is a lack of public domain data available on the effects of VG shape.

Figure 19 presents, in terms of negative lift coefficient, the comparison between rectangular and triangular turning vanes in parallel configuration at 20 degrees, orientated with respect to the freestream flow direction. The experiment carried out by Katz et al. [19] focused on testing geometrically different vortex generators: large type and short type (half-length of large VG). The area was described as the main parameter of concern. It is shown that both sizes of rectangular VG´s produced higher vertical aerodynamic loads than triangular designs as the ground clearance was reduced. However, as the distance from the ground increased the effect of the shape was diminished. The larger vane of each type gave higher values of negative lift, as was expected, due to the larger area.

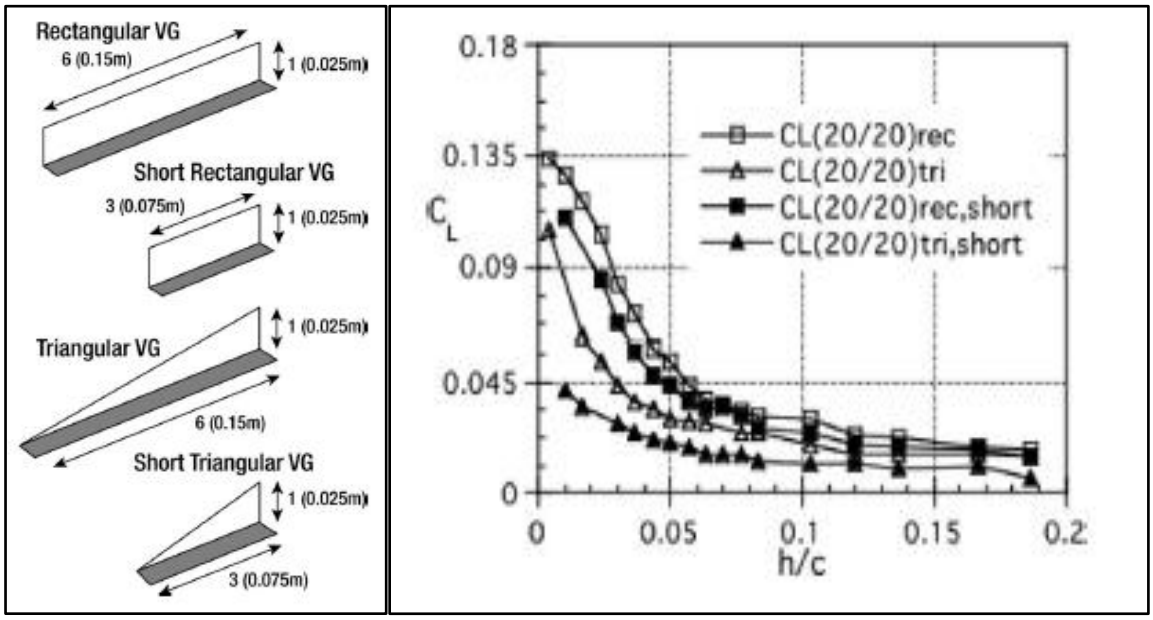

Figure 19: Comparison of rectangular and triangular VGs. Reproduced from [19]

In order to extend the previous analysis, Katz et al. [19] explored the study of additional geometries of vortex generators as depicted in Figure 20. It should be pointed out that triangular and ogive designs have the same area.

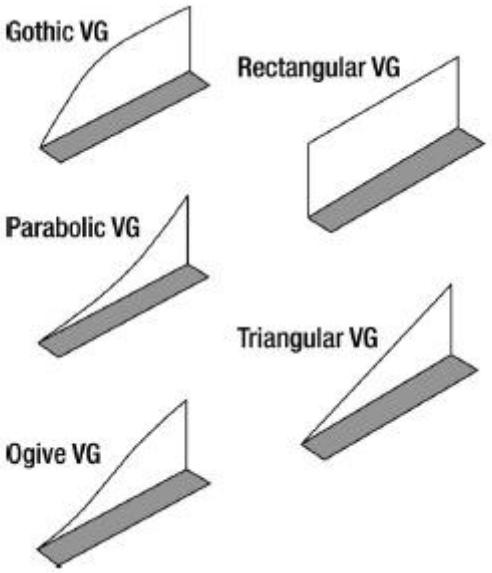

Figure 20: Additional VG shapes. Reproduced from [19]

Figure 21 and Figure 22 summarised the data obtained by Katz and Morey [19] in terms of negative lift and drag coefficients, for five different VG designs. It was clearly shown that the rectangular vane was responsible for generating the largest downforce and drag forces, whereas gothic design produced higher lift than the triangular design. As stated above, the noticeable differences between the evaluated results were suggested to be mainly dependant on the described area by each of the vortex generators.

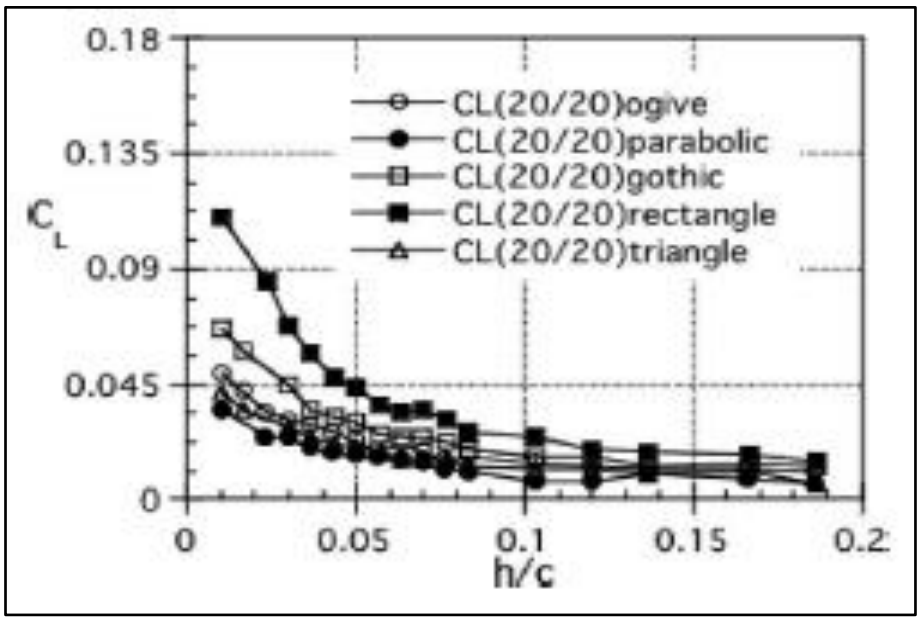

Figure 21: Lift coefficients for VG shapes. Reproduced from [19]

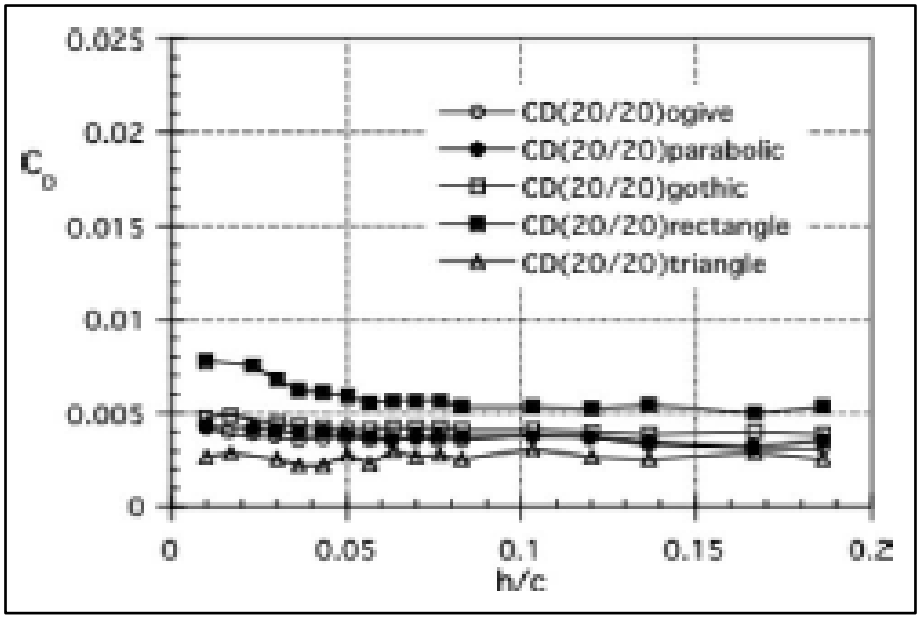

Figure 22: Drag coefficients for VG shapes. Reproduced from [19]

Finally, the authors summarised a general increment of downforce at low distances from the ground, while the triangular design demonstrated the major effectiveness.

Van de Wijdeven et al. [23] mounted a NACA 0012 shaped aerofoil aerodynamic device into a flat plate in order to study the blockage effect between the lower surface of a race car and the ground plane. As a result, the influence of the vortex wake in increasing the local effect of the turning vanes, reducing the pressure in the underbody region was highlighted.

2.3 Endplates

Endplates are commonly identified as vertical surfaces mounted on the wing tip of aircraft or on the wings of racecars. Lanchester et al. originally designed them as induced drag reducers under high lift conditions [24].

Early aerodynamic studies centred on aircraft wings, showed that there was a tendency of the flow to migrate from the lower surface (high pressure) to the upper surface (low pressure), generating strong trailing-edge vortices. Thereby, the pressure at the tip will not be as high as on the wing [24].

In order to block the airflow that continuously looped around the wing tip vertical plates were introduced. This way the induced drag would be reduced, decreasing the strength of the vortices generated at the wing tip, hence improving aircraft´s performance.

Roberts [25] assessed a numerical and experimental analysis of the optimization of a well-designed endplate to reduce the effect of the drag on the planar wing of a PA-18 Super Club aircraft. The author surmised that the implementation of a cambered tip plates allowed an effective increment in aspect ratio of the wing, which would theoretically reduce the induced drag. The experimental results, from wind tunnel testing and from full-scale flight experiment, showed that the addition of cambered tip plates generated a larger diameter edge vortex with a reduced rotational velocity. An improvement of the aerodynamic efficiency of the aircraft for some values of circulation was observed.

The study completed by Soltani et al. [26] reproduced several wind tunnel experiments to evaluate the influence of the endplates in the aerodynamic forces over a wing. The authors demonstrated that attaching endplates on the tips of the wings altered significantly the pressure distribution over the wing and had significant impact on lift and drag coefficients.

As an extension of the work presented by Arguelles [6], the present project aims to investigate the effect on the aerodynamic forces and moments through the implementation of two vertical fences or side skirts on each side of a flat plate. As was previously mentioned, due to the generation of potentially dangerous aerodynamic loads the FIA banned side skirts on motorsport competitions. This reduced the investigations of racecar underbodies equipped with vertical fences and most of the cases are focused on the study of inverted aerofoils fitted with endplates in ground proximity, simulating the front wing of a racing car.

Galoul et al. [27] stated that the presence of endplates was intended to avoid three-dimensional effects as much as possible. The authors conducted a study of an inverted wing with rectangular endplates in the ground proximity in order to explore the aerodynamic performance, using Laser Doppler Anemometry (LDA) and flow visualisation; see Figure 23.

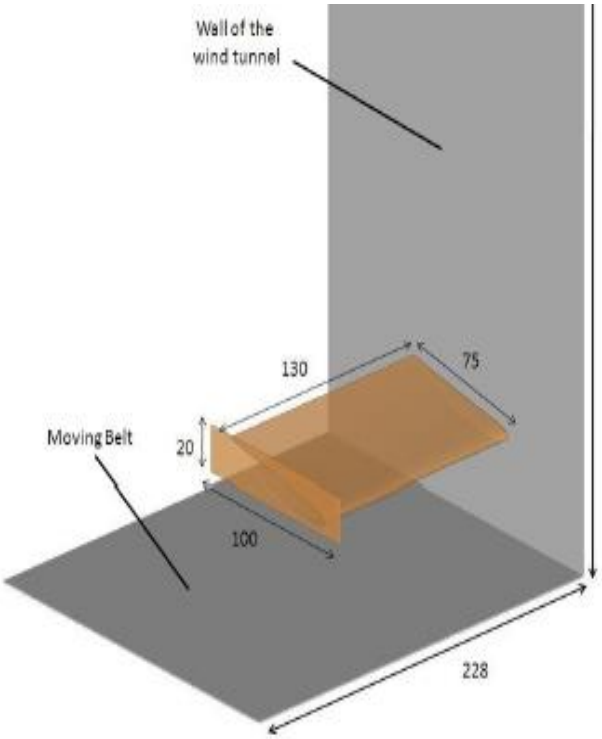

Figure 23: Wind Tunnel set up of the inverted wing. Reproduced from [27]

Flow visualisation revealed that the size of the endplates was an essential parameter, as the wing vortex behaviour was completely dependent on them. In this investigation, the formation of two co-rotating vortices at the top and the bottom of the plates was observed. The length of the endplate dictated the shape of the vortex while the width varied the development of the vortex downstream. The experimental studies reported that the velocity of the vortex was lower than the freestream velocity, as reproduced in Figure 24, attributing this effect to the low pressure induced in the core by the rotatory motion of the vortex. Accordingly, the vortex generated on the bottom edge was found to be stronger than upper edge vortex, in which the size of the lower vortex was estimated in 0.12c and the upper vortex size in 0.05c.

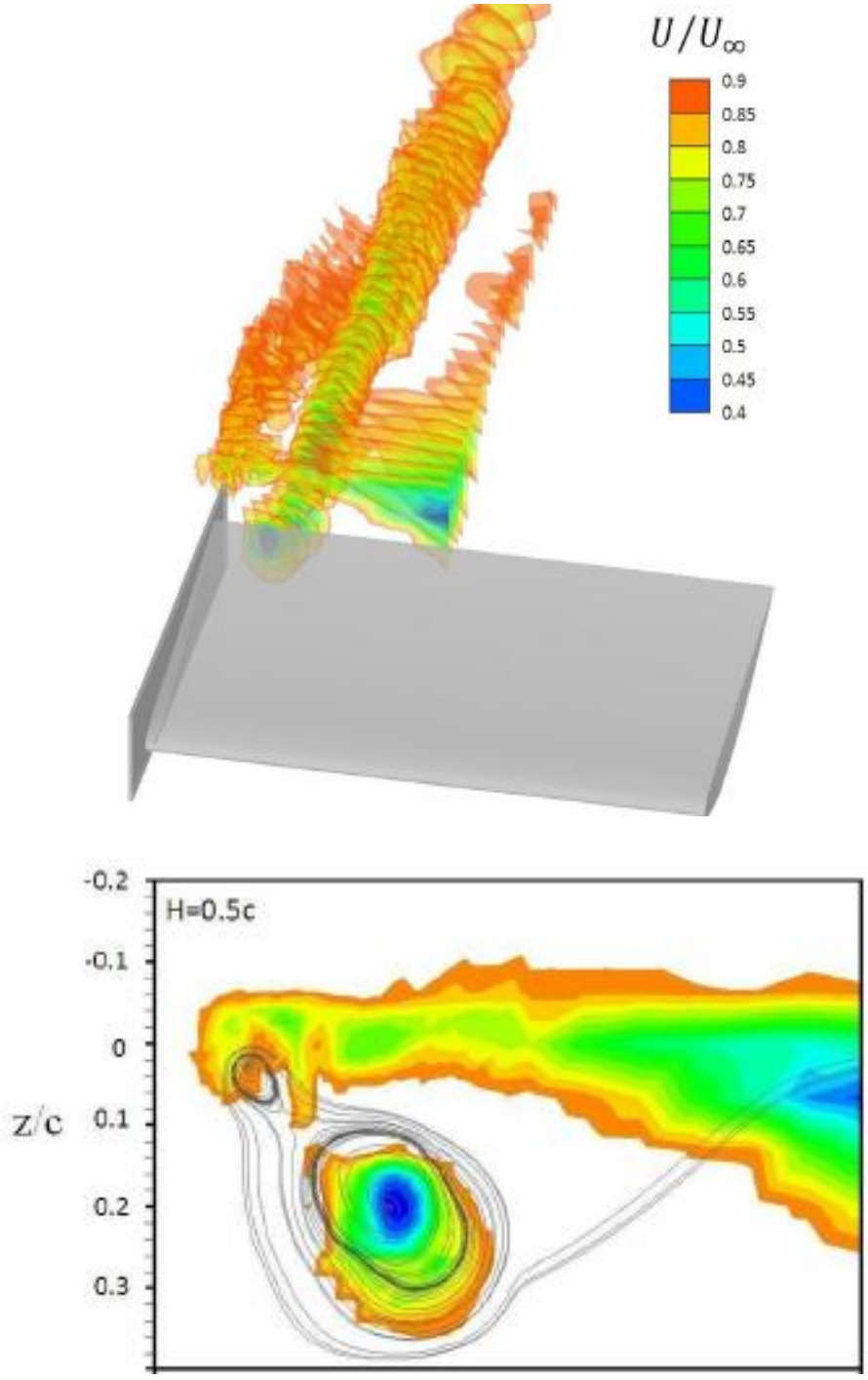

Figure 24: Vortex path development downstream. Reproduced from [27]

The authors stated that the shape of the vortex was found to be non-symmetrical and non-homogenous, and the longitudinal velocity of the lower vortex increased as the distance downstream was augmented.

Finally, the proximity of the ground did not seem to induce significant changes on the vortex behaviour although it had a remarkable effect on the aerodynamic load generated over the wing, increasing the downforce and pressure on the upper surface of the wing as the distance to the ground was reduced [27].

2.4 CFD Numerical Model

Nowadays, computational fluid dynamics (CFD) simulations are very powerful tools used by engineers and researches to predict the physics of the flow-field of respective investigations. Although, in recent years, it has undergone great development and has improved the ability to accurately predict flow structures, an experimental data is still needed to validate a solution. CFD analyses are commonly used to predict before or after experimental tests the characteristics of the flow-field development of the study. In addition, they allow obtaining more data than experimental tests themselves and obtain an approximation of the expected result of the test programmes.

Regarding the application of CFD simulations to characterise the streamwise vortex development, four key parameters can be considered of great importance to study according to Yao et al. [28]: vorticity (concentration), circulation (strength), trajectory (path) and vortex radius (size).

Allan et al. [29] published a numerical investigation of a single small-scale vortex generator vane on a flat plate, configured at 23º and 10º with respect to the free flow. The aim was to evaluate the flow physics downstream of a turning vane, comparing the strength and trajectory of Reynolds-averaged Navier-Stokes (RANS) computational simulations with experimental Particle Image Velocimetry (PIV) data gathered previously. At the same time, a comparison between Spallart-Allmaras (SA) and k-ω SST turbulence models was conducted. Simulations of k-ω turbulence presented more accurate predictions than SA model, in terms of vortex path and vortex peak decay. However, the circulation of the vortex (see Figure 25) was similarly predicted and SA turbulence model showed a more diffuse vortex motion.

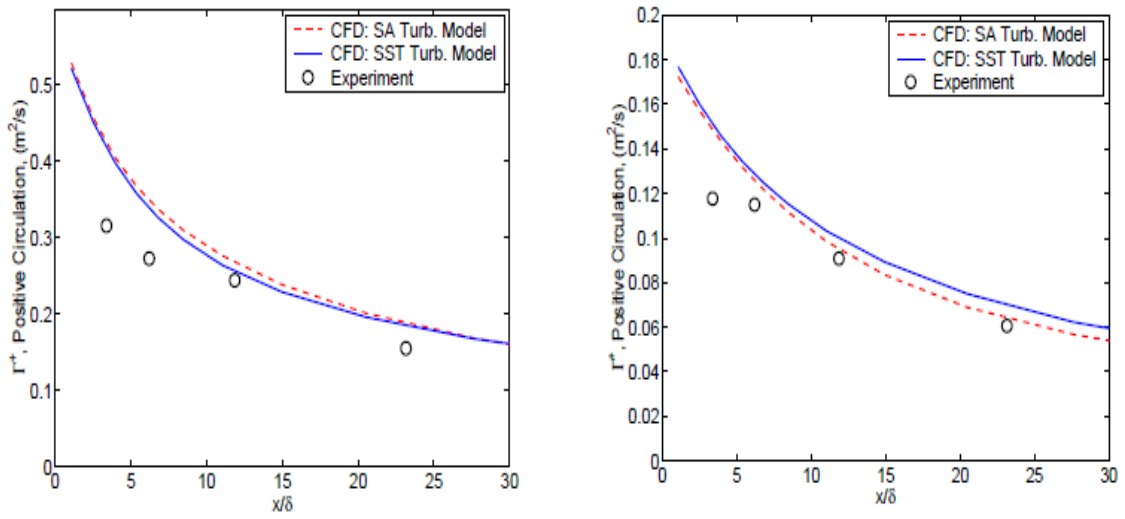

Figure 25: Comparison of Positive Circulation at α=23º (left) and α=10º (right). Reproduced from [29]

A comparison of experimental and computational streamwise vorticity contours is shown in Figure 26. These plots presented an under-prediction of the computational vortex contours and a more rapid diffusion of the vortex development as the distance downstream for the VG increased. Additionally, the vortex shape gathered experimentally indicated a more circular tendency in which a concentrated vortex core at the early stages of the vortex formation was highlighted. Overall, a better prediction of the flow was surmised for the turning vane configured at 10º comparing with experimental studies.

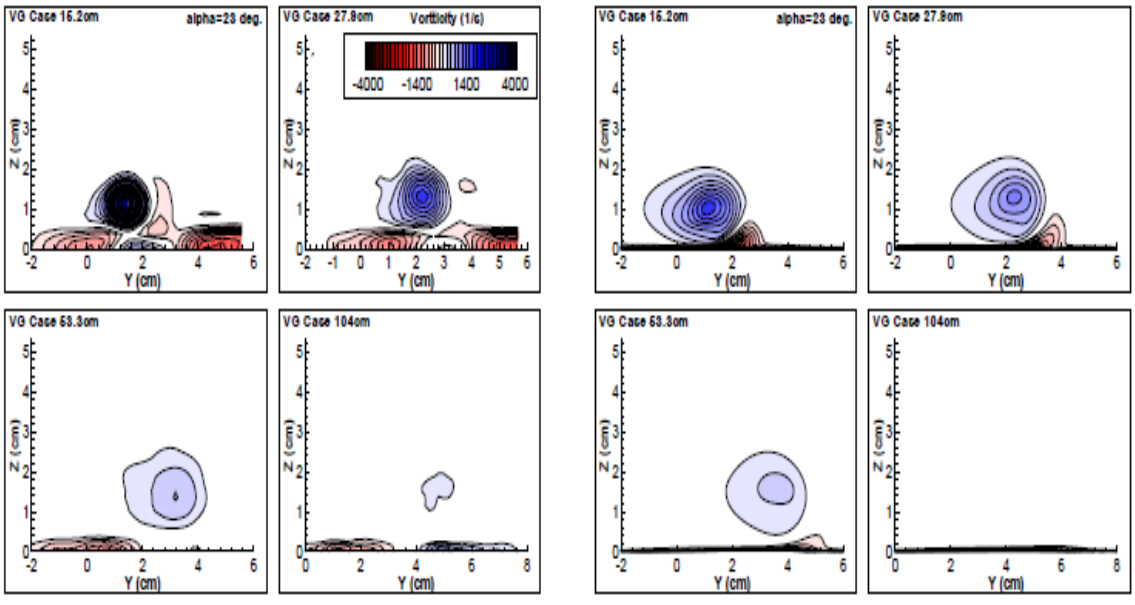

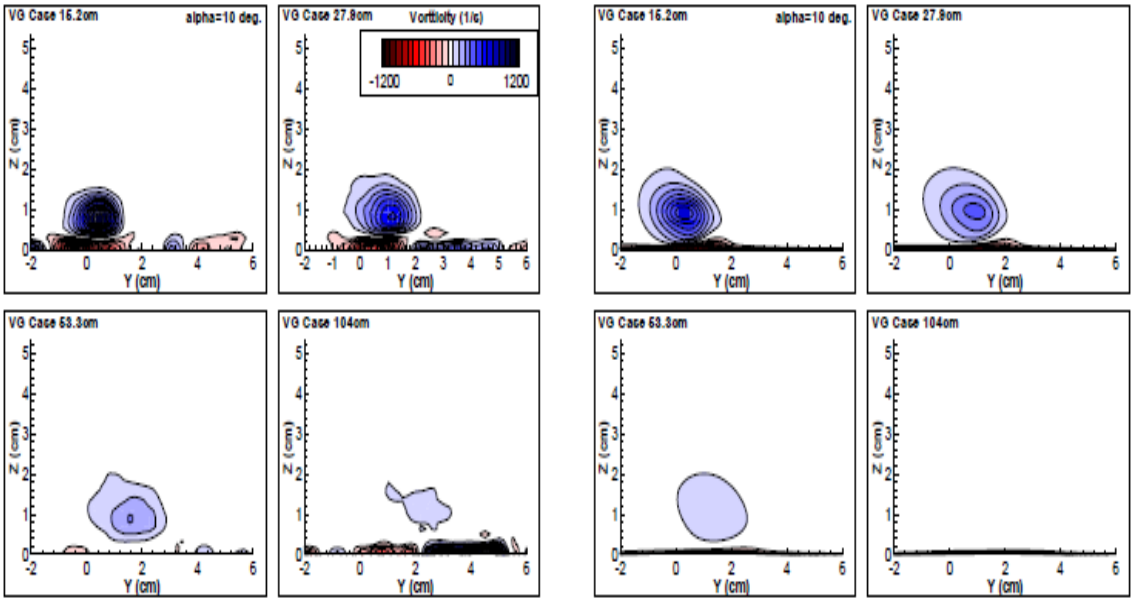

Figure 26: Streamwise Vorticity Contours of Experimental and CFD data (left to right) (Up α=23º and down α=10º). Reproduced from [29]

Jung et al. [30] conducted a computational investigation for a better understanding of the aerodynamic characteristics introduced by the assembly of an endplate on a NACA-4406 3D wing tip. To effectively resolve the unsteady flow physics, Navier Stokes equations were used with k-ω SST turbulence model and SIMPLE implicit scheme. The authors found that the blocking effect generated by the endplates created a decrease in the pressure produced below the surface of the wing, considerably improving (by 46%) the aerodynamic efficiency of the body, especially at low ground clearances as can be seen in Figure 27.

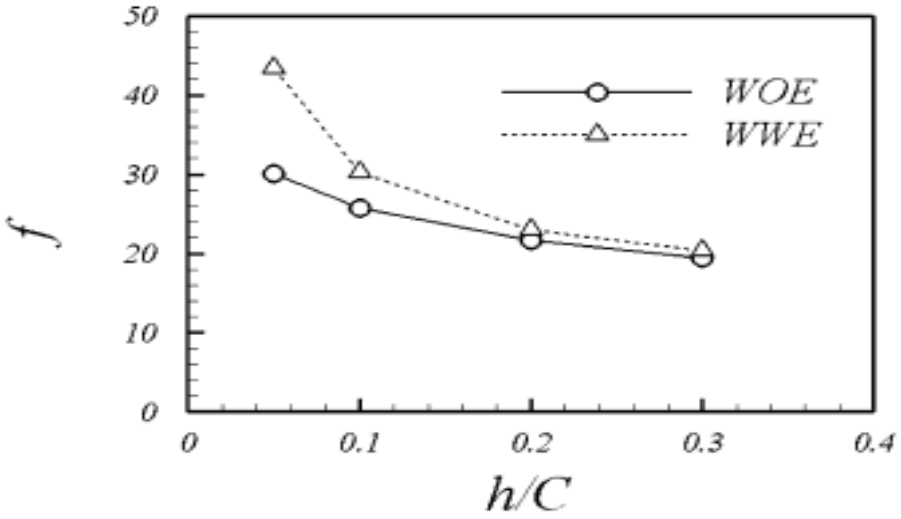

Figure 27: Aerodynamic Efficiency of the 3D wing with (WWE) and without (WOE) endplates. Reproduce from [30]

The analysis of the vortex trajectories reproduced in Figure 28 indicates the formation of wing tip vortices independently of having or not endplates. Based on these results, it can be clearly observed the generation of the vortices, in the case of wing without endplates, occurred from the leading edge backwards and the secondary vortex (V2) presented a higher rate of diffusion. By contrast, the wing with endplates created the vortices at the leading edge, extending further downstream of the wing and a tertiary vortex was also formed at the leading edge.

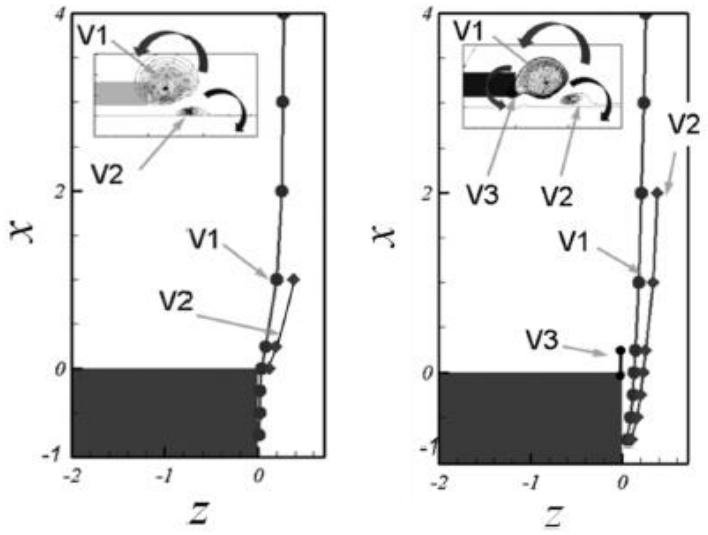

Figure 28: Trajectories of tip vortices for WOE (left) and WWE (right) at h/c=0.5. Reproduced from [30]

Shear Stress Transport (SST) k-ω Turbulence Model

In order to perform the present computational investigation of the vortex generated underneath the flat plate, Shear Stress Transport k-ω turbulence model was selected. This turbulence model consists on a two-equation eddy viscosity model that predicts more accurately adverse pressure gradient flow conditions and data in the near-wall regions. In the near-wall zone of the boundary layer employs turbulent kinetic energy (k) equations and specific dissipation rate (ω) equations. However, since it is very sensitive for k and ω values outside the shear layer, k-ε turbulence model is used in the freestream region exhibiting less sensitivity to freestream conditions, [31]. Coming up next, equations employed by k-ω SST turbulence model are presented:

$$\frac{\partial}{\partial t}(\rho k) + \frac{\partial}{\partial x_i}(\rho k u_i) = \frac{\partial}{\partial x_j}\left(\Gamma_k \frac{\partial k}{\partial x_j}\right) + \bar{\mathrm{G}}_k - Y_k + S_k$$

$$\frac{\partial}{\partial t}(\rho \omega) + \frac{\partial}{\partial x_i}(\rho \omega u_i) = \frac{\partial}{\partial x_j}\left(\Gamma_\omega \frac{\partial \omega}{\partial x_j}\right) + \mathrm{G}_\omega - Y_\omega + S_\omega + D_\omega$$

2.5 Previous Race Car Undertray Studies

The aforementioned experimental study conducted by Garcia et al. [3] involved the development and the strength of the streamwise vortices beneath a flat plate for a wide range of ground clearances. At the same time, aerodynamic loads were recorded when varying the incidence of the VGs and the aspect ratio, in which a fixed wind tunnel ground was used.

Based on the work noticed by Garcia et al. [3] large scale VG´s in ground proximity were assessed by Holt et al. [32]. A numerical and experimental project was carried out with the objective to analyse the effect of a moving ground and the vortex behaviour in the underbody region. For that purpose, the influence of different rectangular VG angles and lateral spacings on a flat plate was investigated.

Experimental downforce and drag coefficients at different vane angles are reported in Figure 29, against several ground clearances. A clear increase in

downforce was noticed as the distance to the ground was reduced, except at 25 degrees where a decrease in downforce was observed. This reduction of negative lift was attributed to the instability of the vortex movement due to its vicinity to the ground. On the other hand, drag coefficient showed the same general trend.

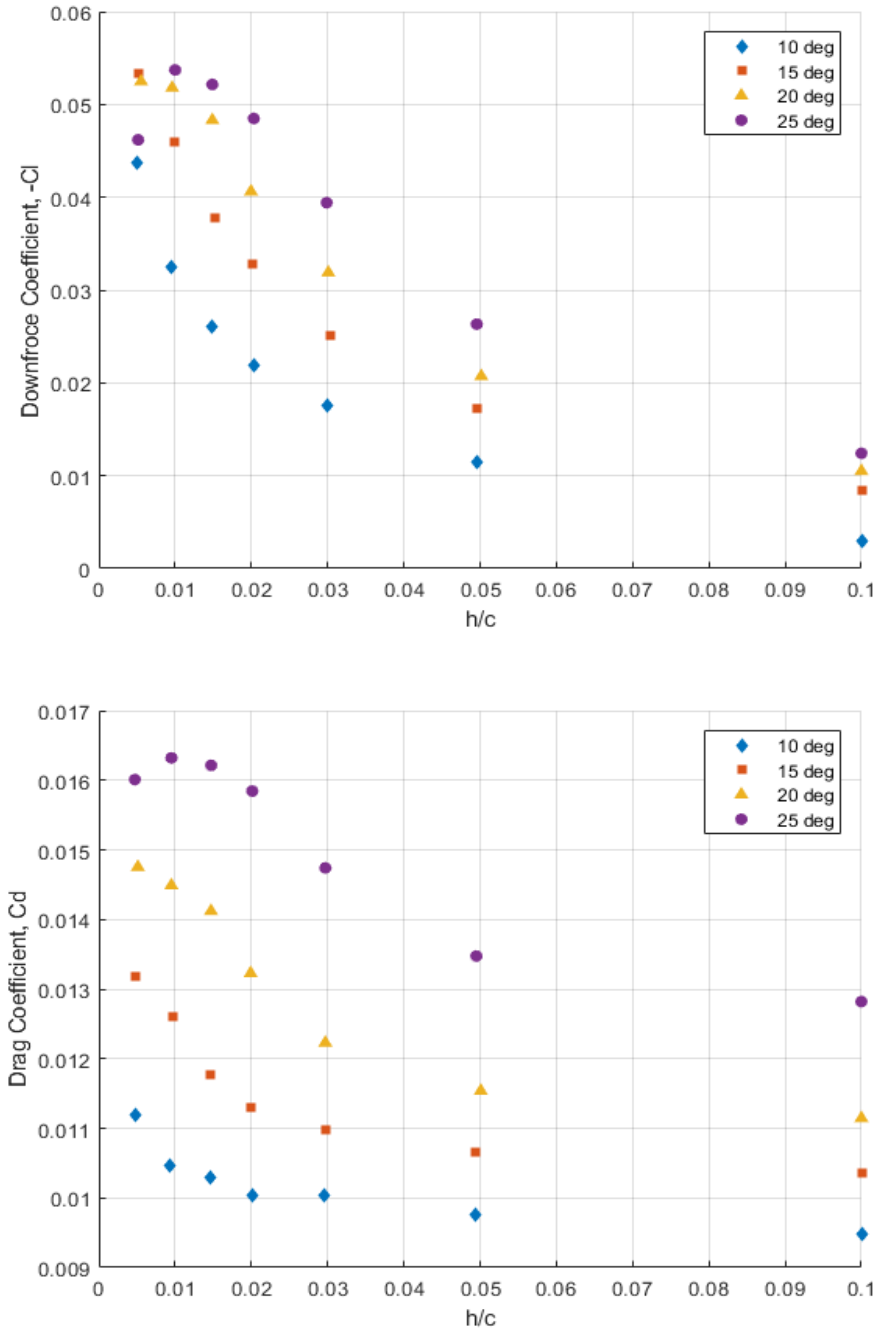

Figure 29: Angle influence on C_L and C_D. Reproduced from [32]

Wind tunnel data, where the aspect ratio (AR) was modified, gave rise to higher negative lift values in the case of AR=2. In contrast, as expected, the plate without flow control devices generated very low aerodynamic loads. However, as Garcia et al. [3] suggested, the presence of a second vertical fence to model the vortex is unnecessary, as can be seen in Figure 30. For AR=0.5, the exerted forces were almost the same as in the configuration of a single vane. Similar trend was seen for drag coefficient.

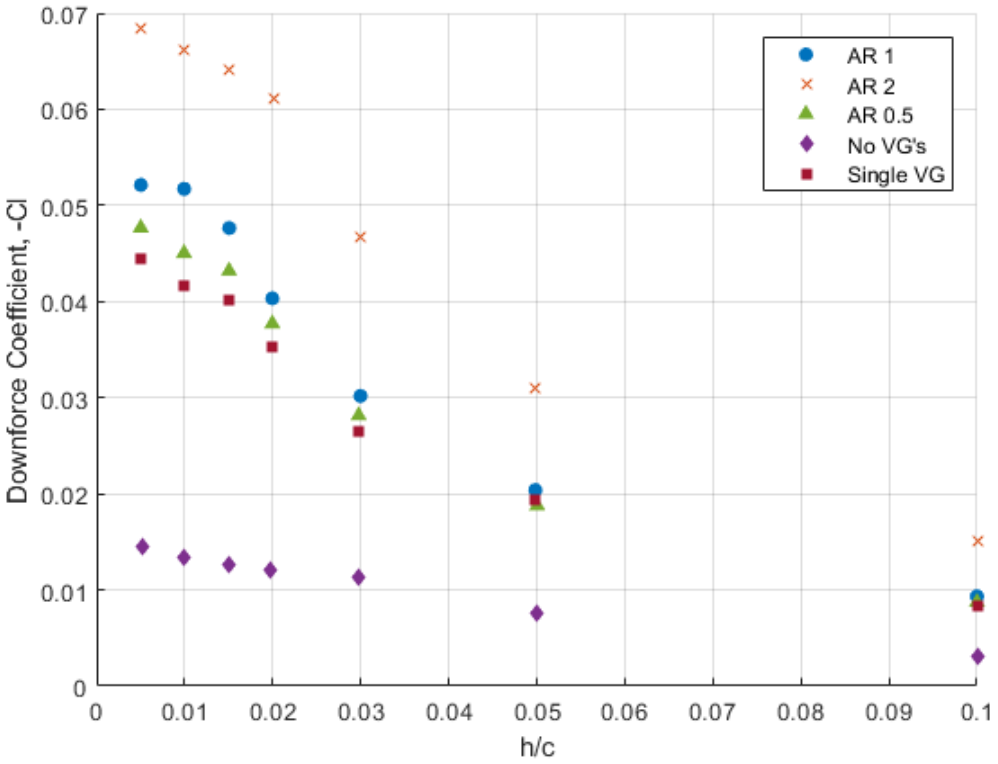

Figure 30: Experimental C_L data for different spacings. Reproduced from [32]

The comparison with fixed ground data of Garcia et al. [3] showed a good agreement with the general trend of the curves. However, the absolute values differed, highlighting the difference between the tests with static and moving belt configurations.

Arguelles [6] extended the previous study, investigating the effect of a pressure gradient change on the vortex flow beneath the plate, controlled by the addition of an adjustable flap-like element at the trailing edge of the plate. Although Holt

et al. [32] and Arguelles [6] conducted a similar research (manipulating the same VG parameters on a flat plate and studying the aerodynamic loads), the results were not comparable since the variation of the diffuser angle heavily influenced the forces measured on the flat plate. A series of wind tunnel tests and numerical simulations were carried out in order to obtain aerodynamic loads and moments acting on the flat plate.

The experimental tests were conducted varying three main parameters: VG spacing (AR), flap angles and VG incidence angles (β). Each parameter was investigated for a range of ground clearances. Figure 36 shows a simple sketch defining how the way of movement of each parameter is.

Effect of varying the angle of the flap (δ)

Figure 31 compares experimental and numerical aerodynamic forces, in terms of lift and drag coefficients, for different configurations of diffuser ramps. The AR and the incidence of the vortex generators were fixed at values of: AR=2 and β=10º. The results obtained showed an excellent agreement between numerical and experimental data. For negative flap angles, an increase in negative lift was observed as the distance from the ground was increased, while the drag values remained practically constant. As the flap angle was increased, higher aerodynamic efficiency was seen, in which the downforce was increased for low ground distances. However, at higher values of flap deflection (δ>= 10º) at low ground clearances, lift and drag coefficient were found to be reduced and as Garcia et al. [3] and Holt et al. [32] suggested, was attributed to the vortex burst.

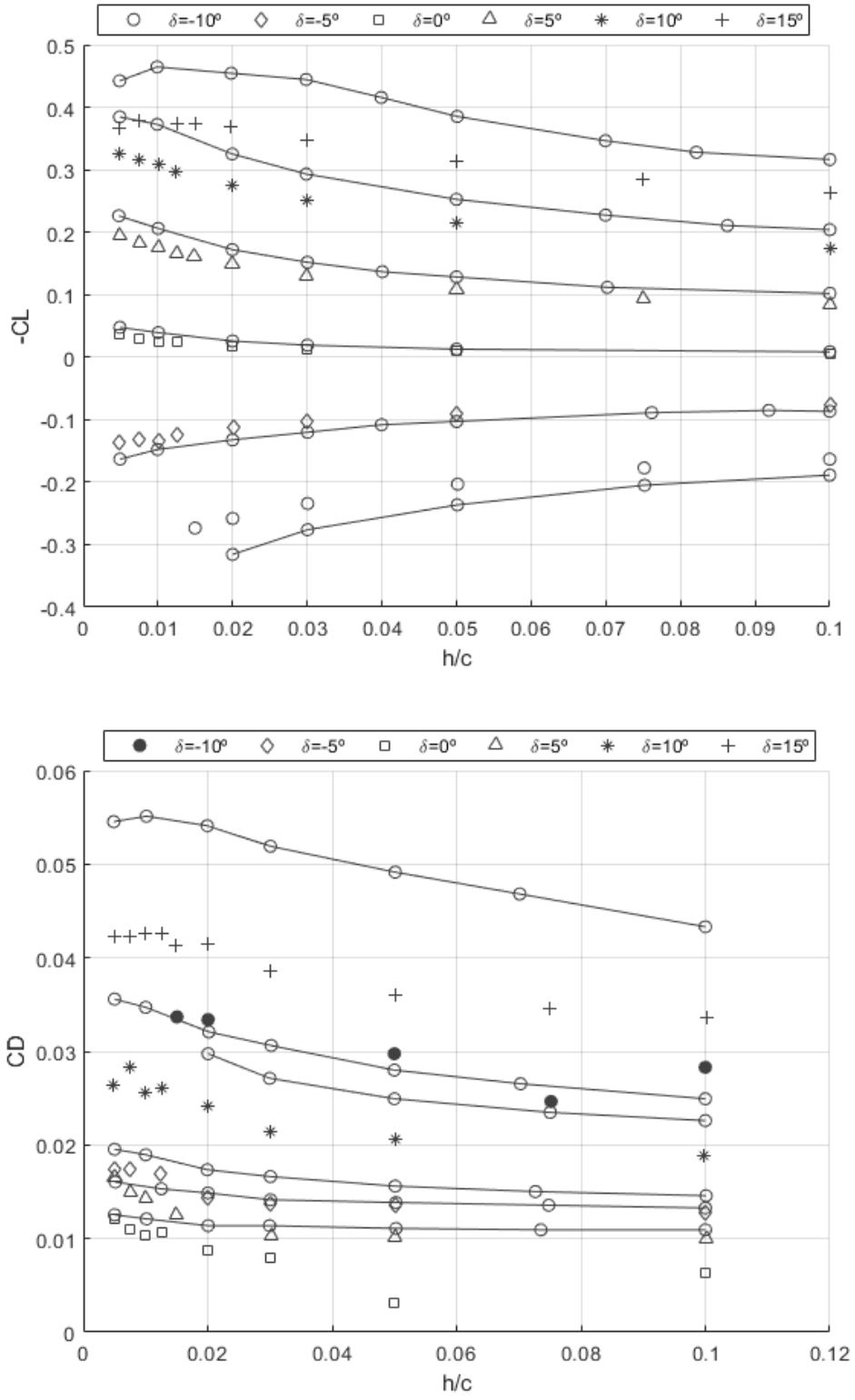

Figure 31: Downforce and drag coefficients for different flap deflections. CFD (line with markers) and Experimental (only markers) Reproduced from [6]

Effect of varying the distance (AR) between the VG´s

Vortex generator spacing was assessed for different angles of diffuser as the ground clearance was varied and the turning vanes were configured at β=20º, respect to the centre line of the plate. Figure 32 presents a general increase of aerodynamic efficiency as the flap augmented the inclination and the distance from the floor was reduced. A general downforce enhancement was seen as the spacing of the VGs increased and ground clearance was reduced. This effect was mainly attributed to the lack of vortex interaction that was observed when the spacing was increased. Furthermore, different vortex developments were noticed while the AR was varied. For AR=2, the vortex generated by the inner aerodynamic device disappeared fairly quickly and only the external vortex could develop to the trailing edge. While in the case of AR=4, both vortex configurations reached the trailing edge while being exposed to a vortex breakdown and it was concluded that they acted in favour of further downforce reduction.

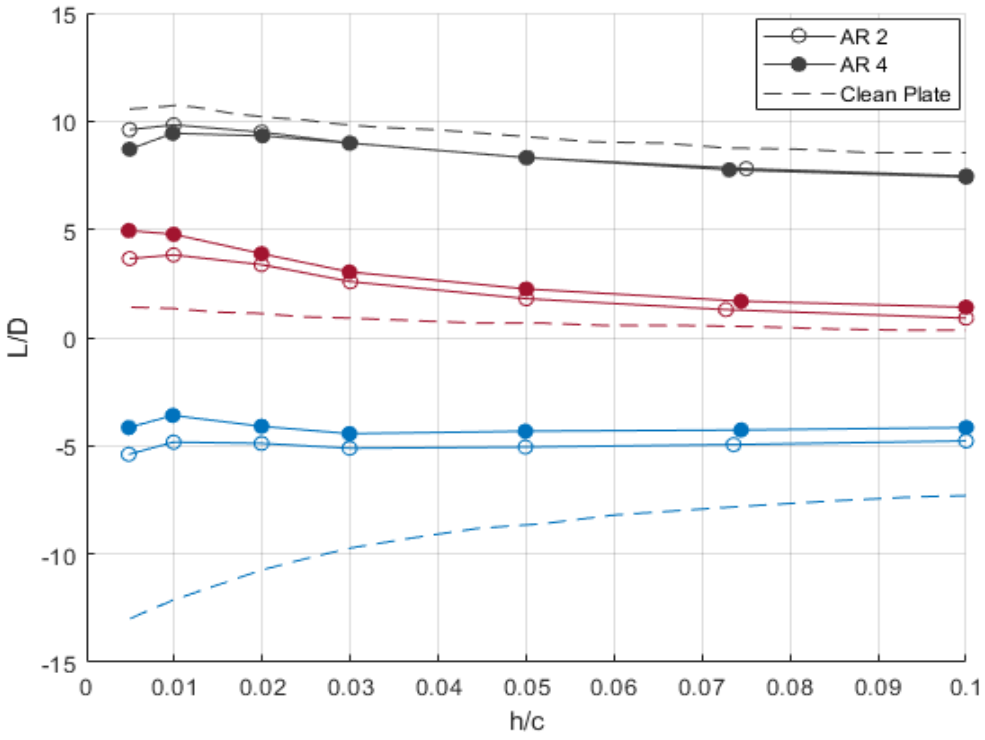

Figure 32: Comparison of the aerodynamic efficiency. δ=10º (black), δ=0º (red), δ=-5º (blue). AR=2. Reproduced from [6]

Effect of varying the angle of the VG (β) respect to the freestream flow

A comparison of downforce and drag coefficient data is reported in Figure 33, where the AR was configured at 2 and was tested for δ=-5º, δ=0º, δ=10º cases. Two different turning vane incidence angles were set up: β= 10º and β= 20º.

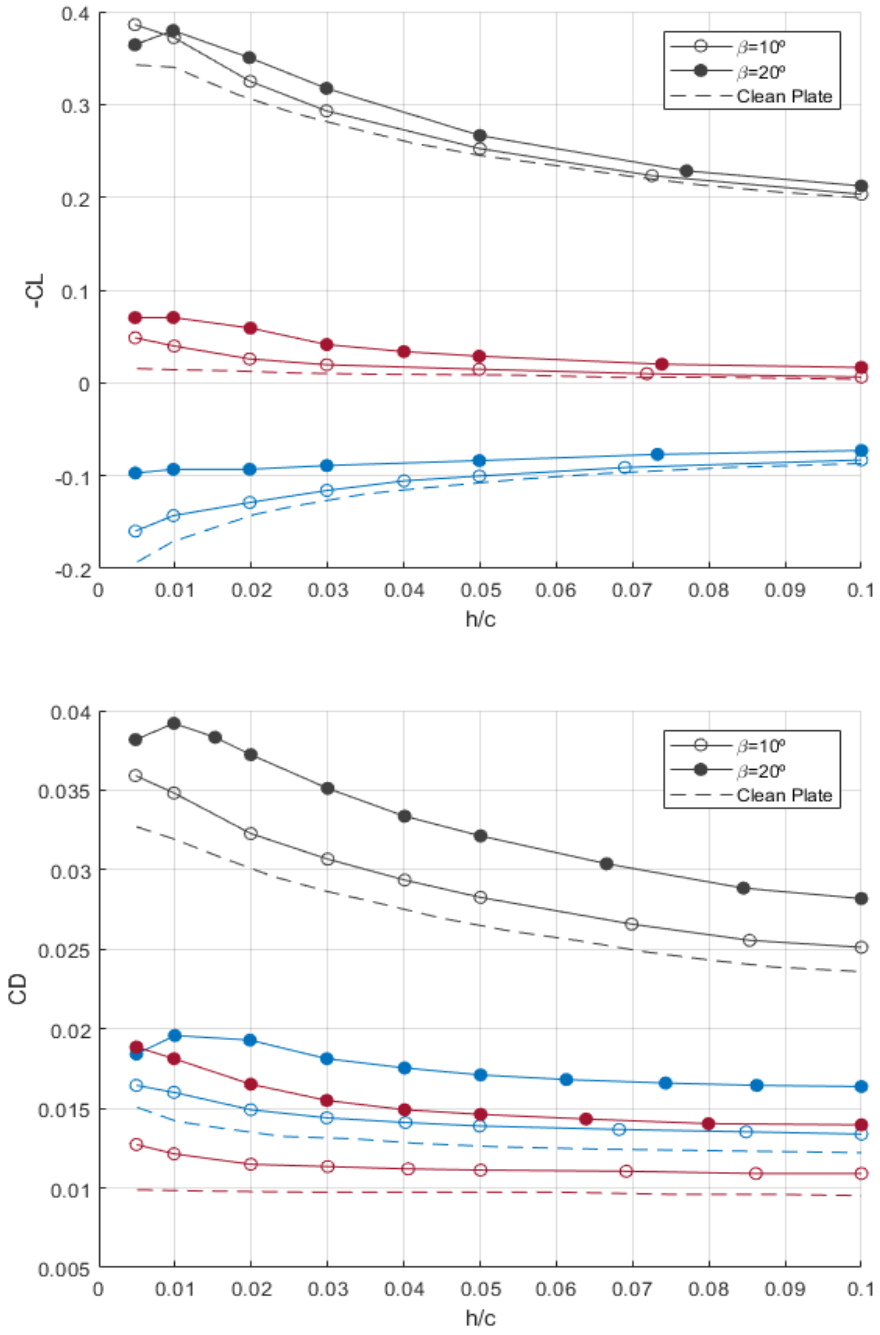

Figure 33: Comparison of C_L and C_D. δ=10º (black), δ=0º (red), δ=-5º (blue). AR=2. Reproduced from [6]

In the case plotted above (Figure 33), an increase in drag and lift forces was seen as the incidence angle of the guide vane system was raised. An important feature to note is the decrease in the downforce coefficient when the plate was configured at low ground clearances with high flap deflections, $\delta=10^{o}$. This situation was attributed to a vortex breakdown as the angle of the vane respect to the free flow increases. This situation was also observed by previous studies conducted by Holt et al. [32] and Garcia et al. [3]. This effect could not be extended to all cases. For the analysis of a positive diffuser value ($\delta=10^{o}$) combined with short distances to the ground, a slight loss of negative lift was stated. As previously discussed, this phenomenon was attached to the vortex breakdown generated beneath the lowermost part of the model. An evident conclusion that was surmised in this task was the strengthening of the vortex structure as the incidence was increased. At the same time, the vortex breakdown effect was affected, which suggested that the risk of vortex burst emergence increased with the angle of the VG.

The lower values of drag coefficient emerged at higher values of ground clearance. These results were also proved by Garcia et al. [3] and Holt et al. [32], which were surmised as a change in flow trajectory that reduces the induced drag.

3 EXPERIMENTAL TESTS

3.1 Proposal of the Wind Tunnel Model

As it was previously mentioned, one of the objectives of this project is to support the planning of an experimental test that could extend the experimental studies conducted by Holt et al. [32] and Arguelles [6]. Following this, Figure 34 shows the experimental model used in the tests by Arguelles, which is the modified model employed by Holt et al. Consists on a flat plate of 600mm width, 12 mm thick and 1000mm long, from which the last 200mm correspond to an adjustable flap device. These characteristic measurements will result in a planform plate area of 0.66m^2.

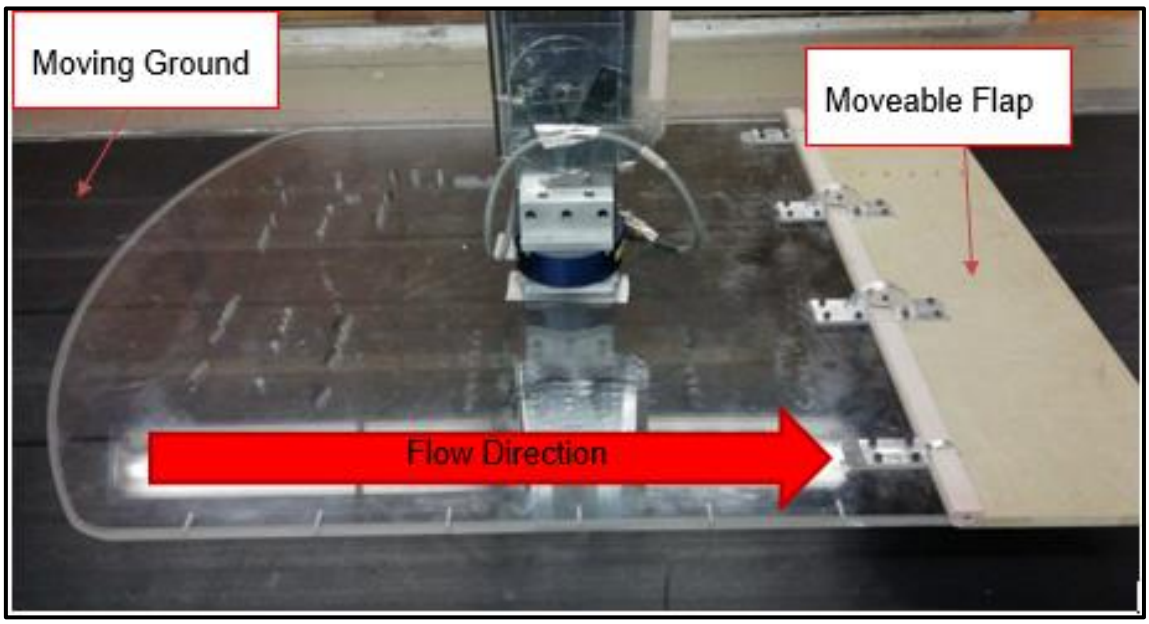

Figure 34: Wind Tunnel Experimental Setup

The adjustable flap can be positioned in a wide range of deflection angles varying between $-10^o \leq \delta \leq 20^o$, which will allow to alter the pressure distribution of the flow underneath the plate. It is interesting to note that the edges of the model have been rounded with an elliptical shape in order to maximise the quality of the measurements of the flow structure bellow the plate and decrease the likely appearance of edge vortices. The wind tunnel model was manufactured in Perspex Acrylic (transparent thermoplastic material) facilitating the visualisation of the flow beneath the plate in case of using any flow visualisation techniques.

Furthermore, several designs (Figure 35) of vortex generators were designed and manufactured in order to analyse the formation of different flow structures and vortex core strengths. As such, the VG´s are 150mm long and 25mm tall in the trailing edge with a thickness of 1.6mm, built in aluminium. It should be pointed out that due to manufacturing restrictions the leading edge of not rectangular VG´s was modified, in order to facilitate the installation of the pin attachment mechanism. Hence, this fact will be considered in the computational study.

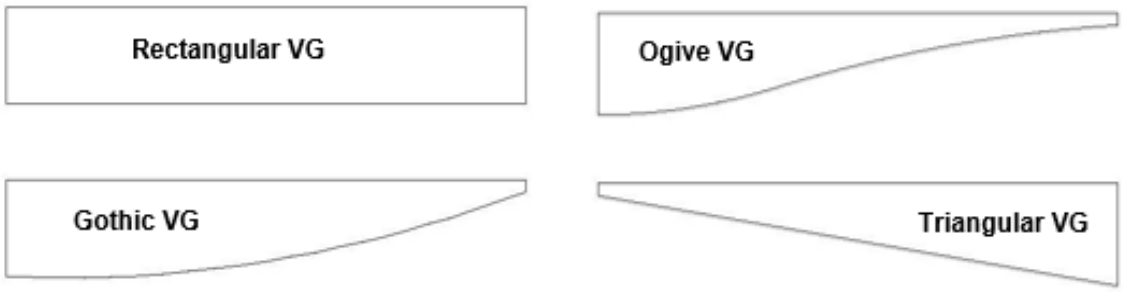

Figure 35: Vortex Generators Designs

During the experimental tests the vortex generators will be configured in different positions, in terms of spacing distance between them (AR), and the incidence angle of the VG´s will be varied respect to the freestream flow direction (β), Figure 36.

3.2 Cranfield´s 8'x6' Automotive Wind Tunnel

Cranfield University has a Low Speed Wind Tunnel that allows a continuous airflow in a clockwise direction inside a closed return design. The working section of 2.4m x 1.8m allows performing automotive, sub-scale full aircraft performance and development tests. A 5-blade fan that allows a wind speed in a range between 5m/s and 50m/s powers the wind tunnel with a very low turbulence intensity level, less than 0.1%. In order to replicate real road conditions the wind tunnel has a moving ground system that can be powered up to 45m/s with a fixed test-model attached to an internal structure. All aerodynamic loads and moments can be gathered through a six-axis internal strain gauge balance that is directly attached to the body of interest. Cranfield University´s wind tunnel is a closed section that is equipped with an automated system, which allows automatic

changes of ride heights and pitch conditions. In addition, it is equipped with glass windows that guarantee visual monitoring of the tests from the control room.

3.3 Experimental Tests Programme

To correlate all the computational simulations some experimental flat plate configurations need to be tested. All tests will be transition free and under controlled ambient conditions of temperature and pressure. Test programme, as the computational study, has to be divided into two parts: the effect of different VG shapes and the effect of adding endplates, as side-skirts, to the flat plate.

The test speed would be set up to 35m/s establishing the same velocity for the moving rolling road system in order to avoid the formation of a boundary layer in the ground. This configuration will lead to a Reynolds number of:

$$Re = \frac{\rho\, v\, L}{\mu} = \frac{1.165\ kg\ m^{-3}\ 35\ ms^{-1}\ 1\ m}{1.86x10^{-5}\ kg\ m^{-1}\ s^{-1}} = 2.26x10^{-6}$$

In order to compare aerodynamic forces and pitching moments a wide range of tests would be run in which different variables has to be modified: lateral spacing (AR), incidence of the VG (β) and the angle of the flap (δ). All the data will be gathered using a LabView software that will allow generating an output post-processing file.

Firstly, the difference in performance of the different VG shapes will be tested in a zero pressure gradient condition, so the differences in the results can only be attributed to the vane designs. For that purpose, the flat plate with previously mentioned VG shapes will be mounted and for each configuration will be tested for a range of ride heights.

Table 1 resumes the experimental tests of the first set and Figure 36 defines the parameters.

	β	δ	AR	h/c
Rectangular				0.005
Triangular	20 deg	0 deg	2	0.01
Ogive				0.02, 0.03
Gothic				0.05, 0.1

Table 1: Wind tunnel experimental tests, part 1

For the second set of experiments, endplates and rectangular VG´s will be mounted on the flat plate. In this case, the spacing, the VG incidence and flap angle will be varied for a range of ride heights.

	β	δ	AR	h/c
		0 deg		0.005
Rectangular VG´s with endplates	10 deg	10 deg	2	0.01
	20 deg	15 deg	4	0.02
				0.1

Table 2: Wind tunnel experimental tests, part 2

The selection of this configurations lies in the thesis conducted by Arguelles [6], with which later results will be compared. Finally, certain configurations must be repeated several times in order to perform a complete uncertainty analysis and obtain the base error level.

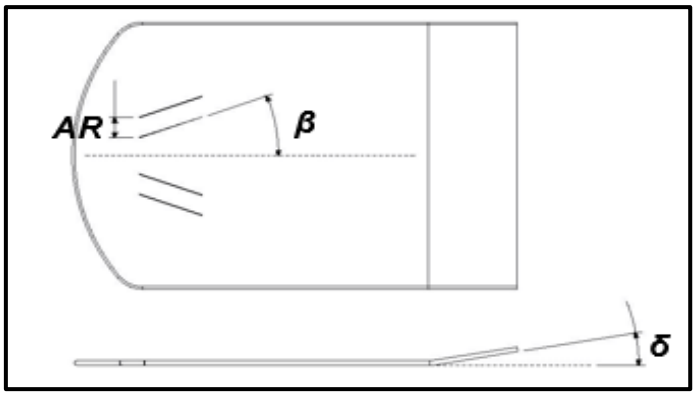

Figure 36: Definition of the parameters on the flat plate

4 COMPUTATIONAL SIMULATION STUDY (CFD)

The present MSc Thesis consists of a fully computational analysis report. Therefore, the main objective was focused on obtaining the most accurate and reliable results so it can be compared with experimental data in future works. In addition to the study of the performance of the model, in terms of downforce and drag, the streamwise vorticity and flow structure downstream of the vortex generating devices will be characterised. For that purpose, experimental data gathered by Arguelles will be used to validate the computational model and afterwards will be used in order to investigate the flat plate configurations and VG shapes designed. It is worth noting that these CFD simulations will not validate the obtained results until experimental tests are performed in order to execute a proper correlation of the data.

In the present report, steady-state pressure based flow simulations will be conducted using *ANSYS Fluent 18.2* software and *ICEM CFD 18.2* as a meshing software, based on a previous thesis carried out by Arguelles [6].

4.1 Computational CAD model

Starting from the computer aided design drawings presented in the thesis conducted by Arguelles [6] the geometry of the flat plate was built in *Catia V5 Student Edition* software. In addition to this, in order to achieve one of the objectives of this thesis, the design of rectangular vertical fences was drawn, which have been located on each of the sides of the model to evaluate the differences on performance of mounting them. Different shapes of vortex generating vanes (Figure 35) were modelled based on a previous research published by Katz and Morey [19], considering previously explained manufacturing restrictions in the leading edge of all the VG´s. Overall, the model can be divided in three main parts: flat plate with a movable flap, endplates and vortex generators.

For the sake of simplicity, as can be seen in Figure 37 and Figure 38, the six-axis strain gauge balance was omitted as well as the attachment mechanism designed for the experimental model that assembles the flap with the plate, Figure 34.

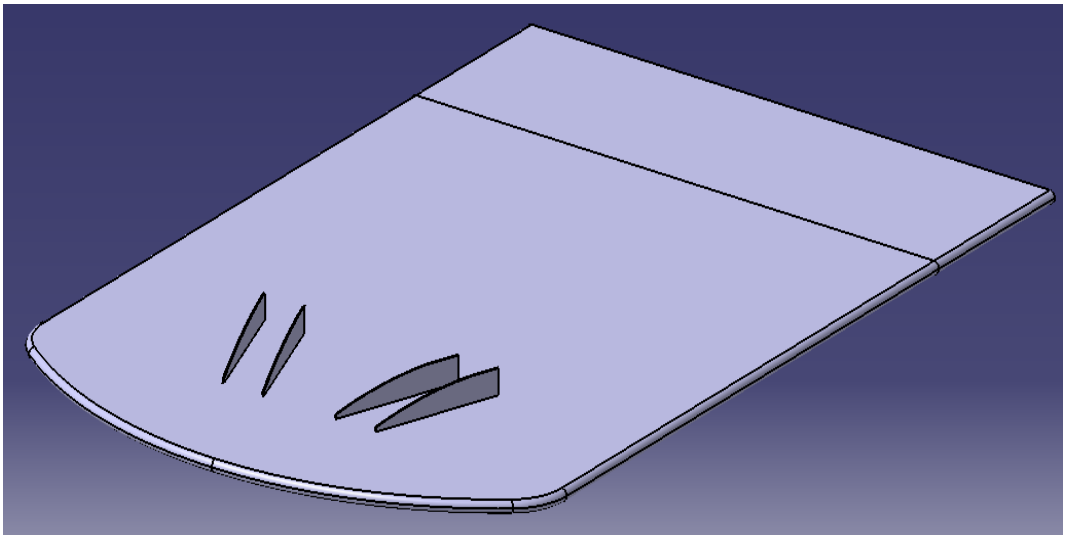

Figure 37: Computational Model for part 1 of the research (Lower surface)

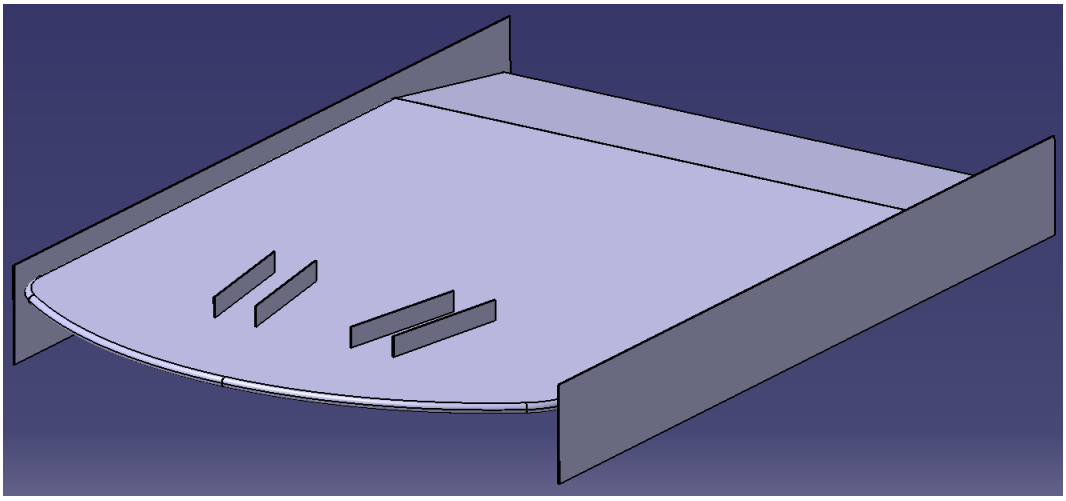

Figure 38: Computational Model for part 2 of the research (Lower surface)

Although these simplifications made on the model might slightly affect the results of the experiments, it has been considered negligible, as those elements were located on the upper surface of the plate, whereas the principal interest of study lies on the flow patterns underneath the flat plate.

Another geometric characteristic avoided was the pressure tab holes that already exist on the manufactured wind tunnel model. Although they could create some suction or blowing effects in the vicinity of the hole, once again this effect has been considered minor and therefore, neglected. The same reason has been

adopted regarding the porosity of the plate material, considering a perfectly polished surface in the whole body.

All the drawings handed in for the manufacturing of the elements have been extracted from the designs used in the CFD simulations, in order to reproduce the same conditions and accurately replicate the experimental data.

4.2 Numerical Methods

In the present thesis, Reynolds-Averaged Navier-Stokes (RANS) turbulence modelling was decided to use. It is an option widely chosen by many investigations [5], [6], [33] of this level and it is extensively demonstrated of delivering accurate results, being “low” in terms of computational cost. This thesis is based on the work carried out by Arguelles [6] and therefore, the same mesh parameters will be used. In order to evaluate the research K-ω SST turbulence model was selected. The advantage of employing large scale VG´s allows generating a less sensitive mesh to the y+ value. Therefore, in this case, the turbulence model chosen has a larger range of y+ values, in which a y+>30 has been ensured in the entire surface of the plate, being unnecessary to apply a y+ of 1 in which the number of cells would have been increased.

4.3 Computational Domain and Mesh Definition

The study completed by Arguelles assumed symmetrical flow conditions for which half of the model and domain were generated. However, in the present thesis has been chosen to simulate the full domain. The main reason for that was because the first steps of this work were carried out together with Cantore [34], since we need to study the same model but with different arrays and forms of vortex generators. Common baseline mesh parameters and flat plate configuration were selected in order to validate the computational simulation, comparing the results with the experimental data provided by Arguelles [6]. Cantore [34] explored lateral forces and flow patterns using axisymmetric vortex generator arrays in the under-body of a flat plate. This fact implied the need to define a complete domain as different yaw conditions were simulated, obtaining non-symmetric flow behaviours.

In the vast majority of automotive and aerospace applications, the wake generated behind the body of study is of a great importance, being essential to create a large longitudinal domain after the model. In this case is not less and to achieve this goal, a cuboid shaped 4m x 2m x 10m fluid domain was generated. The flat plate model was placed 2m behind the domain entry plane (inlet) in order to elude any type of interferences and obtain reliable results in the wake section.

Figure 39: Planform view of the fluid domain structure

Figure 39 shows the fluid domain generated to carry out the simulations, which was divided into different boundaries: inlet, ground, farfield and outlet. With the aim of simplifying the execution of the simulations, thus saving computational cost, several assumptions were defined in the domain boundaries. Firstly, farfield boundary condition was considered too far from the model, so the formation of a boundary layer was omitted by defining as slip condition. Secondly, the ground plane was completely contemplated as a moving ground instead of creating the same rolling road dimensions as the wind tunnel.

Regarding the mesh generation, it should be noted that there was a slight difference compared to Arguelles, in terms of the software used to carry out. While Arguelles used the tool *Mesh Modeller*, included in *ANSYS*, the software employed for this work was *ICEM CFD*. However, as the mesh is the same all the parameters provided by Arguelles were translated from one software to the other in order to achieve the same characteristics. Figure 40 shows the comparison, in

terms of negative lift coefficient, between both computational simulations for the plate configured at β=20deg, AR=2 and δ=0deg.

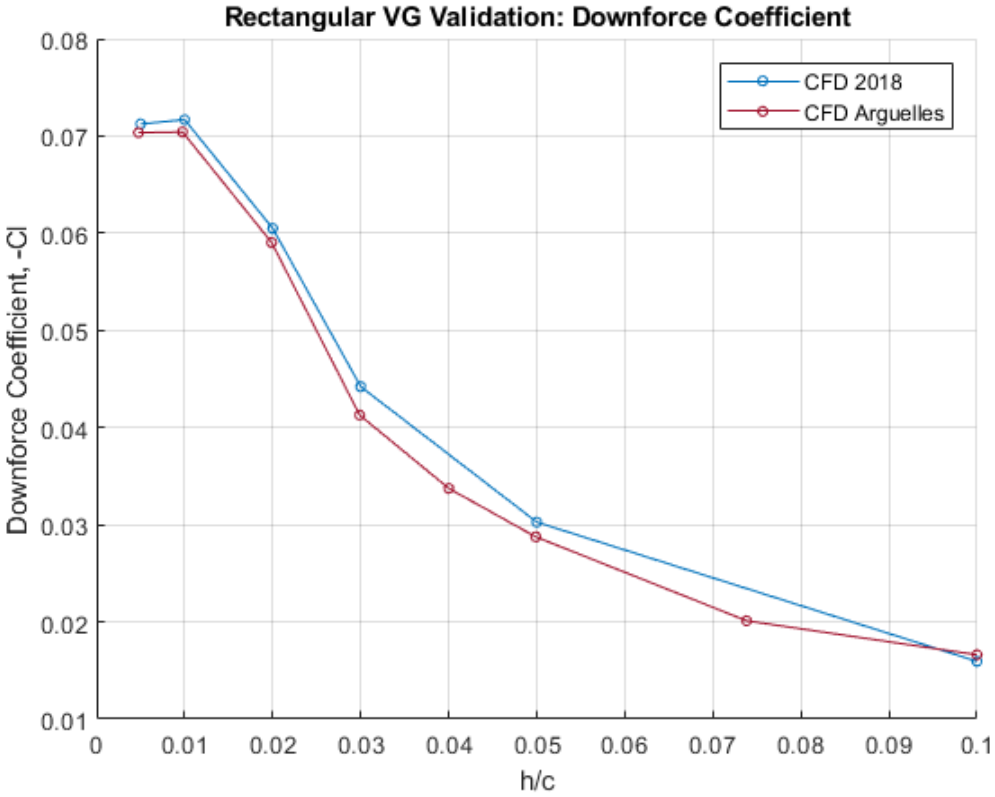

Figure 40: CFD comparison between Arguelles [6] **and actual model**

It can be observed in the previous picture a slight difference in the prediction of the downforce coefficient that can be attributed to the use of different software to generate the mesh. Later, these results will be analysed more thoroughly.

As can be seen in Figure 41 and Figure 42 an unstructured tetrahedral mesh was setup. This configuration saved mesh setup time, reduced computational expenses and allowed an efficient cell distributions avoiding unnecessary oversaturation of cells in places they were not essential [35].

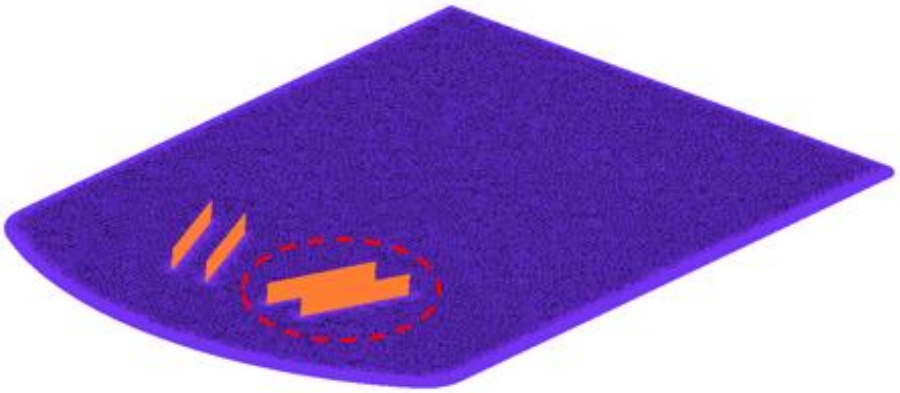

Figure 41: Unstructured Tetrahedral Mesh (Surface Mesh)

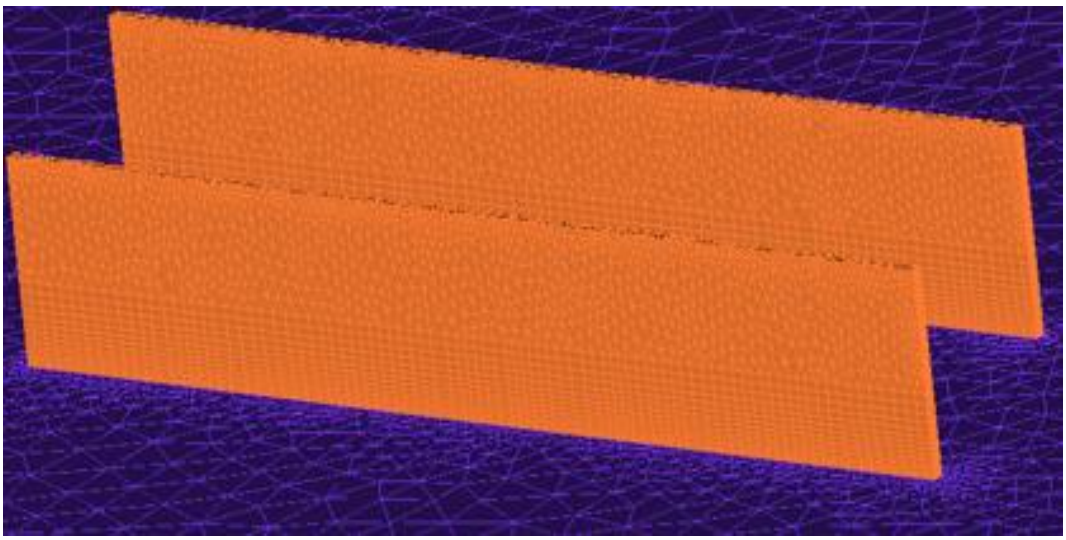

Figure 42: Detail of the tetrahedral mesh near the VG´s

One of the main issues of using discrete equations to define the flow to generate a numerical scheme is the numerical diffusion. A tetrahedral grid has the disadvantage of having misalignment problems between the flow and the cells. This factor increases the numerical diffusion on the mesh. For the purpose of reducing diffusion, density boxes in the most important parts of the domain were created. In this case, the flows around the plate itself and, more specifically, underneath the model were considered. The density boxes allowed to create a more refined mesh obtaining a better alignment of the flow with the cells and therefore, reducing the numerical diffusion. Table 3 shows the properties of density boxes that were created, which were equally defined to the “bodies of influence” defined by Arguelles [6]. It should be noted that the size is a non-

dimensional value that depend on the *Global Scale Factor* selected for the generation of the mesh and defines locally the biggest element size [35].

BOX	1	2	3	4	5	6
Size	0.08	0.05	0.08	0.05	0.08	0.1

Table 3: Density box size information

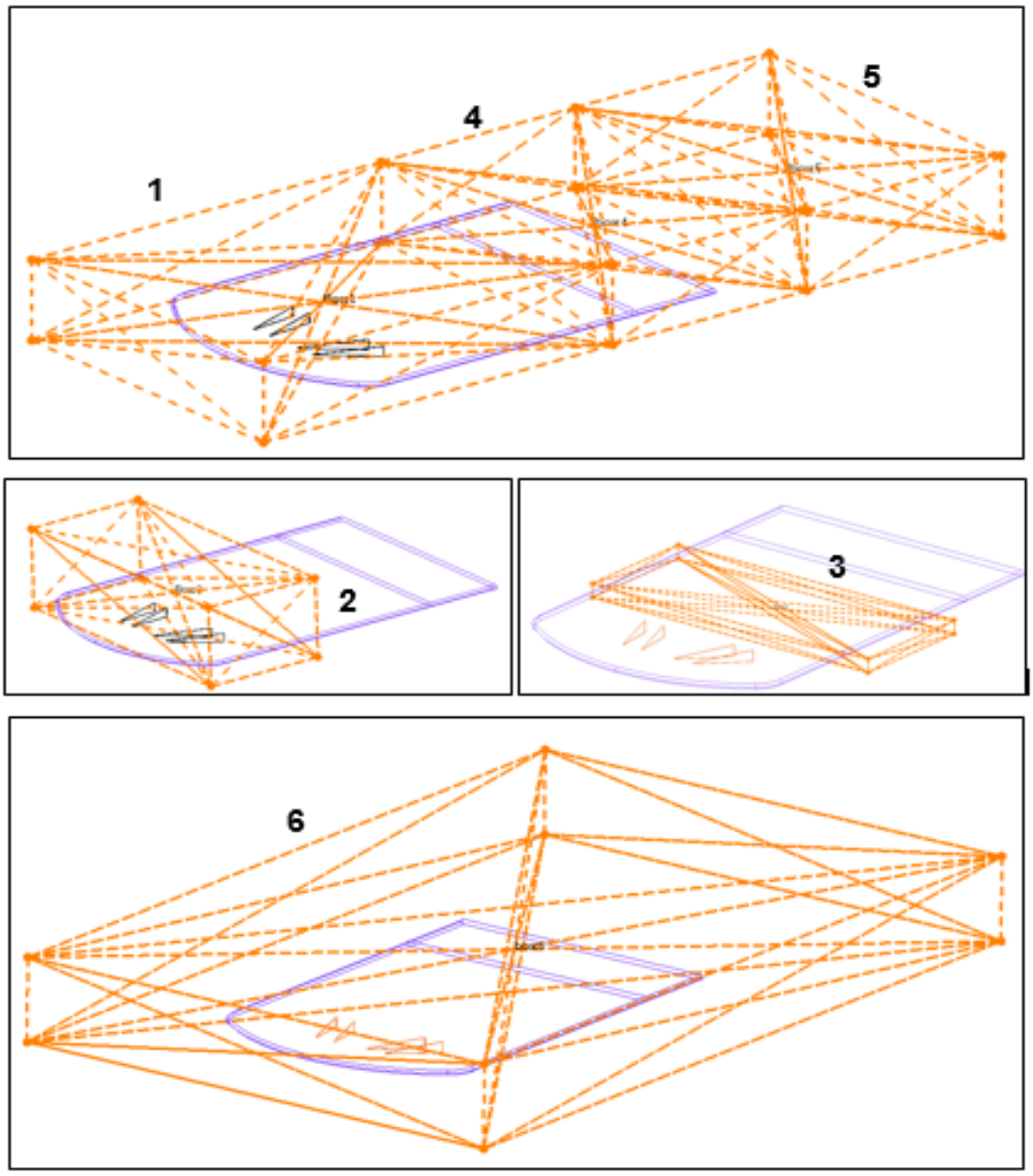

Figure 43: Mesh Refinement Density Boxes

As noted above, the flow around the flat plate is of great importance and the characterisation of the boundary layer must be properly defined. It is quite interesting to note the geometrical characteristics of the VG´s, since the height of these is greater than the boundary layer thickness, which allows defining a y+ value different from one. A y+=1 implies the definition of high aspect ratio cells in the nearby of the plate surface, becoming a problem for a tetrahedral mesh. High aspect ratios in tetrahedral meshes will affect the convergence of the study, delivering less accurate results and lower quality meshes [35]. Thereby, in order to avoid the definition of the first cell in the transition layer (buffer) a y+ value of 30 was selected. Prismatic elements divided in 15 layers with a growth ratio of 1.1 were defined by creating a first prism layer height of 0.325mm, data extracted from [6].

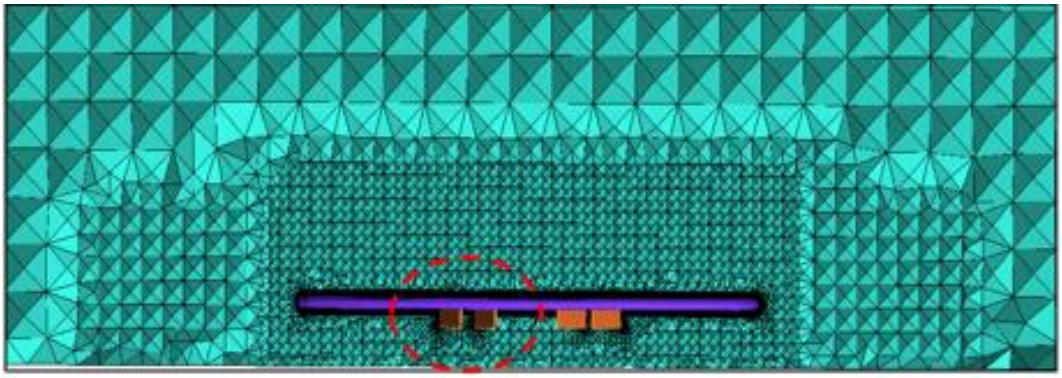

Figure 44: Front View of the mesh at x/c=0.3 (Volume Mesh)

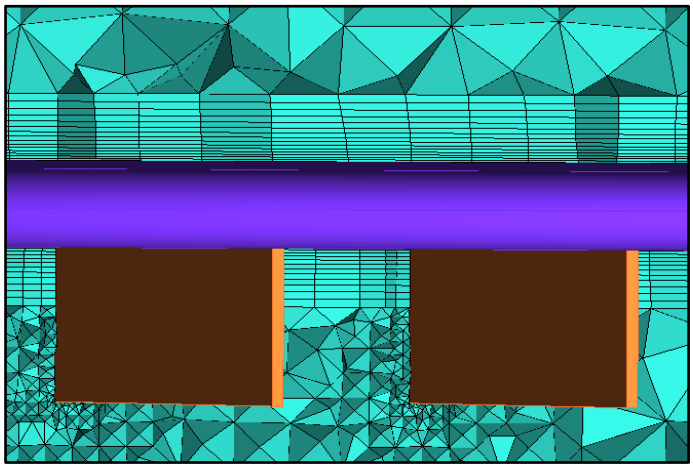

Figure 45: Detail of the Prism Layers around the Plate and VG´s

4.4 Baseline ANSYS Fluent Setup

A pressure-based steady state flow simulation with K-ω SST turbulence model was configured.

Taking into account that the main field of application is found in racing cars under atmospheric conditions at sea level, the fluid definition was considered as an incompressible airflow with a constant density of 1.17kg/m^3 and a viscosity of 1.86x10^{-5} kg m^{-1} s^{-1}. The operating conditions were left as the predetermined values specified by the software, which are a pressure of 101325Pa and a temperature of 300K.

Regarding the boundary conditions, a 35 m/s air speed was set up as velocity inlet matching the velocity of the ground. This last condition was intentionally defined in order to avoid the formation of the boundary layer in the moving wall, applying at the same time *no shear stress* condition.

All the simulations were initialised using *Hybrid Initialisation* option and solution methods were defined as follows: SIMPLE pressure-velocity coupling numerical scheme with a 2^{nd} order spatial discretisation method, which allows to reduce the numerical diffusion previously explained [35]. No convergence criterion was defined and the default values of relaxation factors were left, as the solution smoothly converged before 2000 iterations.

Each simulation was run locally on the university computers for 100 iterations before uploading them into the *Crescent* High Performance Computer (HPC), more details in the *Appendix A: Crescent HPC.*

4.5 Results

Earlier studies performed on aerodynamic devices, used to control the flow, were mainly focused on a flat plate with rectangular vortex generators. To further extend this field, the first set of experiments will evaluate the influence on the flow structure and aerodynamic performance of the different forms of VG´s designed and, secondly, the aerodynamic performance of adding some vertical bits on the sides of the plate will be analysed.

4.5.1 CFD Model Validation

As noted earlier, this thesis report will only be focused on the CFD simulations carried out over the flat plate model. However, in order to perform an adequate analysis of the data and be able to surmise and conclude with respect to them, an experimental correlation is essential to support the results obtained through the computational simulations. For that purpose, a wind tunnel experimental configuration carried out by Arguelles [6] was selected, which was in greater agreement and that would be used for comparison with the current research.

The configuration analysed was the flat plate at zero pressure gradient with the following turning vane setup: rectangular VG, β=20 deg, AR=2 and δ=0 deg. Figure 46 and Figure 47 shows, in terms of aerodynamic coefficients, a direct comparison between the experimental data and CFD data.

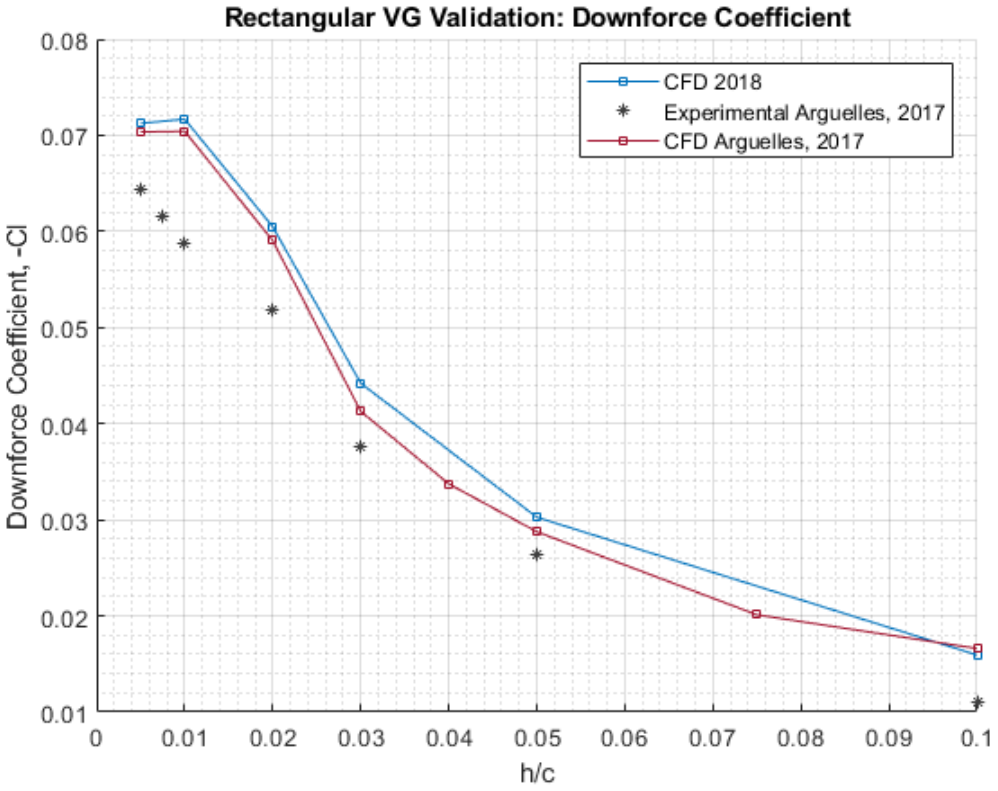

Figure 46: C_L Correlation between wind tunnel and CFD data

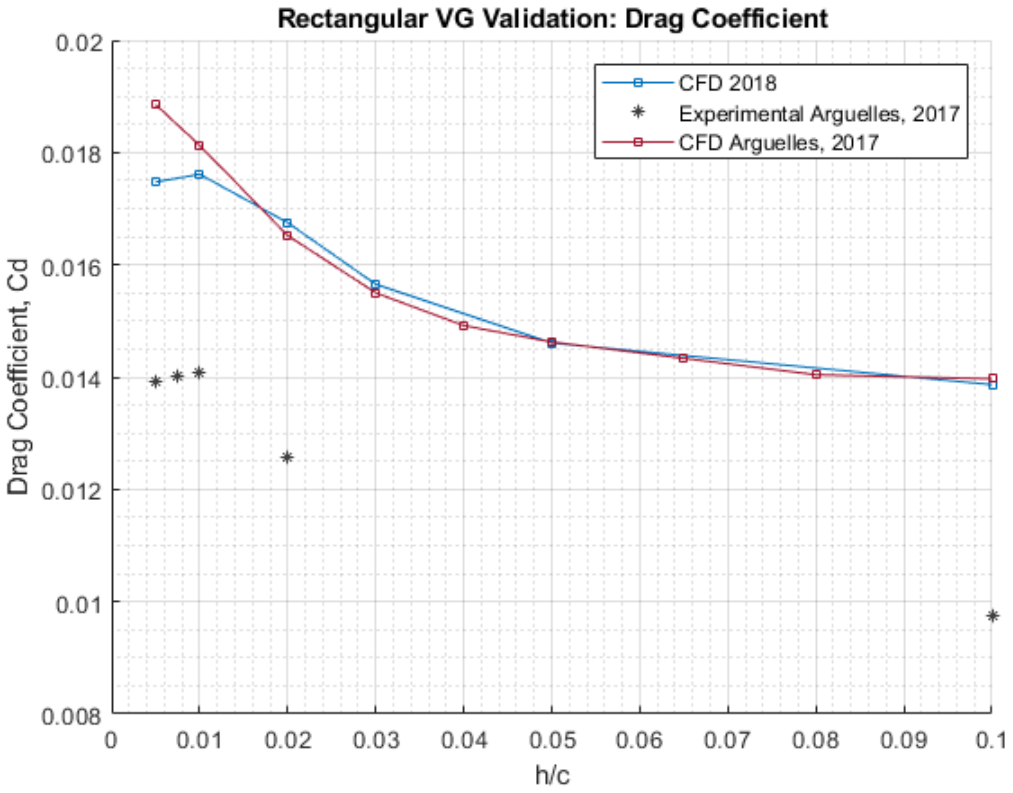

Figure 47: C_D Correlation between wind tunnel and CFD data

The fact of using a different software to generate the mesh with respect to Arguelles [6], despite defining the same mesh parameters, was of utmost importance to make a comparison of the results obtained and whether it was unfavourable, it should have been swapped to the mesh generator employed by the previous author. Both pictures depicted above, in terms of CFD results, present a good correlation that defined almost the same trend. In Figure 46 the maximum percentage difference in negative lift coefficient (for CFD data only) between two measured points was 4.8% and was produced at h/c= 0.03. However, in Figure 47, C_D data at high ride heights is in excellent agreement, while, as the model gets closer to the ground plane it begins to highlight a significant difference in the prediction of the drag coefficient. Data from the present study seem to be more accurately predicted than Arguelles [6] data and replicates better the behaviour at low ground clearances. The maximum disagreement was at h/c=0.005, in which the relative error gap was 8.6%.

Likewise, the sensitivity of conducting a complete CFD study should be highlighted, since a small change could mean a big difference in the results.

Regarding the study between “CFD 2018” and experimental content, the results presented indicate a good prediction of non-dimensional drag and downforce coefficients. However, it can be clearly observed an over-prediction in the magnitude of the computational data. Analysing the drag obtained for this configuration, despite the variation in the magnitudes, there was a good agreement in the tendency of the results. As the plate gets closer to zero ground clearance the drag increases until it reaches h/c=0.01, where a decrease in the value is noticed. As observed, this trend phenomenon was captured adequately by the numerical model obtaining a maximum over prediction of 24.1% along all the evaluated heights.

Additionally, Figure 46 shows a good agreement at high ride-heights of the negative lift coefficient where there are still no causes to attribute it to the ground effect. As the ground clearance was reduced, the largest differences between computational data and experimental data began to emerge. Eventually, the experimental data could not reproduce the stall condition that was generated computationally in the proximity of the ground. This fact could be attributed to the procedure of performing the experimental test. This process starts the measurements at the highest plate position and reduces the height until the lowest ground clearance is reached. Thereby, the vortex can be formed cleanly at ride-heights where there is no ground effect and when it gets to the lowest position, the vortex already generated, can affect the results gathered for the aerodynamic loads. It should be interesting to change the measurement technique and collect new wind tunnel data to compare with CFD and experimental data obtained previously. On the other hand, another factor that may affect the disagreement on the results could be the blockage effect caused by the structural system that holds the model in the wind tunnel. It may be responsible for disturbing the flow direction at the leading edge of the plate yielding a difference in the behaviour of the airflow underneath the plate at low ground clearances and varying the aerodynamic coefficients.

Finally, it is clear that more experimental tests should be carried out close to the ground in order to evaluate and state the discrepancies. However, in general terms, there were no large relative differences between the two CFD models and there was a good agreement in comparison with the previous experimental data. Therefore, the mesh generated with *ICEM CFD* was considered valid for the rest of the study.

4.5.2 Comparison between different Designs of Vortex Generators

In the present task, an in-depth analysis of several VG shapes was carried out. As explained above, four types of VG were studied: rectangular, ogive, gothic and triangular, see Figure 35. This section aims to investigate the best aerodynamic VG design considering different parameters that will be discussed in the following lines. In order to evaluate and compare exclusively the effects generated by the turning vanes a flap configuration of $\delta=0^{o}$ was selected. In this way, the flow will not be affected or disturbed by any change in the angle of the flap, in terms of pressure on the underside of the plate. The VG's were orientated $\beta=20^{o}$ with respect to the freestream flow direction with a distance of AR=2 between them.

The implementation of different VG shapes has a remarkable influence on the aerodynamic performance of the plate. Figure 47 shows the variation in the negative lift coefficient obtained for all the geometries tested. In general, the data presented so far indicate a continuous increase of downforce coefficient, which reaches the maximum value as the distance to the ground was reduced. However, for the rectangular VG configuration, when the plate was located at its minimum distance from the ground, there was a slight decrease in the lifting force. This situation was perfectly captured in the experimental tests performed by Katz et al. [19] and Byrne [5], for the same plate and VG configuration. This effect was attributed to a possible flow obstruction between the VG and the ground plane due to the small gap that exists and therefore, contributed to a vortex breakdown.

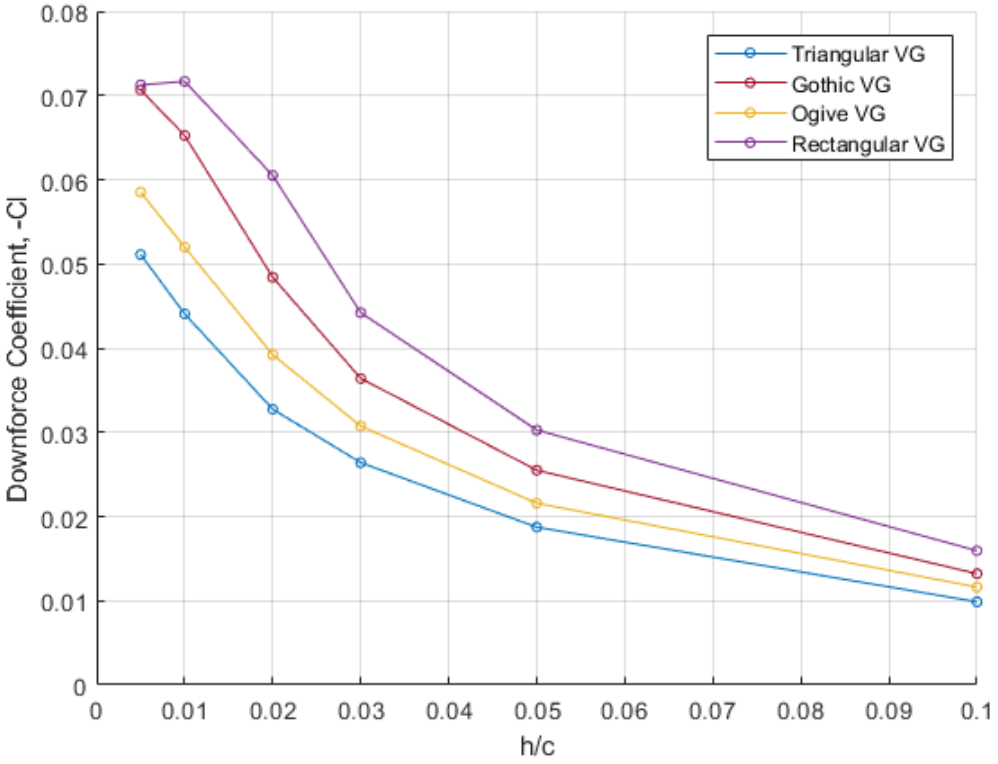

Figure 48: Comparison of Downforce Coefficients between four VG shapes.

Another important feature to note was the clear difference between the coefficient values obtained for different VG´s. The rectangular VG has twice the area of the triangular VG, so a higher downward force value of the rectangular VG was expected. In essence, the negative lift coefficient increased as the area of the turning vanes was larger and the individual comparison of the values presented a bigger gap as the distance to the ground was reduced. However, it is interesting to note an important characteristic for racecar applications. Triangular and ogive VG´s revealed that there are less likely to suffer a reduction in the generation of the lift coefficient in the vicinity of the ground plane. Unlikely, rectangular and gothic vanes do not suggest the same behaviour. These results are demonstrated in the previous figure, which indicates that the area of the VG is one of the most influential parameters for aerodynamic performance, also suggested by Katz et al. [19].

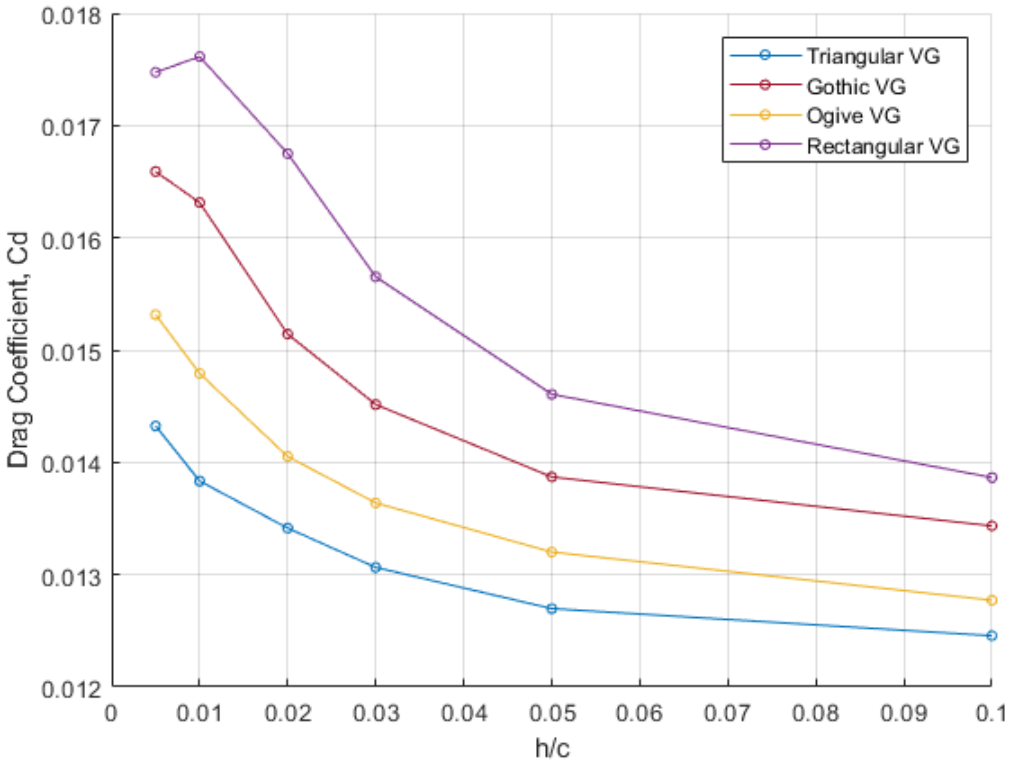

Figure 49: Comparison of Drag Coefficient between four VG shapes.

Figure 49 depicts a comparison of the drag coefficients against a range of ground clearances for the several VG shapes simulated. Similarly, as discussed for the aerodynamic load coefficient, drag coefficient also exhibits a progressive upward trend until it reaches the maximum value at a distance close to zero ground clearance. However, as previously seen, the rectangular VG reproduced the maximum drag force value in h/c=0.01, describing a slight subsequent drop. By contrast, the triangular VG proved to be the most efficient element in terms of air resistance. This situation suggested once more that the main parameter of concern is the area of the vane, in agreement with the experimental results gathered by Katz et al. [19].

Coming up next, a detailed comparison of the L/D relation to different riding-heights presented in Figure 50 described individually the overall aerodynamic performance of the vortex generating vanes. As demonstrated in previous results, it was expected that the triangular and ogive VG´s were aerodynamically less efficient, due to their ability of generating lower aerodynamic loads.

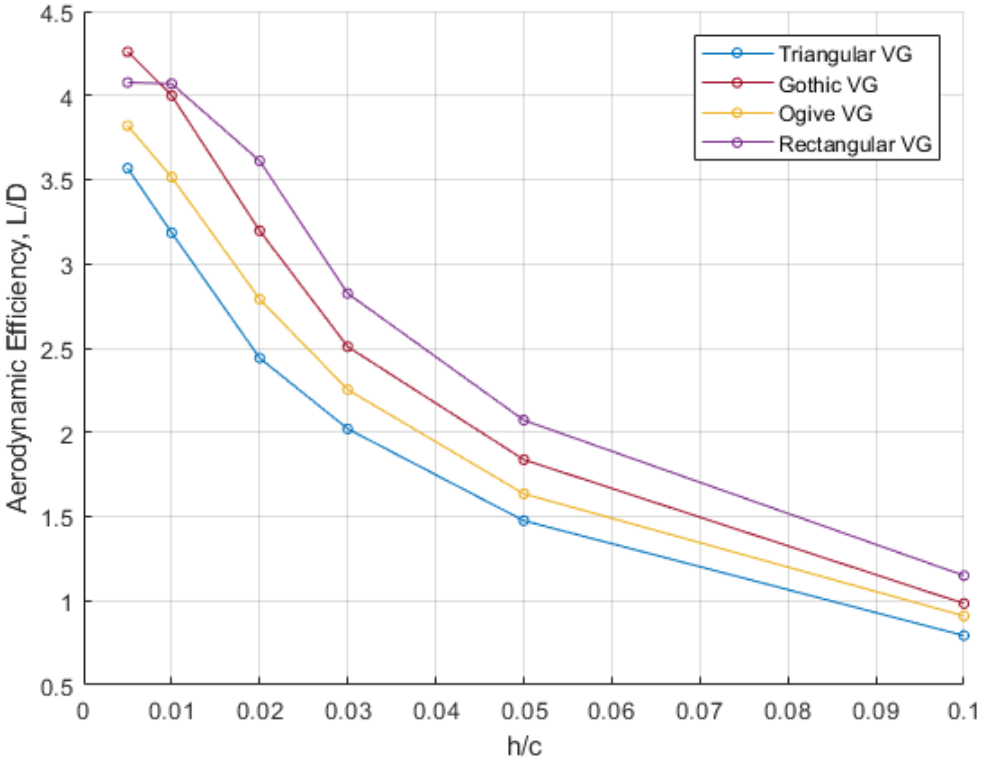

Figure 50: Aerodynamic Efficiency for VG geometries tested.

Overall, the trend shown by the L/D ratio is similar to that depicted for the downforce coefficient in Figure 48. Aerodynamic efficiency improved as the ground clearance was reduced and the area of the guide vane was increased. In this case, the gothic VG turned out to be the most efficient vane at very low ground distances, describing continuous improvements, since the rectangular VG was not able to delay the vortex burst yielding a performance deficit.

Summarising, for a flat plate simulated at a zero pressure gradient, the described VG side area can be highlighted as the main parameter of concern, significantly affecting the performance of the model. On the other hand, not only the area but also the vorticity generated is of great importance for a better understanding and management of flow control, which will be analysed bellow.

In order to evaluate the streamwise vortex development downstream of the aerodynamic guide vanes, the vorticity contours of all the cases tested at h/c=0.02 are depicted in Figure 51.

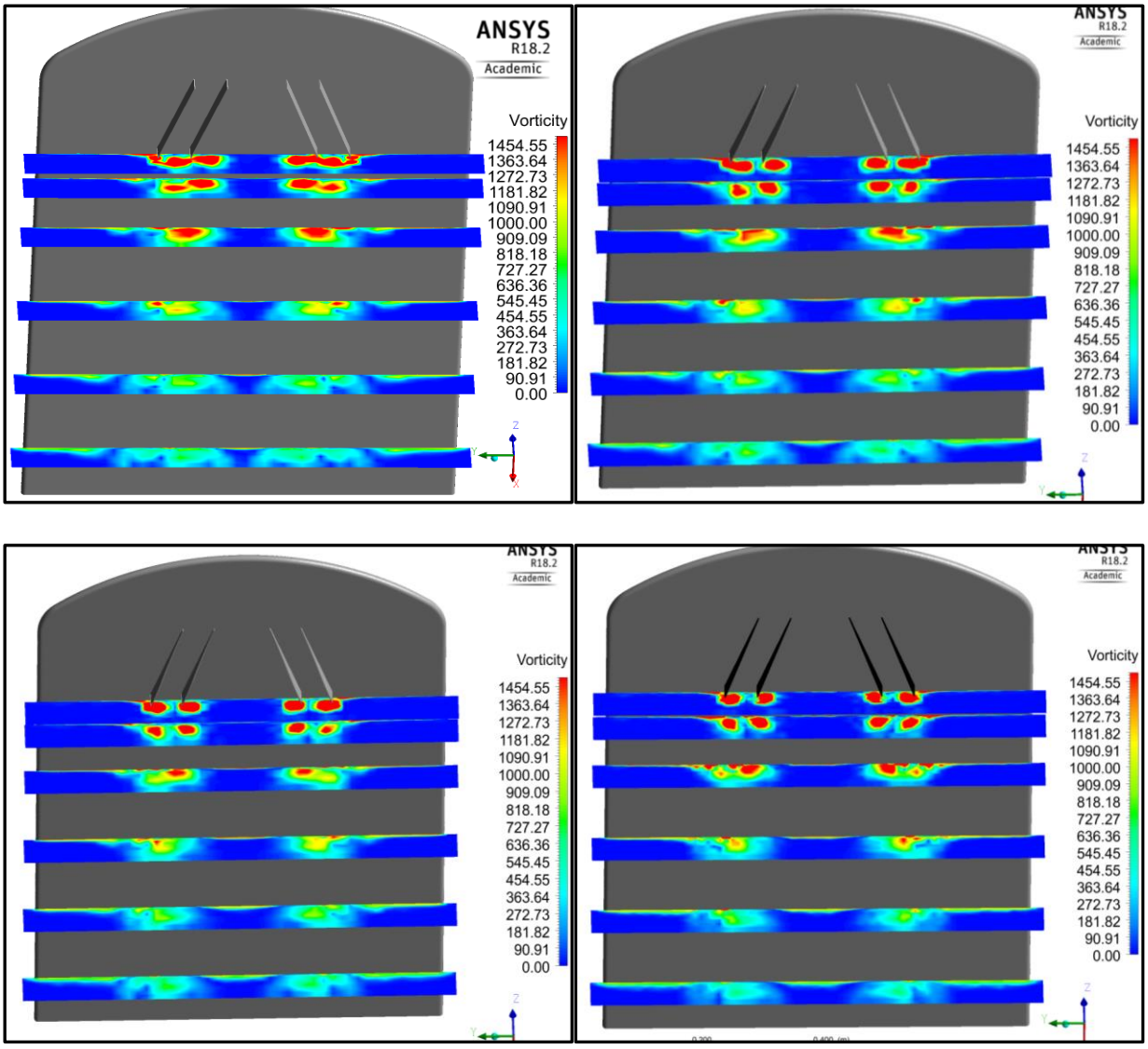

Figure 51: Vorticity contours at h/c=0.02. Rectangular and Gothic VG (Top, left to right). Ogive and Triangular VG (Bottom, left to right)

A similar behaviour can be clearly observed for each pair of vanes. In the early stages of development, there are two distinctive vortices emanating from each pair of generators, with a high core vorticity value that diminishes as the flow moves aft on the plate. Following this, each pair of vortices were merged before reaching half the distance of the plate (in longitudinal direction), describing a progressive and rapid diffusion of the vortices. This will create an aerodynamic "barrier" that increases the suction effect at the lower end of the plate and at the same time, the generation of aerodynamic loads will be enhanced.

To ascertain the diffusion of the vortices throughout the model, Figure 52 quantifies the maximum vorticity values obtained for several longitudinal stations along the plate. For that purpose, the vorticity value of the core was measured in different planes created downstream of the vortex generating vanes.

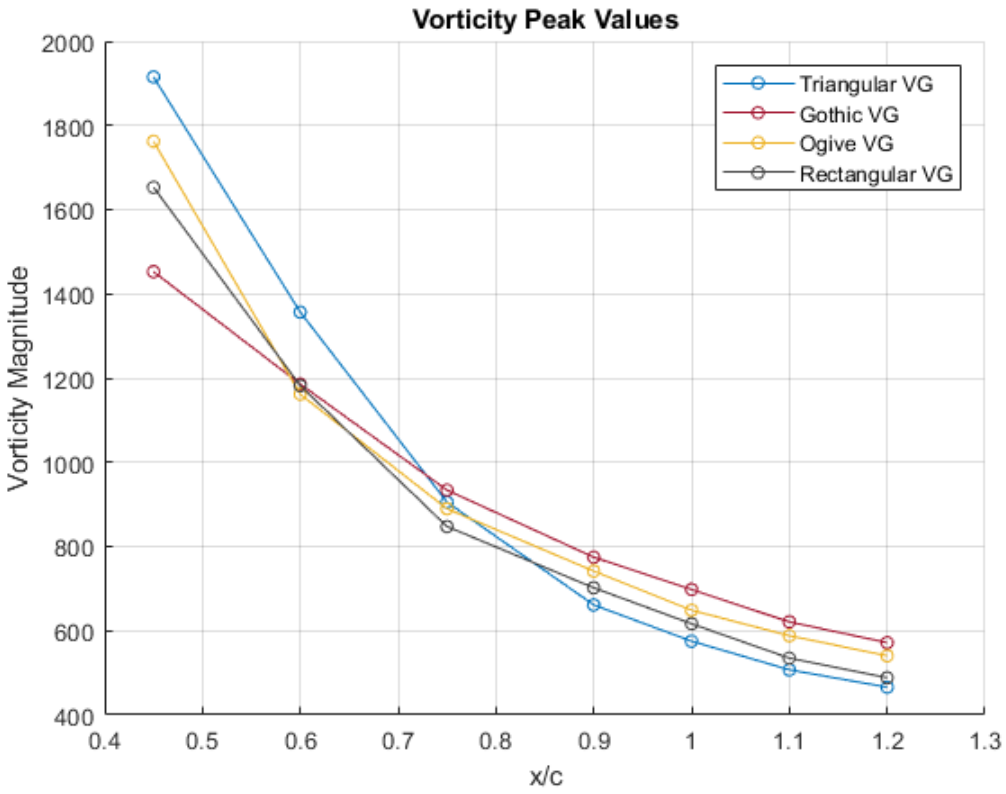

Figure 52: Peak Vorticity Values (at the core) of the four VG shapes.

Based on these data, the vortex strength conforms the diffusion of an "exponential style" curve with a linear attitude once the vortex surpasses the trailing edge of the model. In the case of the triangular VG, the decay of the vortex is the strongest one. It generates the strongest initial core region and then describes a continuous decrease of the vorticity value, suffering a reduction of the vorticity magnitude of approximately 76.3%. Ogive and rectangular VG´s described almost the same decreasing tendency, being the ogive VG more stable and strong than the rectangular vane. Regarding the gothic VG, it was found to yield the most stable vortex movement within the range of study. Despite the fact that the vortex was weakening throughout the plate, it was able to maintain the

highest core value from x/c=0.6 onwards, describing the smoothest reduction of vorticity, 58.6%.

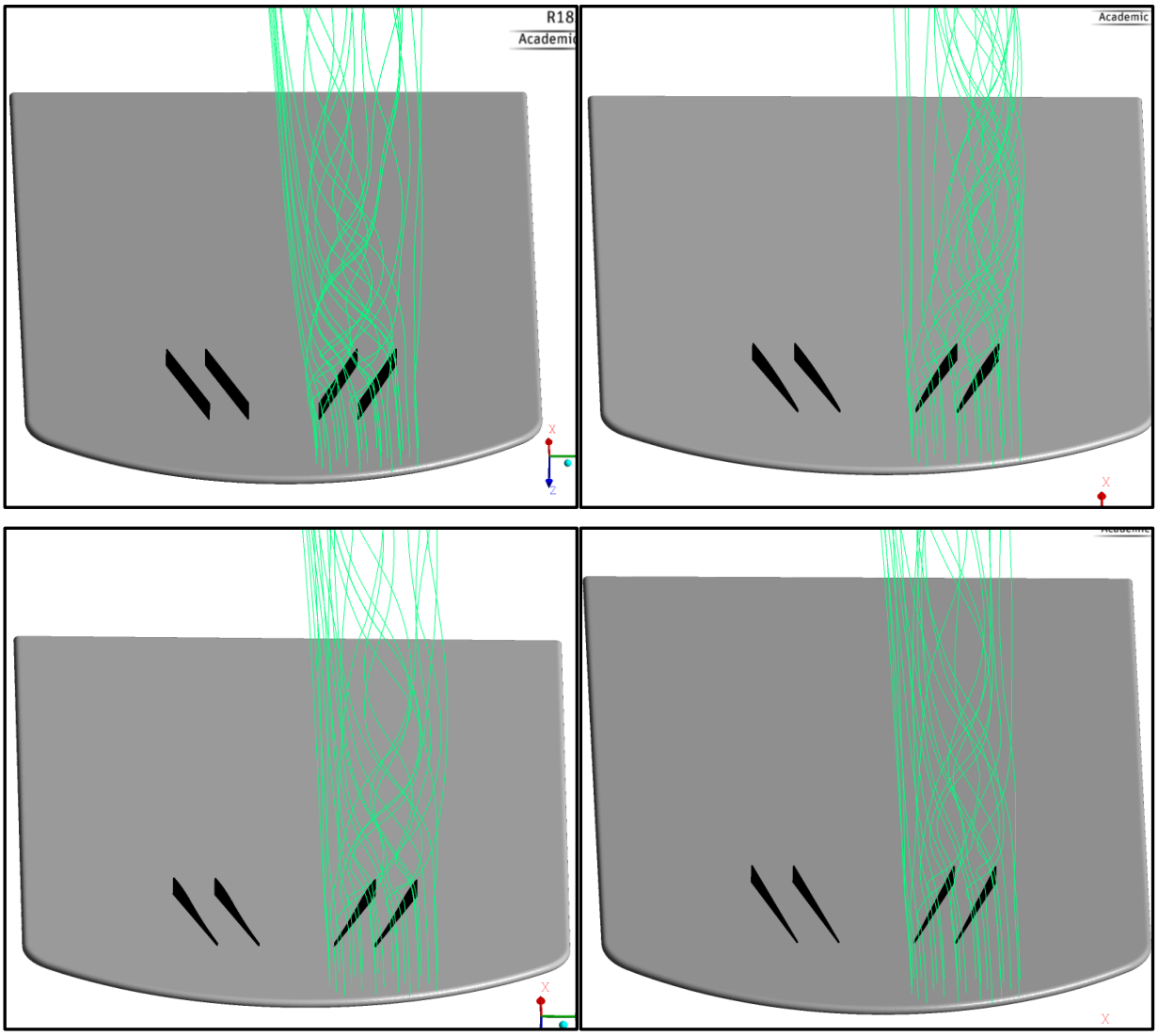

Figure 53: Sketch of the streamlines at h/c=0.02. . Rectangular and Gothic VG (Top, left to right). Ogive and Triangular VG (Bottom, left to right)

Figure 53 shows the streamlines generated for each VG configuration at a riding-height of h/c=0.02. The early fusion of both vortices and the subsequent diffusion of a single vortex can be clearly observed. Ogive and triangular VG´s described a very similar development of the vortex motion downstream the vanes. The strong internal vortex merged with the outer one forming a single vortex that flowed along the plate describing a curved path until at x/c=1.1 was established. It is worth noting that both devices have the same area but distributed differently.

However, rectangular and gothic VG´s describe a completely different trajectory. In order to support the vorticity contours and the streamlines, Figure 54 depicts the lateral trajectory described by the main vortices for a range of longitudinal stages on the plate.

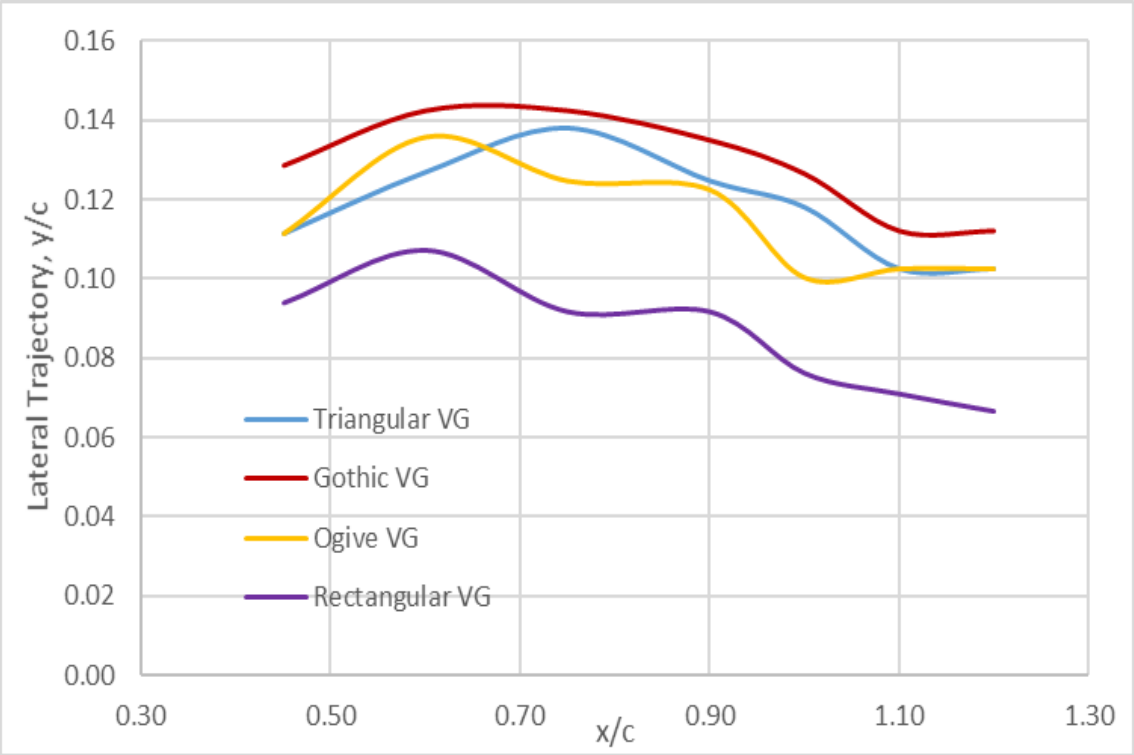

Figure 54: Lateral Trajectory of the vortex peak values at h/c=0.02.

Clearly, the biggest difference can be observed in the fusion and development starting point of the vortices. This, as previously explained, can be related to the vorticity magnitude generated initially by each of the VG´s. In the case of the rectangular VG, it was found the inner vortex to be dominant over the outer vortex, clearly defining an interior path compared to the rest of the turning vanes. The analysis carried out so far, indicated the same vortex behaviour once it was merged. First, it moved outward and approximately in x/c=0.6 the single vortex described a stepped inward trajectory. This effect was also assessed by Arguelles [6], and was attributed to the possible influence of the tip-vortex generated on the edges that forced it towards the inner part of the model.

Regarding gothic VG, the trajectory generated by this vane differs significantly from the others. Initially, there was an outwash of the inner vortex in order to merge with the external vortex. Since then, at x/c=0.6, a smooth transition was observed defining an inward flow trajectory. This behaviour can be attributed to an overall larger vorticity value as seen in Figure 52, so that the effect of tip-vortex is lower.

The distribution of the pressure coefficient through the flat plate model is 3D plotted in Figure 55, in order to assess the evolution of the vortex downstream the VG.

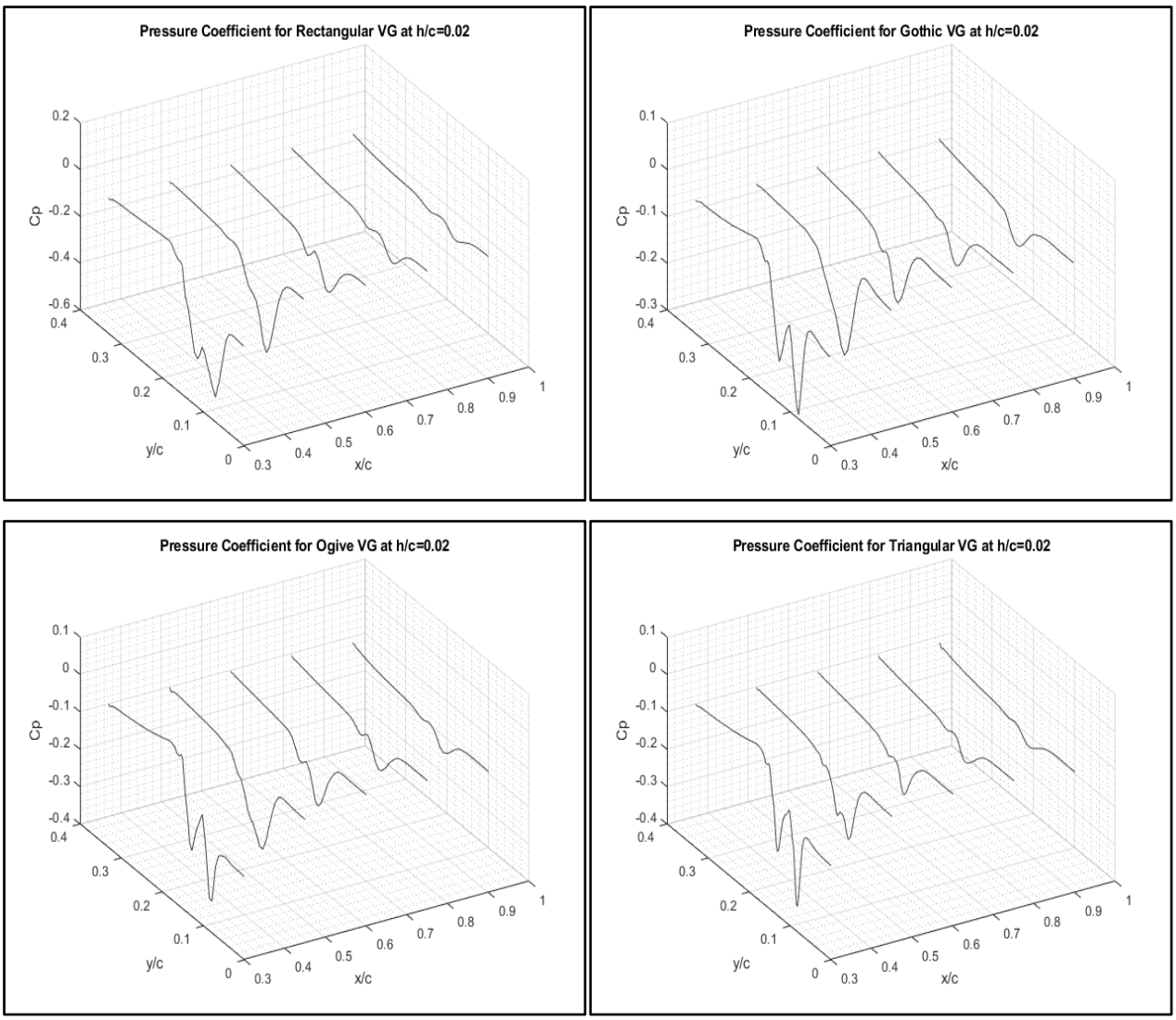

Figure 55: Pressure Coefficient distribution at h/c=0.02. Rectangular and Gothic VG (Top, left to right). Ogive and Triangular VG (Bottom, left to right)

In longitudinal direction (x/c), the zone from the trailing edge of the VG´s to the end of the edge of the flat plate is shown; while in transversal direction (y/c) only half of the model has been exposed, where y/c=0 is the value that defines the centreline of the model.

In general, Figure 55 depicts the decay of the vortex strength as the distance from the VG increases, which is damped from a considerable peak of Cp in a smooth pressure curve. Clearly, at distances very close to the vortex generators (x/c=0.3) two distinctive pressure distribution peaks can be observed, indicating that the vortices had not merged and still flowed separately. Adopting a similar approach, it was discovered that the internal vortex (measured with respect to the centre line) was the strongest and, therefore, the dominant, since it generated a higher initial suction peak. In addition, focusing on the triangular VG, it was found that the fastest vortex decay occurred in this particular element, which supports previous explanations made in the vorticity magnitudes.

Nevertheless, valuable information that can still be extracted from Figure 55 and in detail in Figure 56, is the fusion of the pair of vortices that emerge from the guide vane system. Figure 56 presents a detailed comparison of the pressure coefficient distribution in a plane created at x/c=0.45 and at the same ride-height previously adopted. It is worth mentioning that in this longitudinal location, a complete merge of the pair of vortices was performed, with the exception of the triangular VG case. As can be seen in Figure 56, the pressure coefficient curve of the triangular VG is still defined by two suction peaks, which demonstrates a delay of the vortex mix and could be highlighted as one of the reasons for producing lower aerodynamic drag. From this point, a single vortex was formed and diffused downstream.

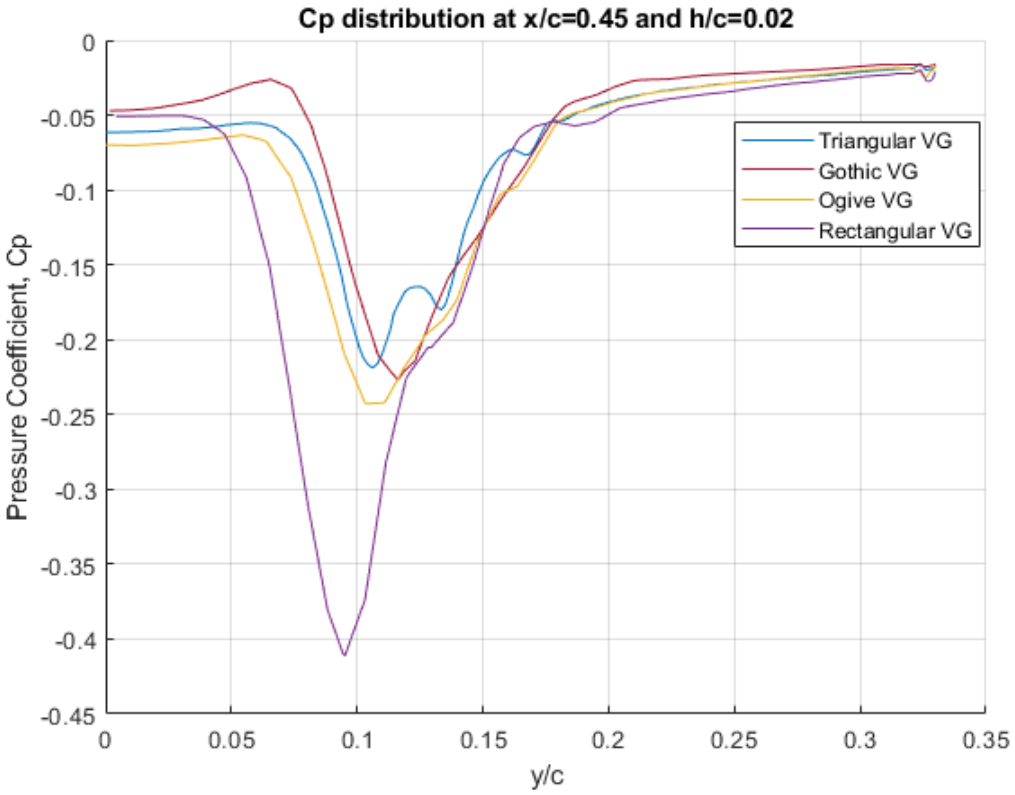

Figure 56: Cp distribution on the plate at x/c=0.45 and h/c=0.02.

The comparison of pressure coefficients in Figure 56 shows a large difference in the suction peak generated in this region. The rectangular VG almost produces twice the maximum value compared to the rest of the turning vanes. This fact can be attributed to the area of the vortex generator, in which a bigger area will denote a higher result of the pressure coefficient. Another important feature to note is the upward tendency of the pressure before suffering a huge drop. It was a reaction developed in all the generators, but it was clearly highlighted in the gothic VG. This effect was also gathered by Arguelles [6], in the study carried out with rectangular VG´s.

Finally, the Cp peak value of each vane described the difference in the lateral trajectories adopted by the vortices. Rectangular VG describes the innermost trajectory, while the gothic VG emerges from the exterior of the plate. This phenomenon was explained above and presented for the completely flat plate model, Figure 54.

4.5.3 Aerodynamic Performance of the Flat Plate with Rectangular VG´s adding Endplates

Coming up next, in the following two sections, an in-depth analysis of the aerodynamic performance and vortex generation on the flat plate with endplates will be carried out and, subsequently, a comparison with the research conducted by Arguelles [6] will be shown. For that purpose, three main variables will be varied throughout the study: angle of the flap (δ), incidence of the VG´s (β) and spacing of the VG´s (AR).

Effect of varying the angle of the flap (δ)

The downforce coefficient plotted in Figure 57 shows the differences and the influence of changing the flap deflection. In this case, the flat plate with endplates was set up with a VG angle, respect to the flow direction, of β=10º and a spacing of AR=2.

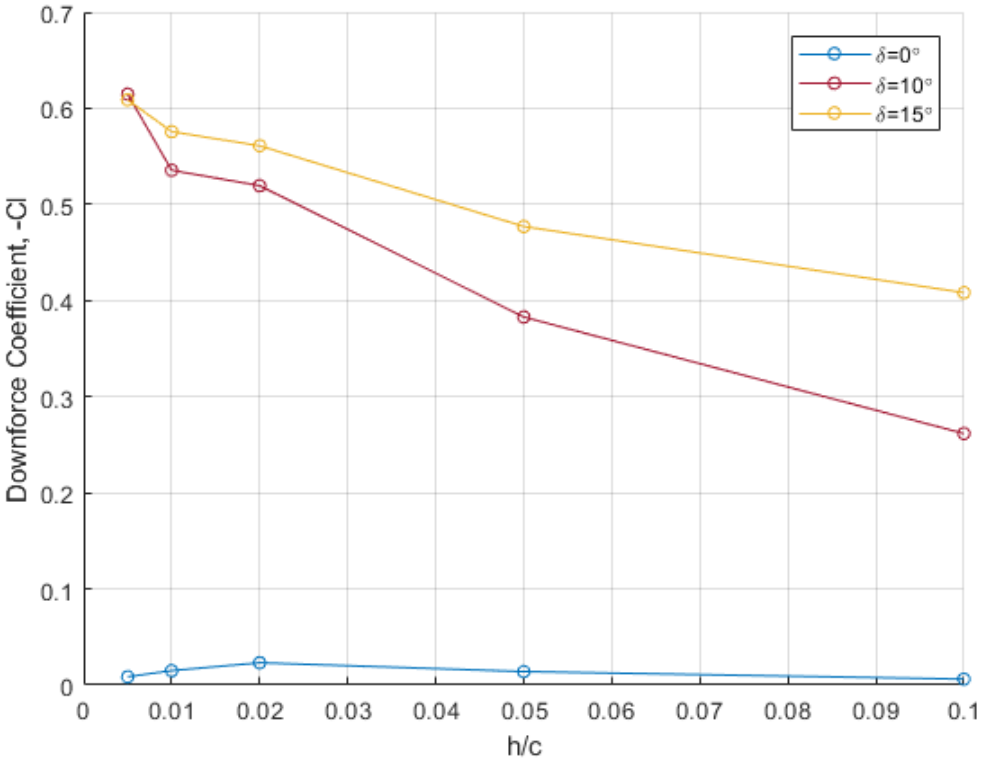

Figure 57: Comparison of C_L for different flap angles

These data clearly proved that the lift force becomes more negative as the ground clearance is reduced and the angle of the flap is increased to positive values. This result is caused due to the reduction of the local pressure induced by the vortices flowing beneath the model. It is worth noting that the upward tendency described by the model with angles of δ=10º and δ=15º is almost the same with different force magnitudes until the lowest measured point (x/c=0.005) was reached. In this location, a sharp increase of the δ=10º model was observed and produced the highest downforce value. The explanation of this phenomenon could possibly be associated to slight flow separation in the flap area. As assessed by Arguelles, when the model was configured without endplates and δ=15º, flow separation on the centre region of the diffuser was observed causing a decrease of the downforce. In this case, the addition of the endplates has probably delayed the appearance of the flow separation, but the change in trend may indicate that it was on the verge of detachment. For δ=0º, smooth and continuous values of lift forces were obtained with a slight reduction in the proximity of the ground.

Figure 58 shows a comparison of the drag coefficients gathered for different flap angles as the ride-height of the test was varied. Unlike the negative lift coefficient, these data produces a similar trend; increase of the drag coefficient until a maximum value with a subsequent reduction when approaching the ground. For δ=0º, the reduction of the drag force is delayed a bit further, until x/c=0.01.

However, a striking situation that could be associated with the ground effect was exhibited, in which at low ground clearances, while the downforce coefficient increases until a maximum value, the drag coefficient undergoes a noticeable reduction. It should be noted that the addition of endplates tends to mimic the function developed by the side-skirts introduced by the Lotus F1 team in 1978. In this case, an edge vortex is produced at the lower edge of the endplates, that being so close to the ground, behave as aerodynamic “barriers” that perfectly seal the air that flows underneath the flat plate, enhancing the suction effect. This effect can be clearly observed for the configurations with certain angle (δ=10º and δ=15º) in the diffuser, since they are probably reproducing the Venturi Nozzle

associated to the ground effect. A similar effect of the decrease in drag while the negative lift increases, at low ground clearances, was found by Holt et al. [32]. It was suggested that the interaction between the low energy of the boundary layer (B.L.) and the high energy of the vortex could reduce the height of the B.L. and, therefore, yield that effect. However, in this case, the angle of the VG´s was set to β=20º and no endplates were added.

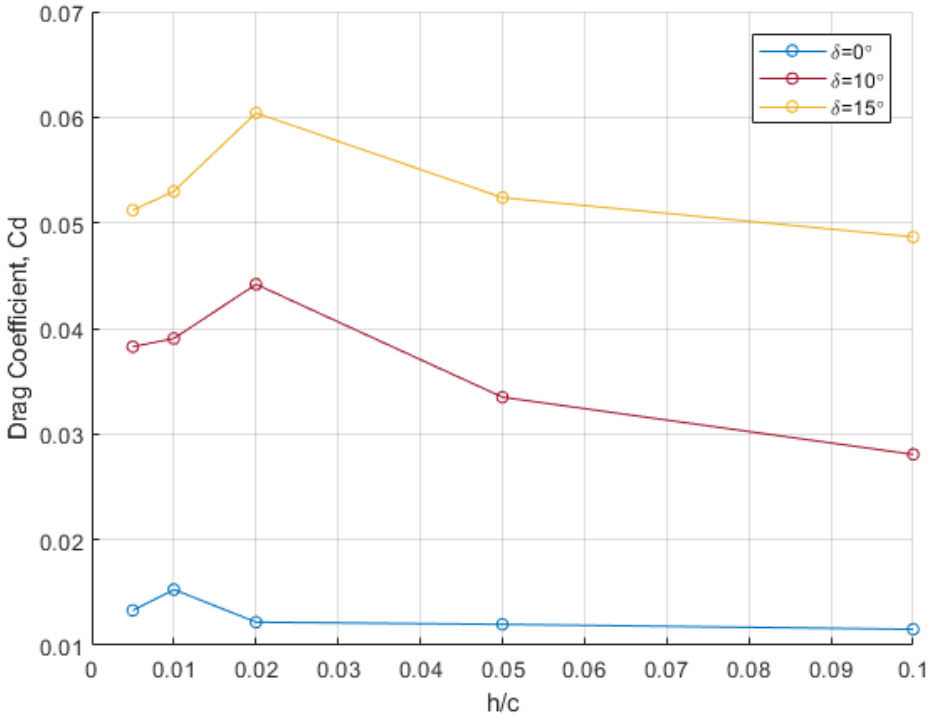

Figure 58: Comparison of C_D for different flap angles

Regarding the analysis of the aerodynamic performance, L/D ratio shows the overall behaviour that can be extracted from a CFD study. As can be seen in Figure 59, the case for δ=10º proved to be the best option in terms of performance, especially at ride-heights lower than x/c=0.02. Likewise, the study conducted by Arguelles [6] also revealed that the δ=10º was the most efficient configuration, even without having the endplates.

In addition, it is believed that the assembly of the endplates will be more advantageous when a diffuser shape trailing edge is expected, since it is able to enhance the performance. In fact, for a complete flat plate, the addition of the

vertical fences does not seem to induce any improvement. (See Figure 79 and Figure 80 for a comparison of the plate with and without endplates).

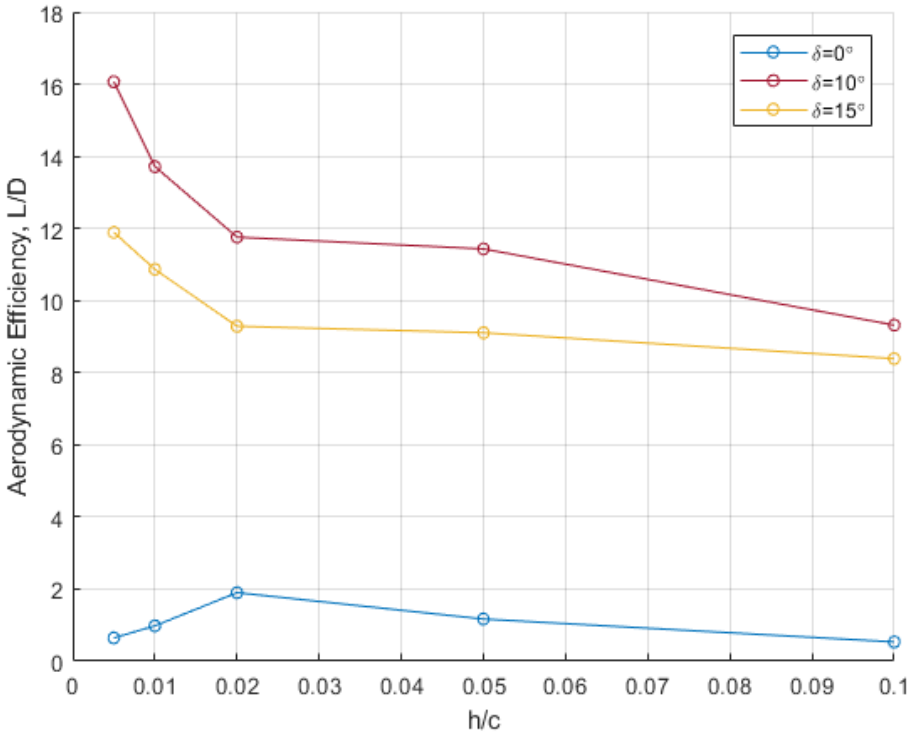

Figure 59: Aerodynamic efficiency for different flap angles

Coming up next, detailed information of the development of the vortices at a number of streamwise locations is depicted through the vorticity contours in Figure 60. For the sake of simplicity and brevity of the analysis, only data associated with δ=0º and δ=10º angles was presented, but data corresponding to the configuration δ=15º will be summarised in the *Appendix C: δ=15º.*

Clearly, two vortices emerged from each pair of vanes and merged rapidly into a single vortex, which flows and diffuses downstream. It can be seen that when the angle of the flap increases, a stronger vortex structure is obtained. However, a significant difference can be observed in the edge vortices emanating from the endplates. While in the case of the complete flat plate, the vortex seems to follow the edge of the vertical plate with a continuous core value, the configuration for δ=10º presents a completely different behaviour. The presence of these longitudinal vortices could be beneficial for a downforce enhancement. Additional

sketches of streamlines are displayed in Figure 61 in order to expand the field of vision of the vortex motion.

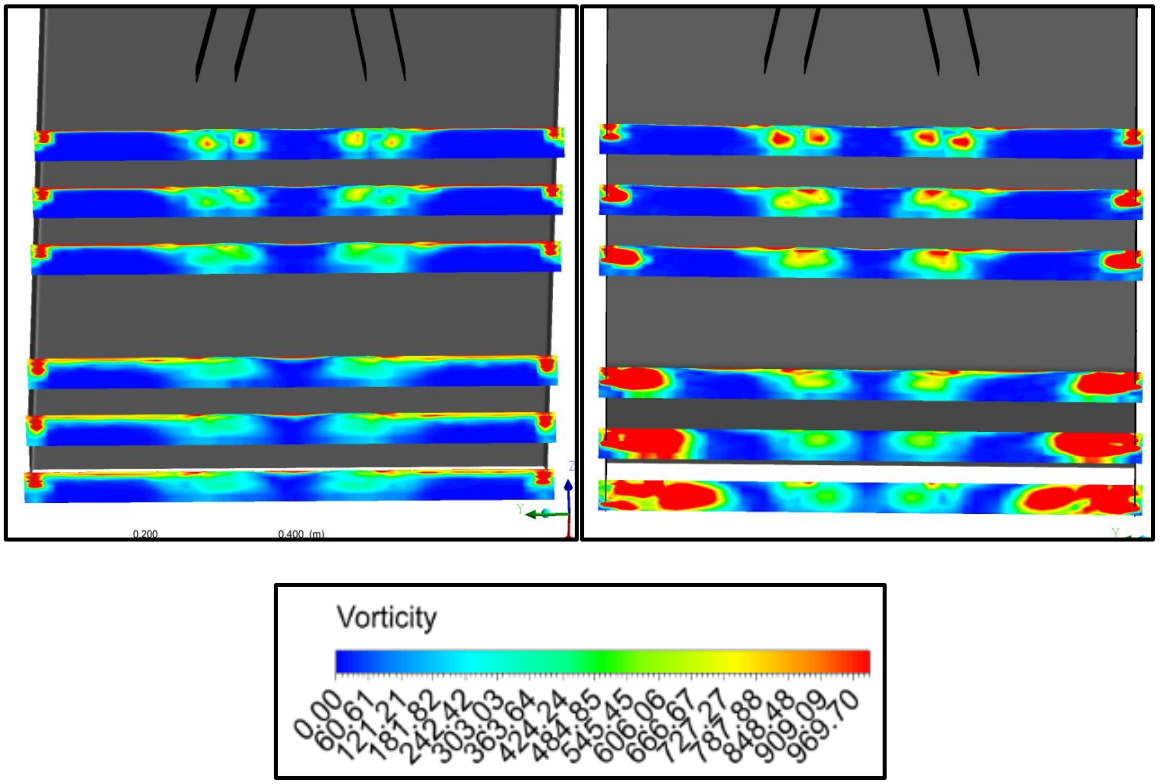

Figure 60: Vorticity Contours for δ=0º (left) and δ=10º (right)

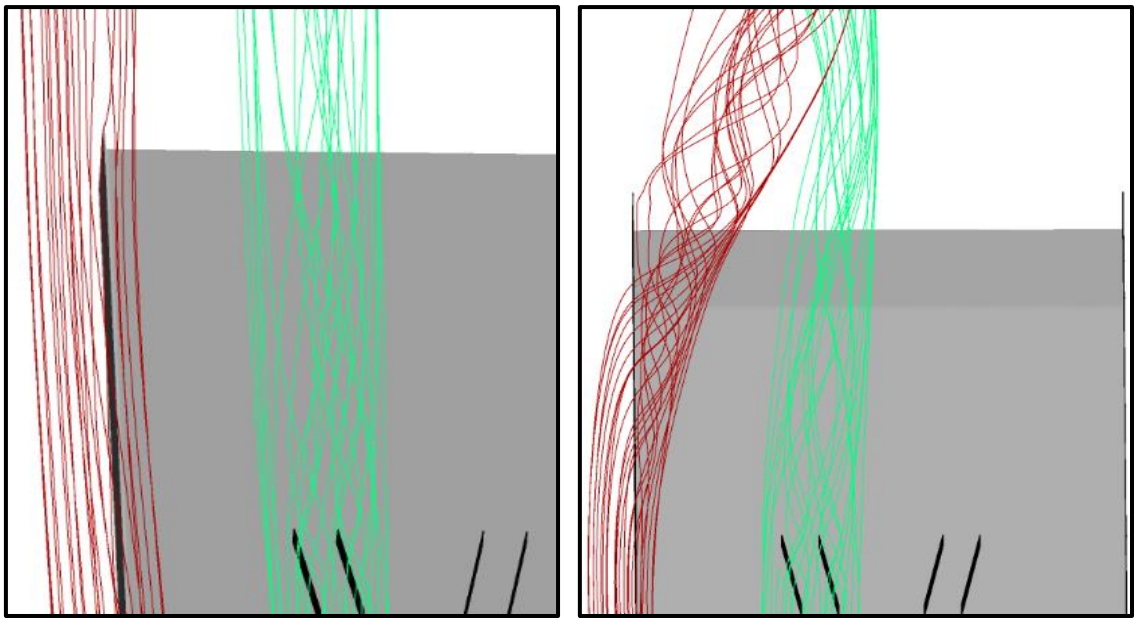

Figure 61: Sketch of the streamlines for δ=0º (left) and δ=10º (right)

The inward tendency described by the lateral vortices could possibly be related to the change in pressure yielded due to the variation of the diffuser ramp angle. These vortices are gaining strength as they flow backwards in the plate and finally, they end up mixing downstream of the plate with the diffused vortex from the flow control devices. The aforementioned aerodynamic “barrier” (red streamlines) can be clearly seen in the previous figures, which will create a reduction of the local pressure in the inner region. Furthermore, the vertical movement of these strong longitudinal vortices can be impeded due to their proximity to the ground plane, causing the aerodynamic force enhancement previously represented for the plate with a flap angle.

Another important feature to note is the swirl motion described by the vortices generated in the lower edge of the endplates. As can be seen in Figure 62, when the model goes from being a completely flat plate to having a flap deflection, the rotational direction of the vortex changes. While for the completely flat plate case the vortex rotates counter clockwise, the configuration of a flap angle causes rotation in the clockwise direction. In the case of the VG´s, as can be seen in the *Appendix B: Rotational direction of the VG´s*, both vortices rotate in a clockwise direction, regardless of the diffuser configuration.

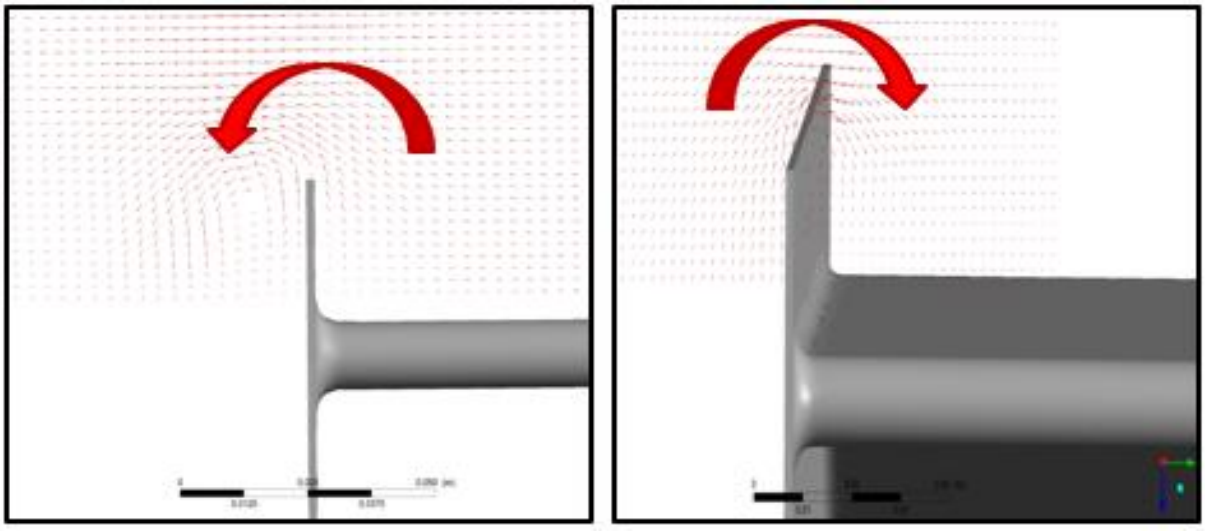

Figure 62: Comparison of Vortex swirl direction. δ=0º (left) and δ=10º (right) (represented upside down)

The pressure coefficient is seen to vary as the air flows backwards on the plate. Figure 63 shows the Cp distribution for the case of the completely flat plate at a number of streamwise locations. As can be seen, in x/c=0.4 two peaks were measured indicating that at this point the vortices were not yet fully merged and that the strength of the inner vortex was higher than the outer one. From this point onwards, a single peak was measured and the gradient of the curve became smoother, representing the diffusion of the single vortex. In addition, following the peak values through the longitudinal direction of the model, the lateral trajectory followed by the main vortex can be highlighted. Clearly, there was almost no lateral displacement from the position of the inner tuning vane, this development can also be observed in Figure 60 and Figure 61.

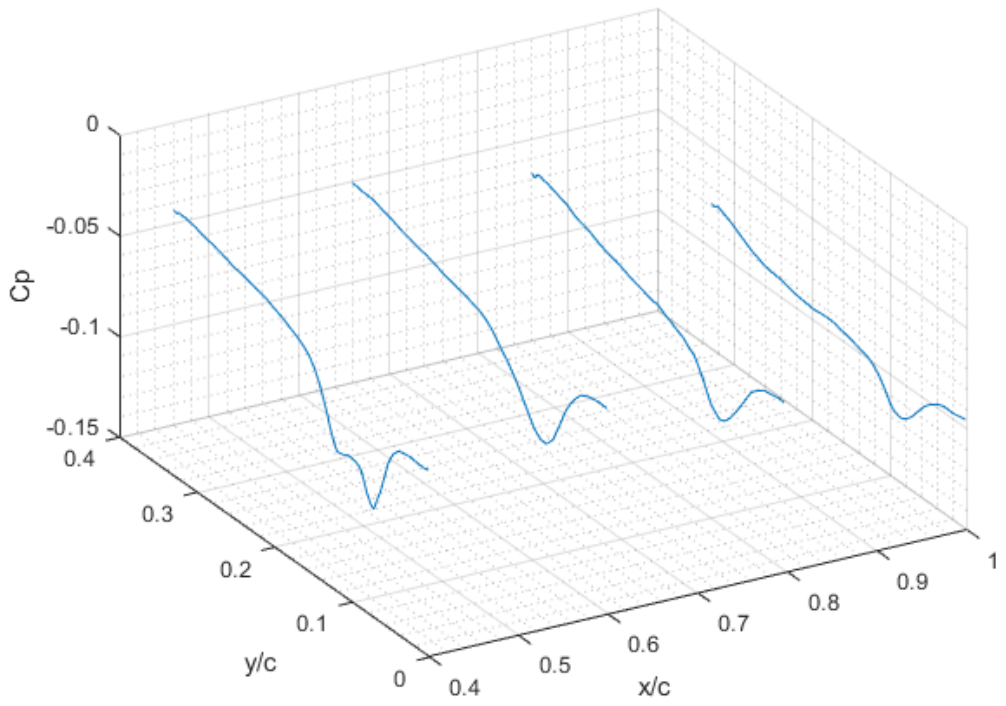

Figure 63: Pressure Coefficient Distribution at a number of streamwise locations. Ride-height h/c=0.02 and δ=0º

The pressure distribution for the model configured with a diffuser ramp angle of δ=10º is shown collectively in Figure 64. In this case, it was decided to present separately in order to appreciate the influence of the lateral vortices generated

on the lower edge of the endplates, since the pressure magnitudes varied significantly from one location to another. As stated for δ=0º case, at x/c=0.4 the vortices were not yet fully merged. However, in this case, a slight influence of the lateral vortex arises at the edge of the plate, at y/c=0.33. Moving back on the plate, the formation of the single vortex appeared and, at the same time, the vortex of the endplates gained more strength and became dominant. An important feature to note is that at the point where a slope change (x/c=0.8) occurs, due to the deflection of the flap, an overall reduction of the local pressure beneath the plate and more specifically the strong peak suction generated by the edge vortex was measured. This effect will cause a pressure drop of the flow on the underside of the model and will explain the increase of the aerodynamic load represented in the negative lift plots.

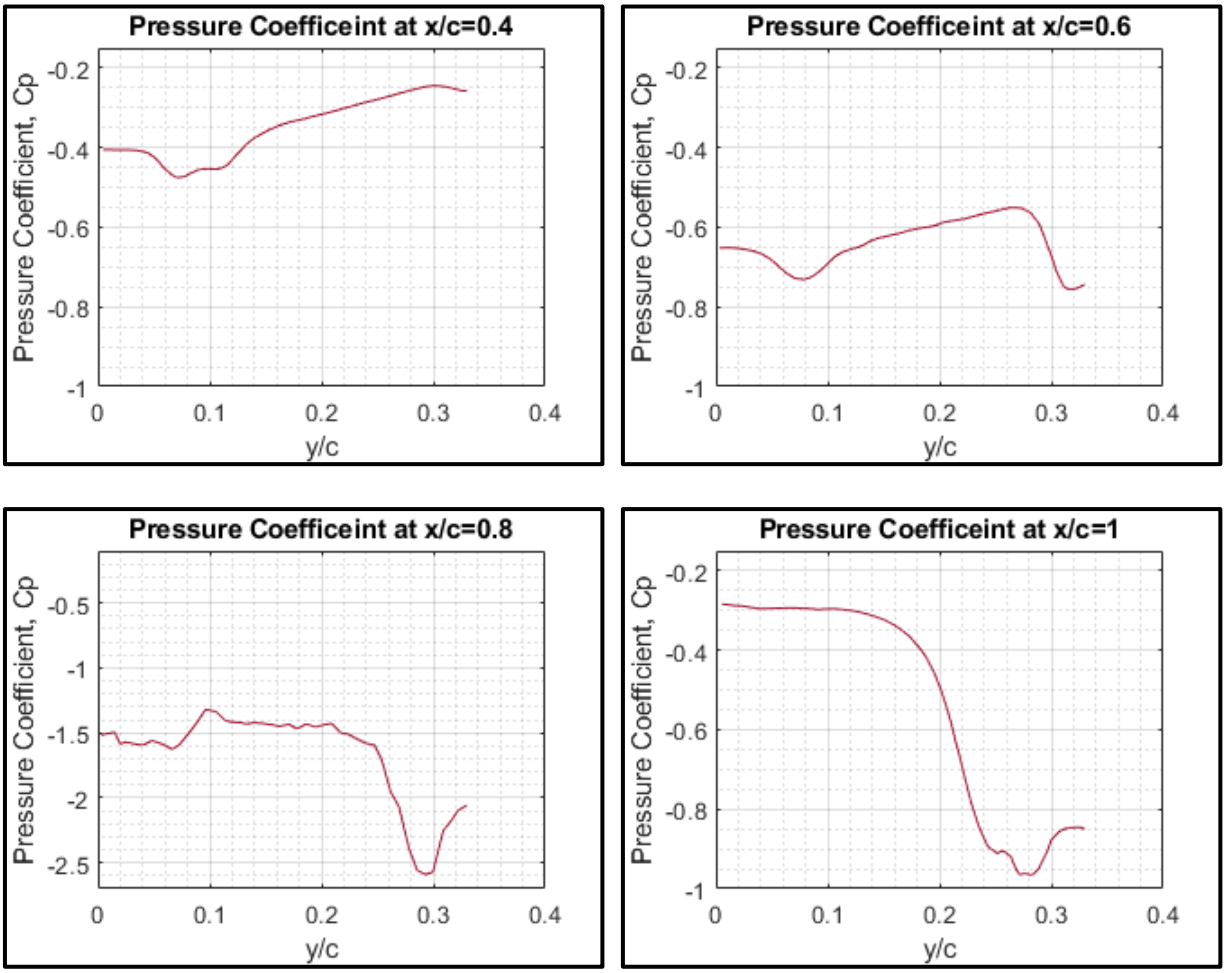

Figure 64: Pressure Coefficient Distribution for a flap set up of δ=10º

Effect of varying the angle of the VG (β) respect to the freestream flow

In the present section, the influence of varying the incidence of the vortex generators will be evaluated. For that purpose, two main VG angles were selected (β=10º and β=20º) and, as the previous section, three diffuser angles were simulated for a range of ride-heights. The spacing of the vanes was configured to AR=2.

The lift coefficient for a wide range of ground clearances is shown in Figure 65, while the angle of the flap and the angle of the VG´s are varied.

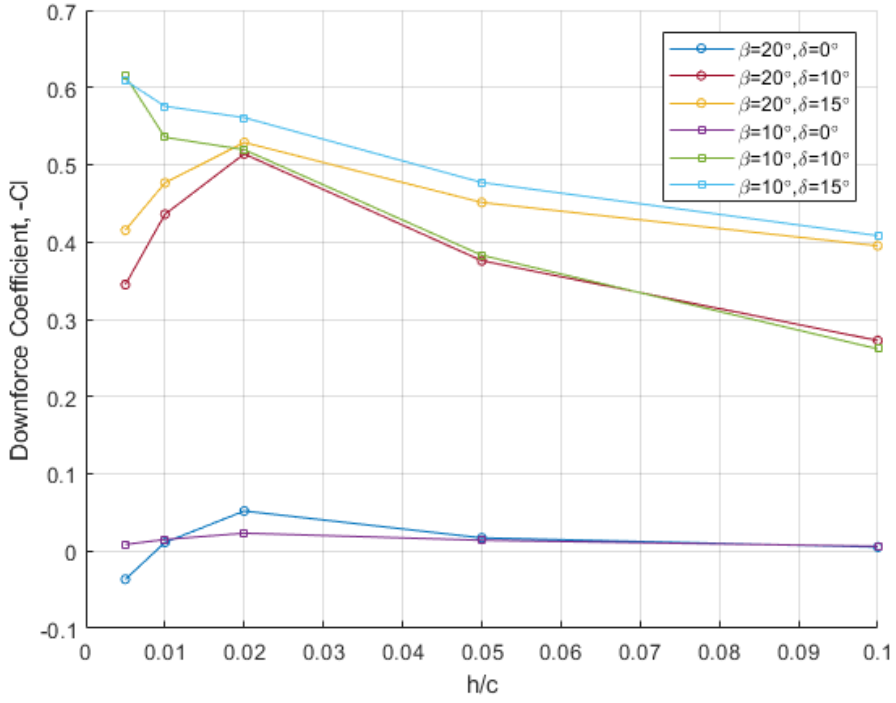

Figure 65: Comparison of C_L coefficients for different VG angles

The data corresponding to the set-up of β=10º is exactly the same depicted in the previous task, in which a progressive increase of the downforce coefficient was obtained for the “flapped” model, while the zero angle diffuser suffered a slight decrease as the plate height was reduced. However, when the angle of incidence of the flow control devices is increased, with respect to the free flow direction, the downforce increases progressively as the ground clearance is reduced. At h/c=0.02 reaches the maximum lift force value and it is followed by a sudden stall

of the flow. In fact, ride-height h/c=0.02 turns out to be an interesting point for the case of δ=10º. It can be clearly seen that for distances far from the ground, in both cases, exactly the same results are obtained. In turn, as the height of the model decreases bellow h/c=0.02, the opposite effect occurs: β=10º increases and β=20º decreases its values. Overall, there has been no improvement compared to the β=10º case, in terms of downforce magnitudes.

The downforce reduction presented when the ground height is reduced is not an unknown effect, since it has been previously reported in studies conducted by other researches such as Holt et al. [32] and Zhang et al. [36]. The main reason of this curve respond was attributed to the vortex burst in the proximity of the ground. Likewise, Garcia et al. [3] reported that the reduction of the exerted lift forces could be related to the untwisting motion of the vortex. As the model approaches the ground plane, the vortex will be developed closer to the plate surface, obstructing the swirl motion leading to the vortex breakdown.

Finally, it can be summarised that low ground clearances and high VG angles seems to be the main cause of the vortex breakdown and therefore, are should be considered as the main parameters to control in order to avoid a remarkable drop of the aerodynamic load.

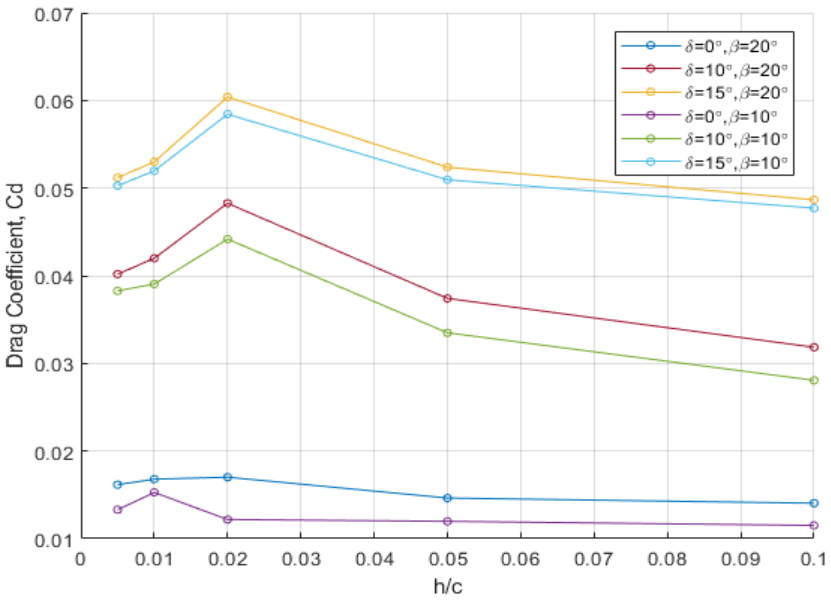

Figure 66: Comparison of CD coefficients for different VG angles

Detailed information about the drag coefficient for different VG and flap angles is presented in Figure 66. Based on these data, the characteristic curve of the drag seems to follow the same trend as that described in the negative lift coefficient. The drag force increases as the model height is reduced until a maximum result is obtained for h/c=0.02, after which, a progressive drop is experienced. Eventually, for the case of β=20º, the drag coefficient that has been recorded is broadly larger than for the case of β=10º. As the angle of incidence of the VG increases with respect to the flow, the exposed frontal area confronting the airflow must also be larger. Hence, the amount of drag generated would potentially be greater.

Finally, in terms of aerodynamic performance, Figure 67 shows that the case of δ=10º and β=10º continues to be the most efficient configuration. However, the rest of the "flapped" configurations performed extremely well, although at low distances to the moving ground, for β=20º cases, it seems to lose a bit of performance. It should be pointed out the extraordinary performance of all models for large heights, maintaining an almost constant efficiency until h/c=0.02. For completely flat plate cases, even increasing the angle of the VG, the addition of the endplates does not seem to be satisfactory, obtaining generally low L/D ratios.

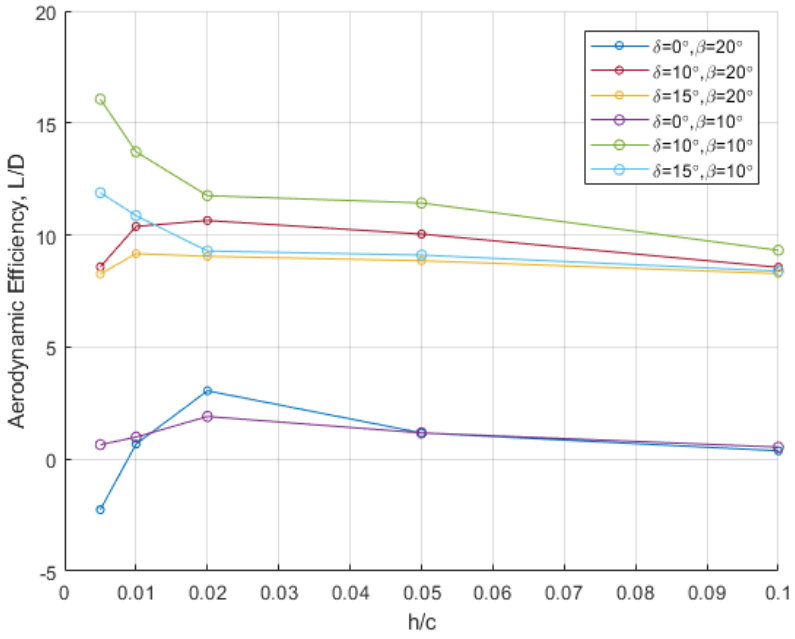

Figure 67: Aerodynamic Efficiency of the plate when δ and β angles varied

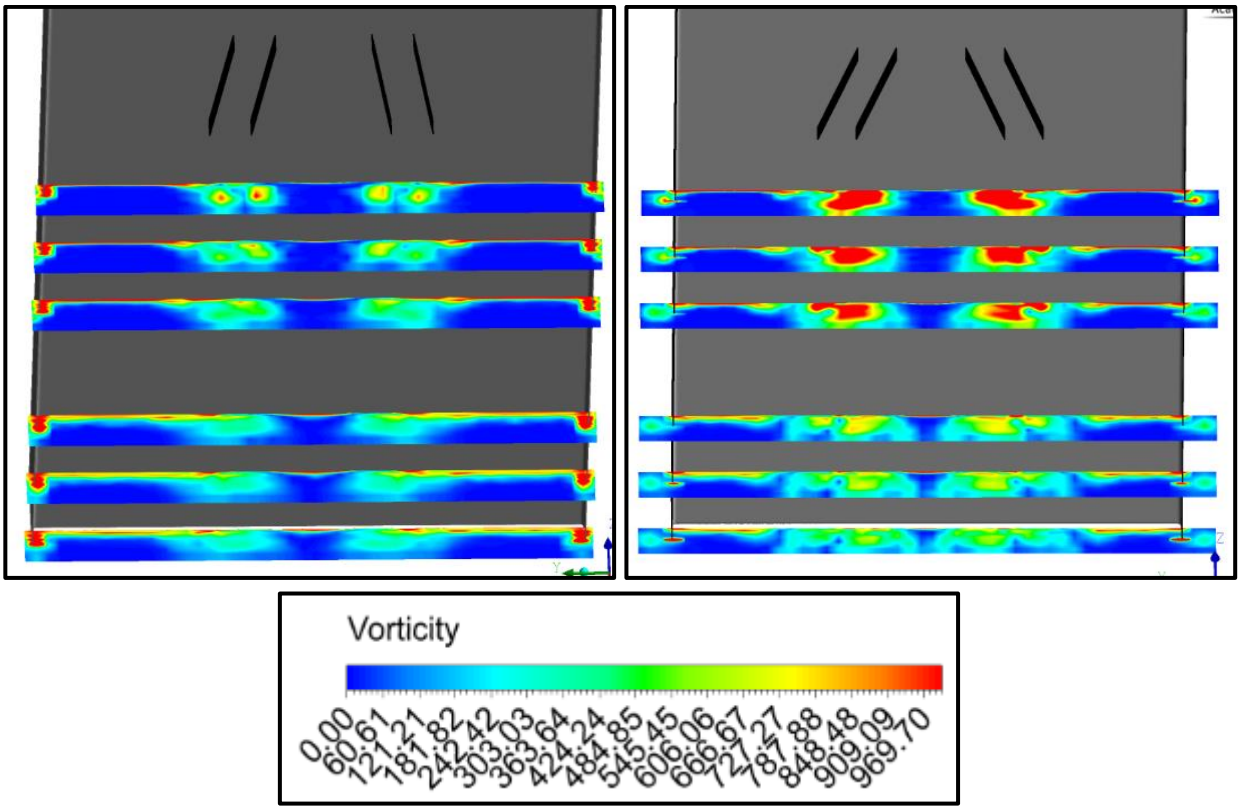

Figure 68: Vorticity Contours: δ=0º, β=10º (left) and δ=0º, β=20º

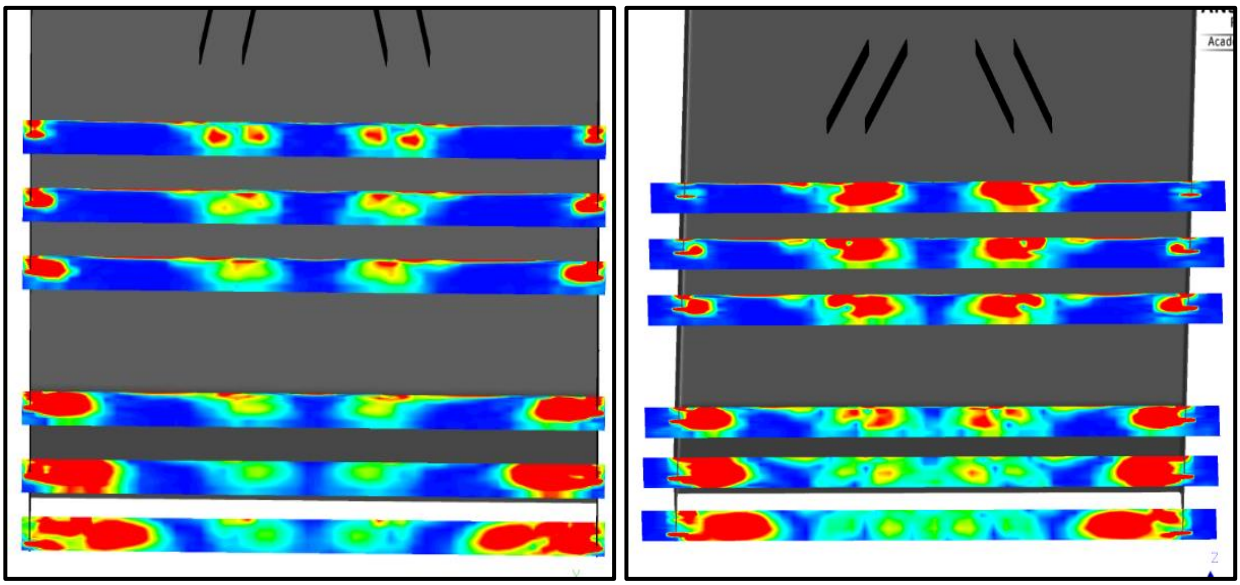

Figure 69: Vorticity Contours: δ=10º, β=10º (left) and δ=10º, β=20º

Figure 68 and Figure 69 compares the vorticity contours for cases depending on the angle of the flap at a ride height of h/c=0.02. The comparison indicates a more concentrated vortex core region when the angle of incidence of the VG was increased to β=20º. Unlike the case of β=10º, it is thought that a change of the vane angle leads to an earlier merge of the vortices emerging from the VG´s.

For δ=0º set up (Figure 68), in addition to what has already been commented, it is quite interesting to compare the different behaviour of the lower edge vortex of the endplate that can be observed. For lower VG angles, the development of this vortex maintains its trajectory through the edge of the side plate, while for β=20º it seems that the vortex defines an outwash trajectory away from the model. This effect can be attributed to the fact that the vortex emanating from the turning vanes appears to be stronger than that created in the endplates.

Adopting a similar approach, when the flap angles is increased to δ=10º, the same endplate vortex trajectory is defined in both cases. However, when the VG angle is increased, it can be observed that when the vortex diffuses along the plate and reaches the trailing edge (x/c=1), the decomposition into small vortices seems to occur. This statement is represented in Figure 70, where the vorticity peak value at streamwise location of x/c=1 has been extracted along the cross section of the flat plate. Clearly, each of the peaks represented in Figure 70 corresponds to the strongest region of the longitudinal vortex cores at that streamwise location. The four peaks in the middle, apparently of the same strength, represent the vortices that emerge from the flow control devices, while the larger peaks and, consequently, those from the sides correspond to the vortices generated in the side plates. The main vortex developed from the endplates turned out to be the strongest, favouring the suction effect that occurs in the lower part of the flap region.

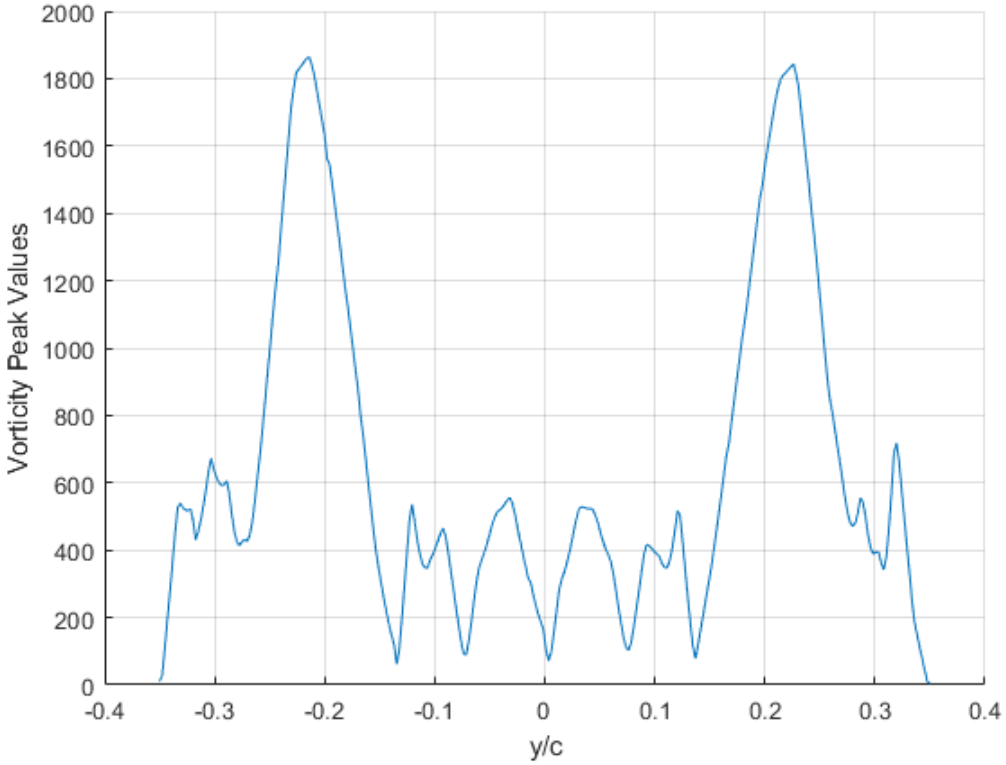

Figure 70: Vorticity Peak Values at the trailing edge of the model (β=20º, δ=10º, x/c=1 and h/c=0.02)

Finally, in order to illustrate in a better way the path followed by the vortices of the VG´s and the endplates shown in the vorticity contours (Figure 69), the lateral trajectory in the flow direction is presented in Figure 71. Assuming a symmetric flow structure on both sides of the plate, only half of the model has been depicted for diffuser ramp of δ=10º.

The main difference that can be extracted from the analysis of this picture is the delay of the vortex fusion when the VG angle is β=10º. Clearly, the presence of the pair of vortices is defined until x/c=0.6 location is reached. In general, the vortex emanating from the turning vanes describes an inward trajectory when moved aft on the plate. Another important feature to note is when the vortex is at x/c=0.8, where a variation of the slope produces a change in the pressure distribution, the edge vortex experienced a progressive inward direction. The development of these vortices will continue and merge further downstream of the

plate. It can be summarised, that the increase of VG angle does not seem to induce great differences, in terms of vortex development trajectory.

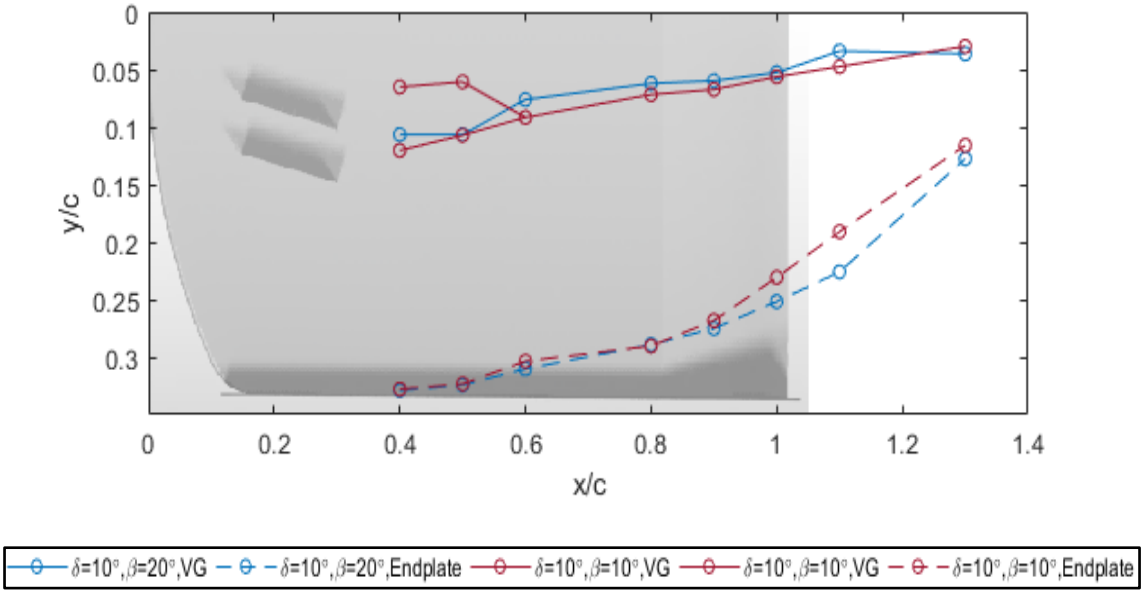

Figure 71: Lateral trajectories of the vortices for δ=10º at h/c=0.02

Effect of varying the distance (AR) between the VG´s

Last influential parameter evaluated was the separation distance between the vortex generators. AR=2 and AR=4 were selected and a comparison between both was conducted. Regarding the others parameters, the angle of incidence of the VG´s was kept configured at β=20º and the flap angle was varied between δ=0º, δ=10º and δ=15º.

Reflecting on the work carried out by Garcia et al. [3], reported that an increase in the aspect ratio of the vanes would induce an aerodynamic load improvement. Considering that the test was carried out with a completely flat plate and with rectangular VG´s mounted, it can be seen in Figure 72 that this statement is no longer valid when some side plates are added in the model. In contrast, when the model is configured with a specific flap angle, it turned out to be valid.

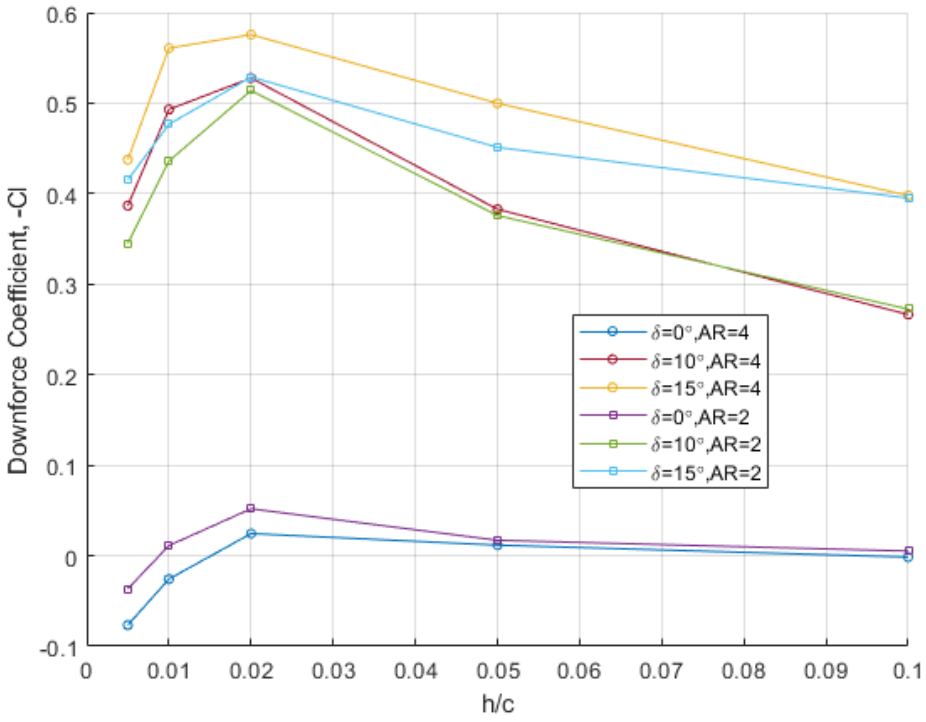

Figure 72: Comparison of Lift Coefficients for β=20º

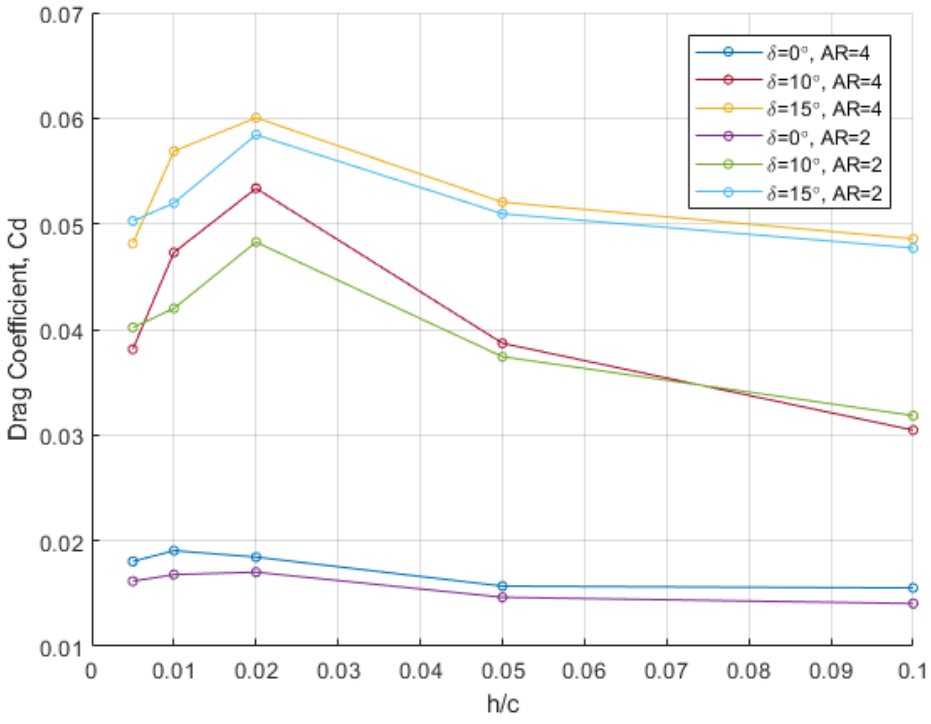

Figure 73: Comparison of Drag Coefficients for β=20º

Figure 72 and Figure 73 shows negative lift and drag coefficients at a number of streamwise locations, where the spacing of the VG´s varied inducing some slight differences. The data presented clearly indicate a common trend for the curve gradient. As the model test height is reduced, the downforce coefficient progressively increases until a maximum value has been reached. It was found that the peak value of the force was located at a ride-height of h/c=0.02 for all cases simulated. As the distance to the ground kepts reducing, a remarkable fall of the downforce coefficient was revealed. As previously stated, the proximity to the ground and high angles of attack for the VG´s will lead to a vortex breakdown that induces a sudden drop of the force. Regarding the drag forces, a similar behaviour described for the downforce coefficient is obtained. It should be noted that for the “flapped” configurations with AR=4, in general, a higher value of the resistance force was measured, with the exception of the lowest ground clearance where a lower value was obtained compared to AR=2 set up.

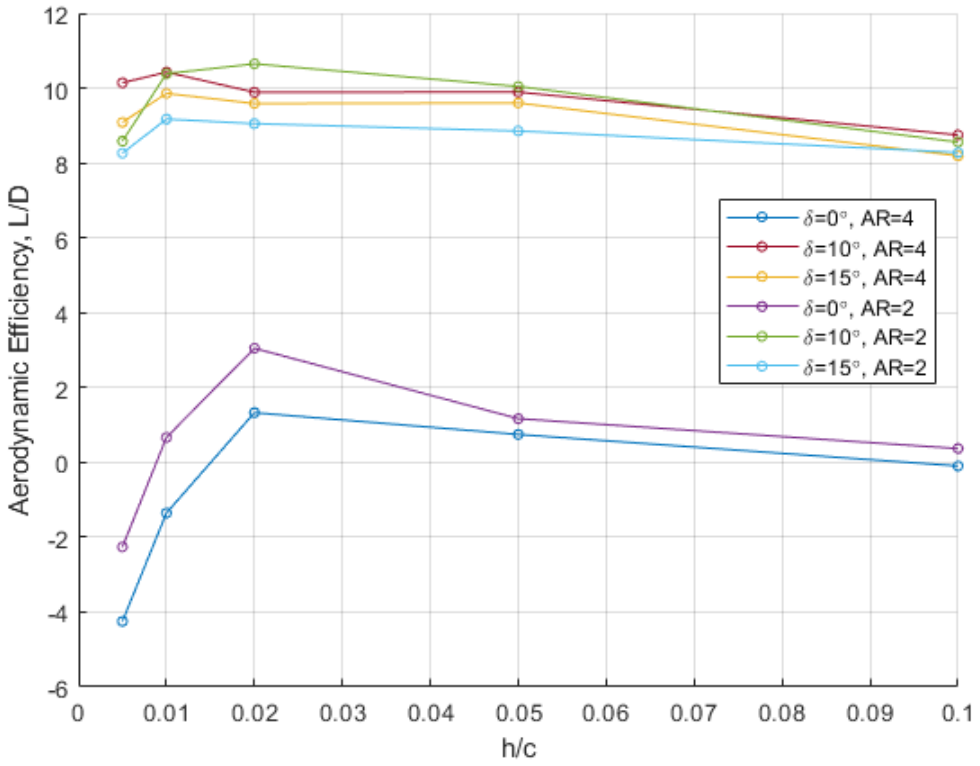

Figure 74: Comparison of Aerodynamic Efficiencies for β=20º

The comparison of the L/D ratios for a range of riding-heights demonstrated, as seen in previous sections, the significant difference between the configuration of the model with or without endplates. In terms of VG spacing, the variation of this parameter does not seem to highlight great differences at larger heights, as can be seen in Figure 74. As the height above the ground is modified, the difference increases slightly, so that the aerodynamic efficiency lies between ratios of 8 and 11, meaning that the maximum difference in a specific location (x/c=0.005) is approximately 28%. Finally, the configuration with AR=4 and δ=10º can be considered as the one that performs best, since it is the set up capable of keeping the highest value of aerodynamic efficiency.

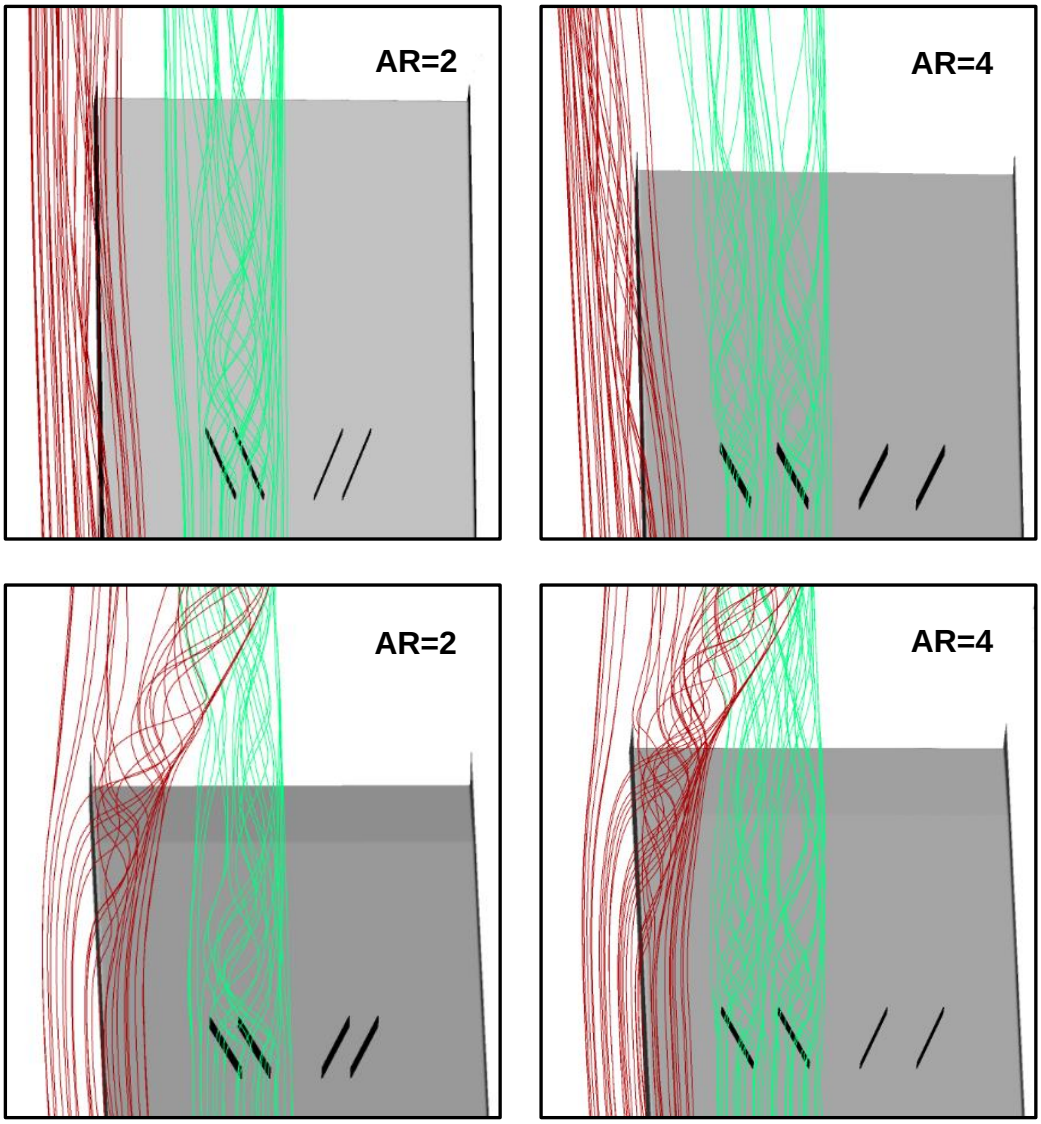

Figure 75: Sketch of the streamlines for δ=0º (Top) and δ=10º (Bottom)

A comparison of the streamlines generated for different VG configurations is presented in Figure 75. The main and most characteristic difference that was found when the distance of the VG´s increased from AR=2 to AR=4, was the lack of interaction between the vortices emanating from the vanes. For the case of no flap deflection, the vortices flowed separately avoiding their fusion. However, in the case of δ=10º, as previously discussed, the change in the pressure beneath the plate and three-dimensional effect of the diffuser will force inward flow. Thereby, the vortices from the VG and the endplates will be merged further downstream of the plate. As assessed by Arguelles [6] and what has been discussed in this task, it can be suggested that the downforce generation can be highly dependent on the interaction between the vortices. When the interaction is low, the aerodynamic load will be enhanced and vice versa.

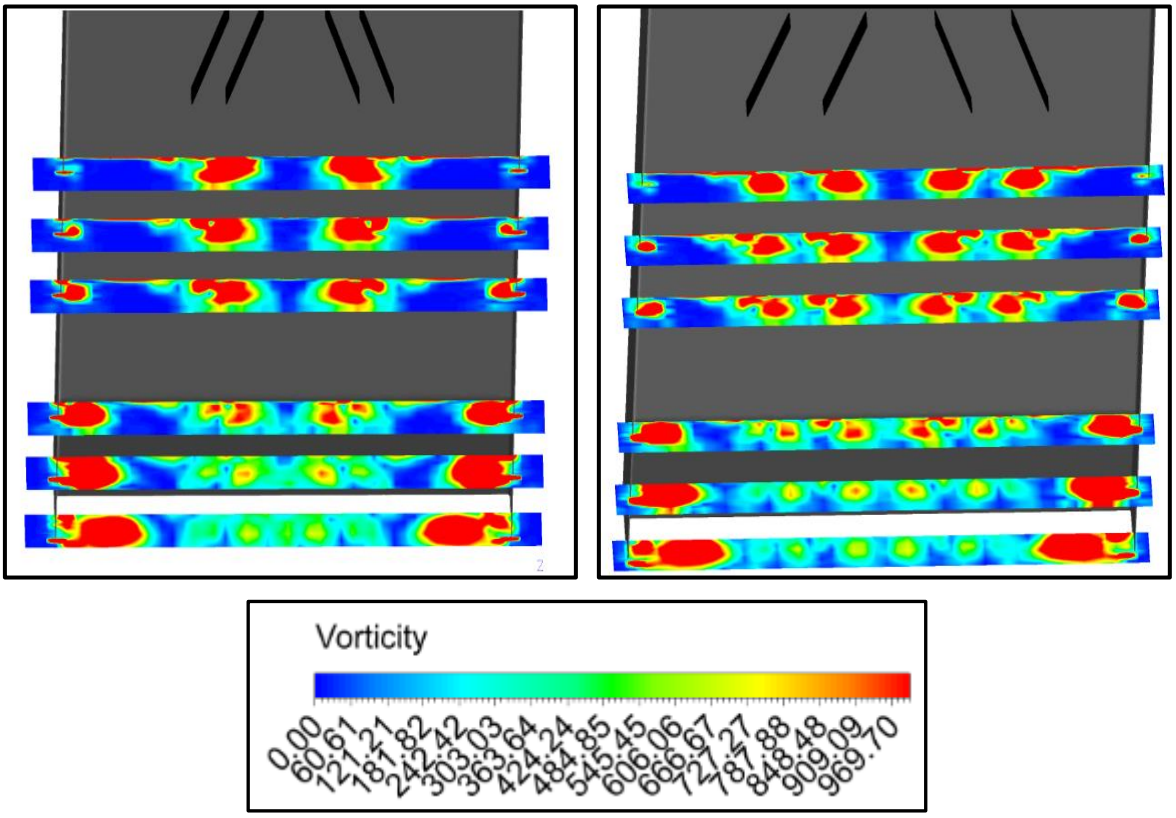

Figure 76: Vorticity Contours for AR=2 (left) and AR=4 (right), δ=10º

Figure 76 depicts the vorticity contours related with a 10-degree flap configuration, in which the effects of the VG spacing can be compared. The figure above represents clearly the differences in the diffusions of the vortices as they

flow backwards. Generally, the diffusion was found to be smoother and more progressive if compared with other configurations (Figure 60), in which it was seen a strong decay of the vortices in the early stages of their development. Based on previous discussions, it was also found that the larger separation of the vanes leads to the generation of separate vortices that will merge downstream with the vortices emerged from the lower edge of the endplates.

Lastly, the measurement of the pressure coefficient at a number of streamwise locations in the flat plate is presented in Figure 77, for case δ=0º. This will provide additional information about the trail development of the vortices, such as the trajectory followed downstream.

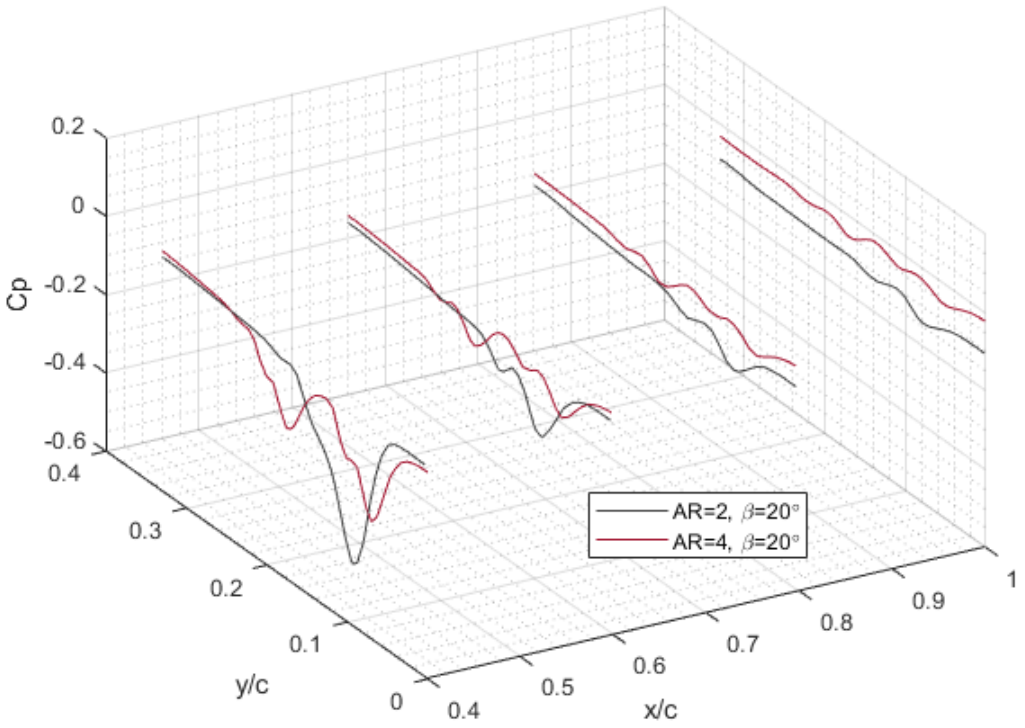

Figure 77: Pressure Coefficient comparison for δ=0º at h/c=0.02

The comparison shows clearly one of the main differences discussed about changing the distance between the turning vanes. The configuration with AR=2 presented a unique suction peak that suffers a strong initial vortex decay with a subsequent smooth diffusion through the flow direction. While the configuration

with AR=4 depicted two principal suction peaks, associated with the previously seen separate flowing motion of the vortices, describing a more progressive and less aggressive curve gradients. The smoothness of the curves is due to the loos of capacity of the vortices to roll up and their subsequent loss of energy. These maximum values indicate approximately the location of the core of the vortices generated by the VG´s, which allow observing the longitudinal and lateral trajectories followed by the vortices.

Finally, in Figure 78 additional data of the pressure coefficients is reproduced in four different streamwise locations for a flap deflection of 10 degrees.

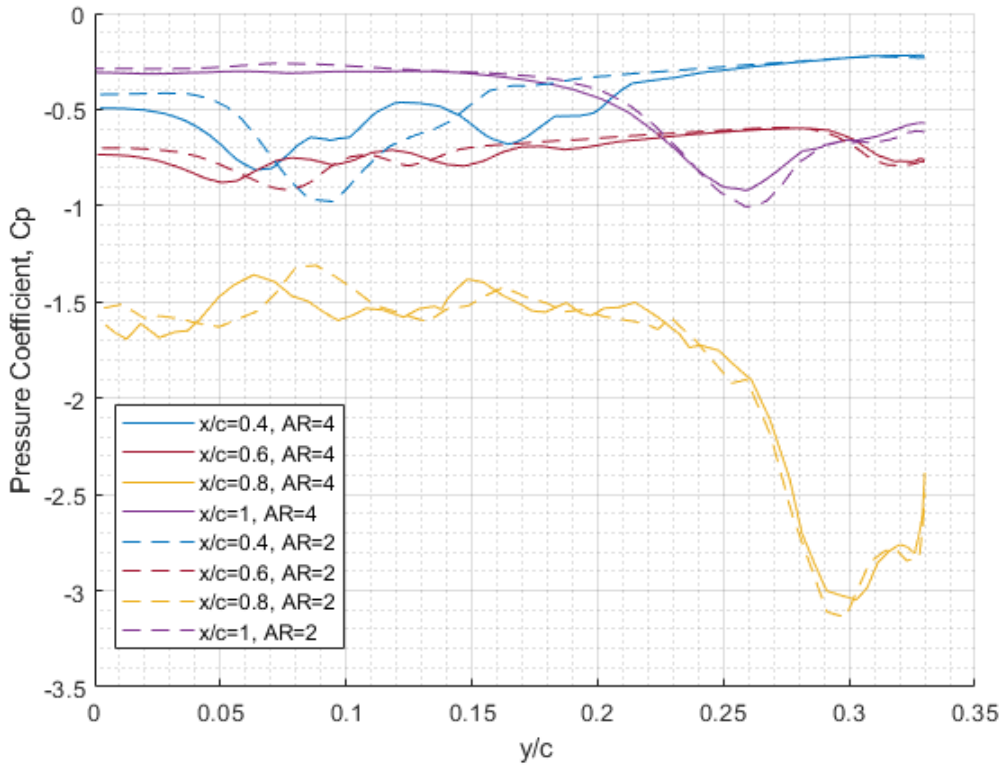

Figure 78: Comparison of the pressure coefficients for δ=10º at h/c=0.02

It can be observed similar curve trends previously explained for the case in which the flap angle is deployed. First, the peaks due to the VG vortices predominate, but as the plate progresses, the peaks due to the vortices of the lower edges of the endplates begin to stand out, managing to dominate the situation at the intersection between the plate and the diffuser. The two peaks are again

observed in the case of AR = 4, and in terms of Cp magnitudes, there is not much difference, except that the configuration with AR = 2 seems to produce slightly higher suction peaks.

4.5.4 Comparison to Arguelles study

Once all the computational data and results related to the flat plate model equipped with endplates on the sides has been explained and analysed, a comparison between the present project and the study carried out by Arguelles [6] will be presented.

In this section, the computational model is the same one used previously. In other words, it consists of a flat plate with endplates and rectangular VG´s, in which the angle of the flap, the angle of incidence of the VG´s and the spacing of the VG´s was varied. On the other hand, the computational model employed by Arguelles [6] had the same plate and rectangular VG´s. Thereby the influence, in terms of aerodynamic performance, of adding some vertical fences will be evaluated.

Effect of varying the angle of the flap (δ)

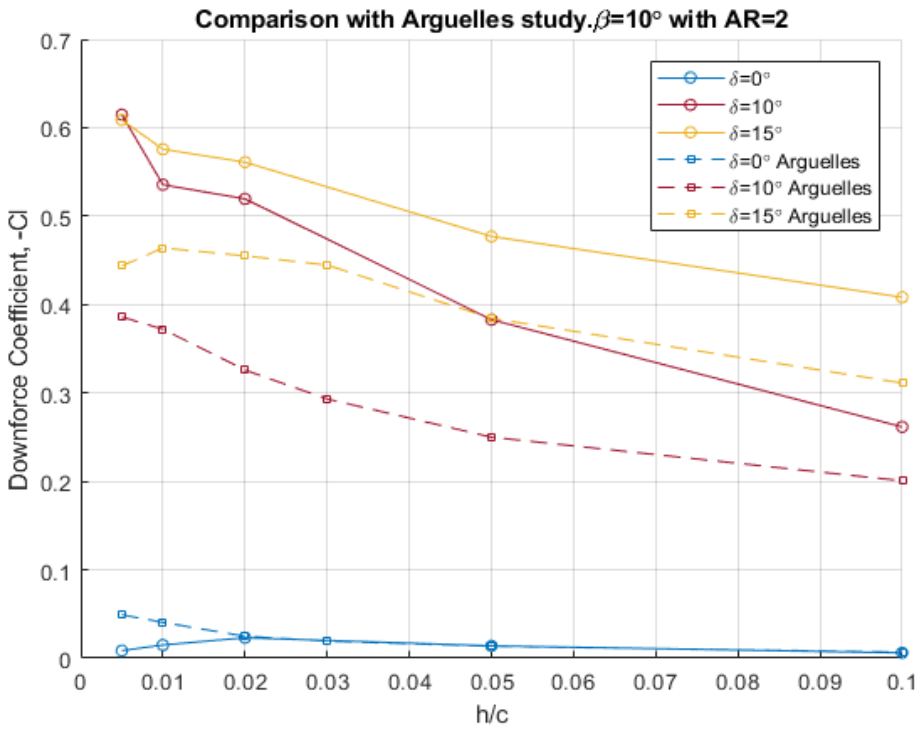

Figure 79: Comparison of the C_L for a range of flap angles

Figure 79 shows the downforce coefficient results obtained for three different trailing edge flap angles. In general, exists an increase tendency of the aerodynamic load when the ride-height was varied, with the exception of two cases in the vicinity of the ground plane, where a slight decrease of the downforce was observed. In addition, the plate with endplates tends to generate bigger aerodynamic loads.

For δ=0º, the comparison shows a similar curve gradient at high distances from the ground, but when the model reaches x/c=0.02 a clear difference of the results was predicted. In this case, the model with endplates obtains a maximum downforce value followed by a sudden reduction, in opposition to the results obtained by Arguelles [6], in which the maximum value of downforce was obtained for the nearest distance to the ground. The study conducted by Zhang et al. [36] also found this remarkable reduction of the downforce at close to zero ground clearances, for a wing model equipped with vertical fences.

Regarding the cases with the plate configured with two different flap angles, it can be seen the significant differences emerged. In this case, the curve describes a stepper path for the model with endplates as the body is getting close to the ground, which means that the enhancement of the downward force is larger. In this way, the change in pressure distribution induced by the deflection of the trailing flap will be better employed by a model equipped with endplates, since it will allow sealing the sides of the plate and control the flow more efficiently under the model. Based on the study conducted by Arguelles [6], he reported that for δ=15º and at x/c=0.01, the decrease in the downforce coefficient was due to the separation of the flow in the diffuser area. Focusing on the same location for the model with endplates, it can be seen that the force continues increasing, which implies that the addition of endplates delayed the flow detachment.

A detailed comparison of the drag force coefficient against a wide range of ride-heights is depicted in Figure 80, configured with three different flap angles. Overall, as can be expected, the drag force proved to be higher in the case of the plate mounted with endplates. However, in the case of δ=15º, when the maximum drag value was obtained a sharp reduce was observed, predicting a lower value

than the model without endplates. As can be seen, the model used by Arguelles [6] defined a very smooth increasing drag curve, while the new model projects a defined trajectory; an increase until the maximum value followed by an abrupt drop.

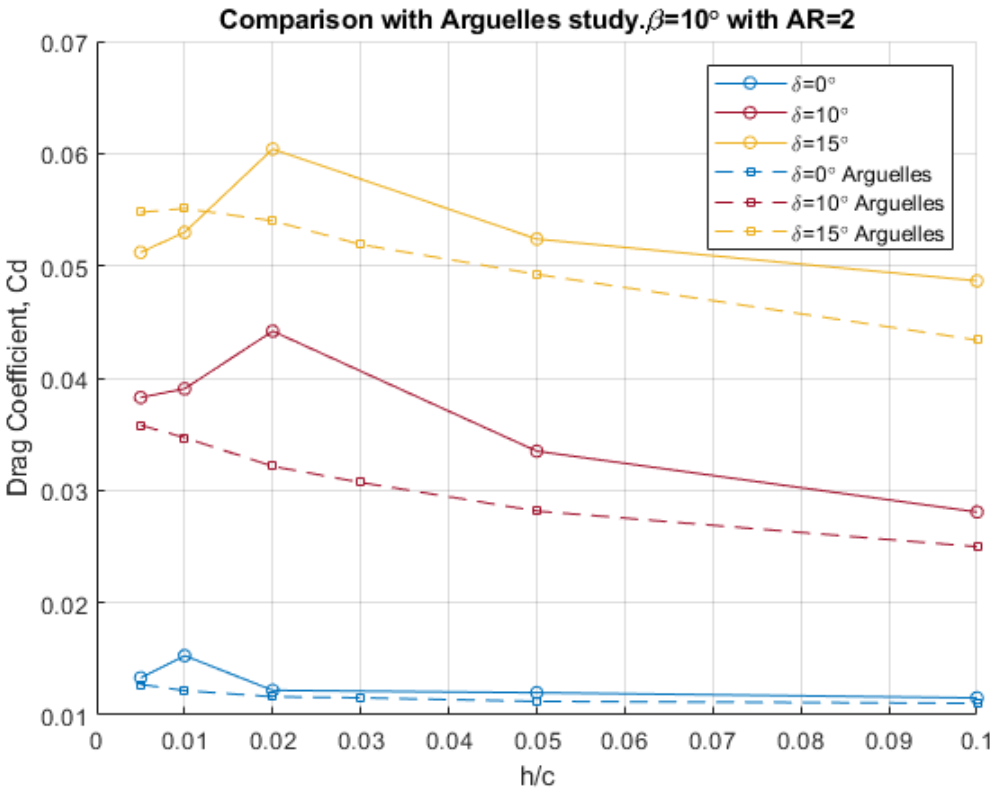

Figure 80: Comparison of the C_D for a range of flap angles

The results presented so far suggest that the addition of vertical fences to the flat plate when it contains a diffuser ramp or moveable flap will report some benefits; in terms of aerodynamic performance, the efficient downforce will be increased.

Effect of varying the angle of the VG (β) respect to the freestream flow

Figure 81 illustrates the downforce coefficient obtained for the model configured with VG angle of β=20º and flap angles of δ=0º, δ=10º. Using these results as a guideline, both computational models showed a similar trend, an increase in aerodynamic load until a maximum value was reached with a subsequent sudden reduction at low ground clearances. As previously stated for the configuration of β=10º and δ=0º (Figure 79), the force generated by both cases at high ride-

heights was almost the same until x/c=0.02, where a discrepancy arose in the results.

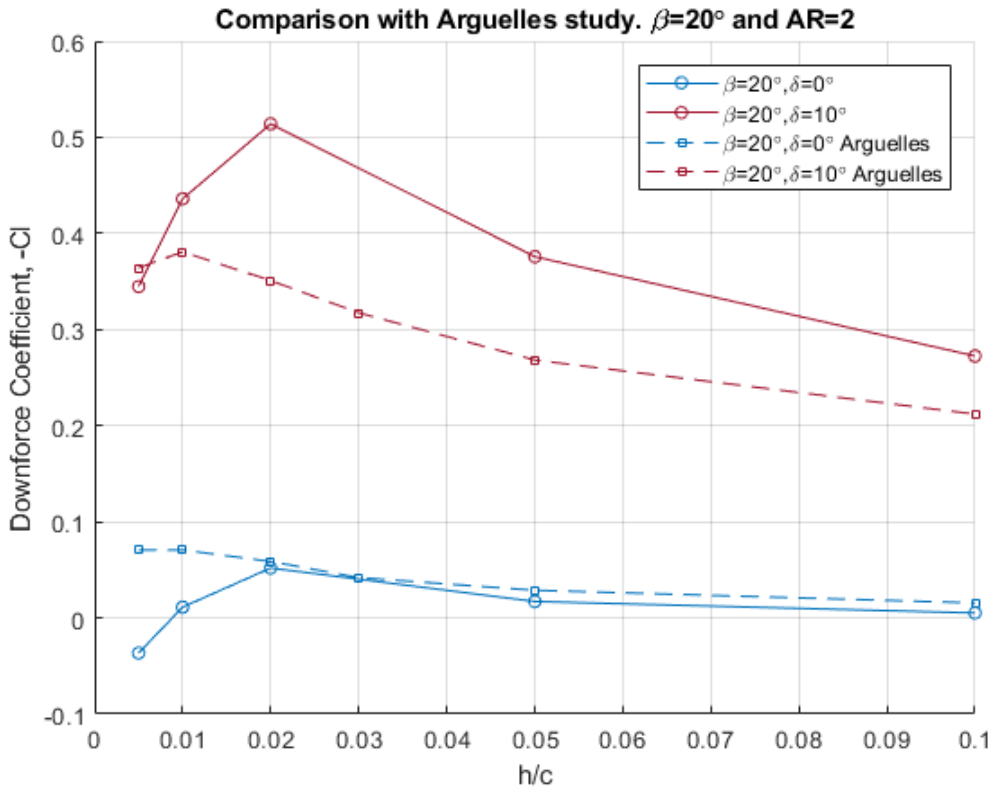

Figure 81: Comparison of the C_L with VG angle at β=20º, for δ=0º and δ=10º

Unlike depicted for β=10º, when the incidence of the vane increases, a drop in the force is revealed (for all cases) at distances close to the ground. The reduction of downforce is greater in the model with endplates and also seems to occur at higher distances from the ground, x/c=0.02 against x/c=0.01 for the model of Arguelles [6]. It can be surmised that the addition of the endplates could possibly move forward on the plate (trailing edge direction) the vortex breakdown, as it was also predicted by Garcia et al. [3].

As can be seen in Figure 82, the drag coefficient predicted the same behaviour with a pronounced increase and a sharp reduction at low ground clearances.

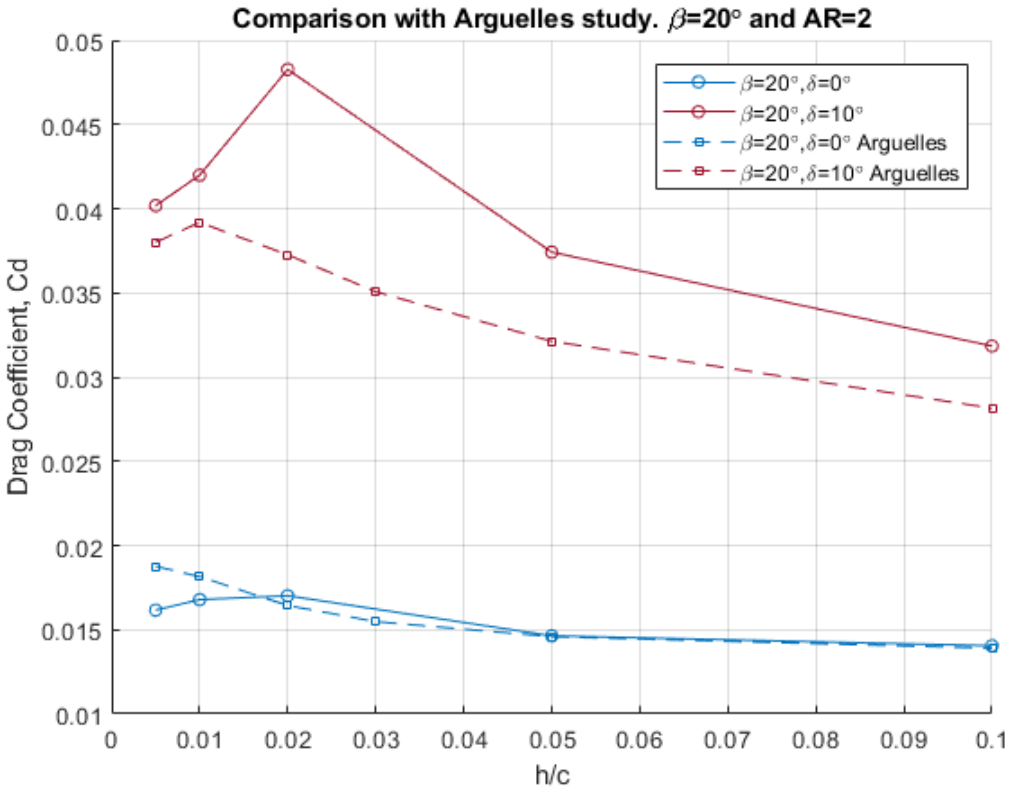

Figure 82: Comparison of the C_D with VG angle at β=20º, for δ=0º and δ=10º

Summarising, when the angle of incidence of the VG is increased, the generation of the aerodynamic forces increases. An important feature to note is that the effect of the endplates is noticeable when there is a change in the pressure below the plate due to a variation on the flap angle. However, a phenomenon also assessed by Holt et al. [32] emerged at low ground clearances and high VG angles: vortex breakdown. This effect can be highlighted in both models, although the intensity was higher for the case with endplates. Following this, the model used by Arguelles [6] proved to be capable of delaying the vortex burst compared to the current model, since, as previously presented, this effect arose at lower distances to the ground plane.

Effect of varying the distance (AR) between the VG´s

Regarding the spacing of the vortex generators, downforce coefficient and drag coefficient are collectively presented in Figure 83 and Figure 84. All the data presented so far, in terms of aerodynamic performance, reproduced almost the

same behaviour. When analysing the case of the plate with β=20º, it can be perfectly appreciated, for all cases, the breakdown of the vortices in a distance close to the ground.

However, it would be interesting to highlight the results obtained when a change in the flap angle is not performed, leaving the model as a complete flat plate. Until now, similar behaviour had been obtained up to x/c = 0.02, where a difference in performance could be observed from that height onwards (in direction to the ground). When the spacing of the generators was varied, a greater aerodynamic force was obtained for the case of the model without endplates. This phenomenon can be attributed to the involvement of the lower vortices generated by the endplates, producing in this case a negative effect.

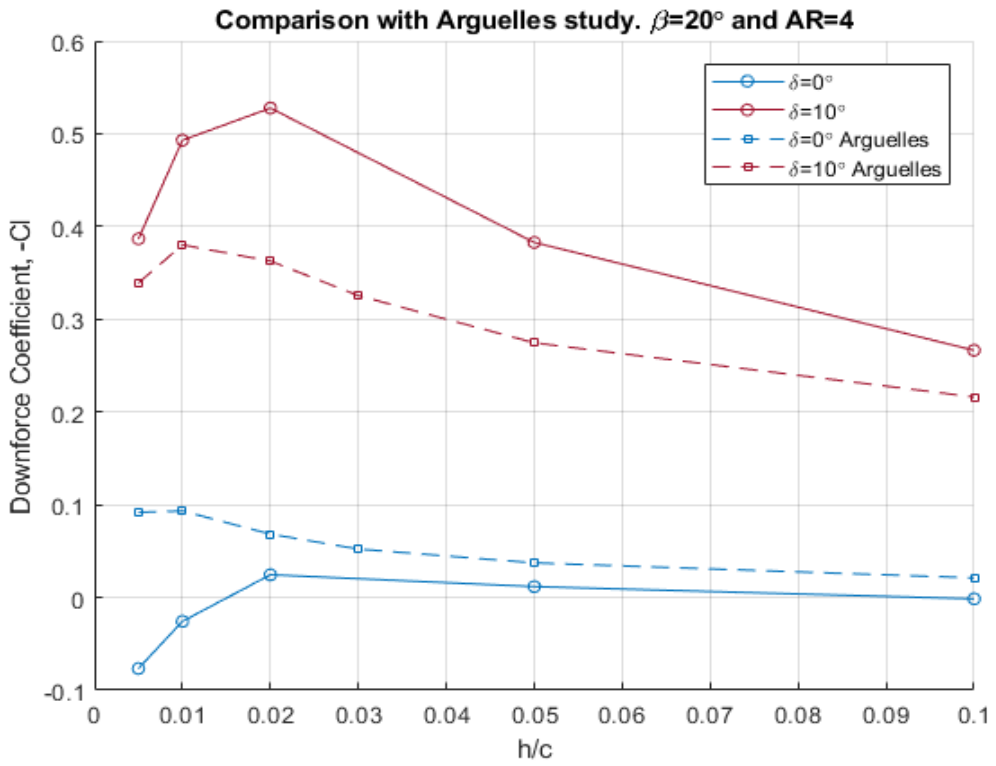

Figure 83: C_L comparison with Arguelles data for =10º

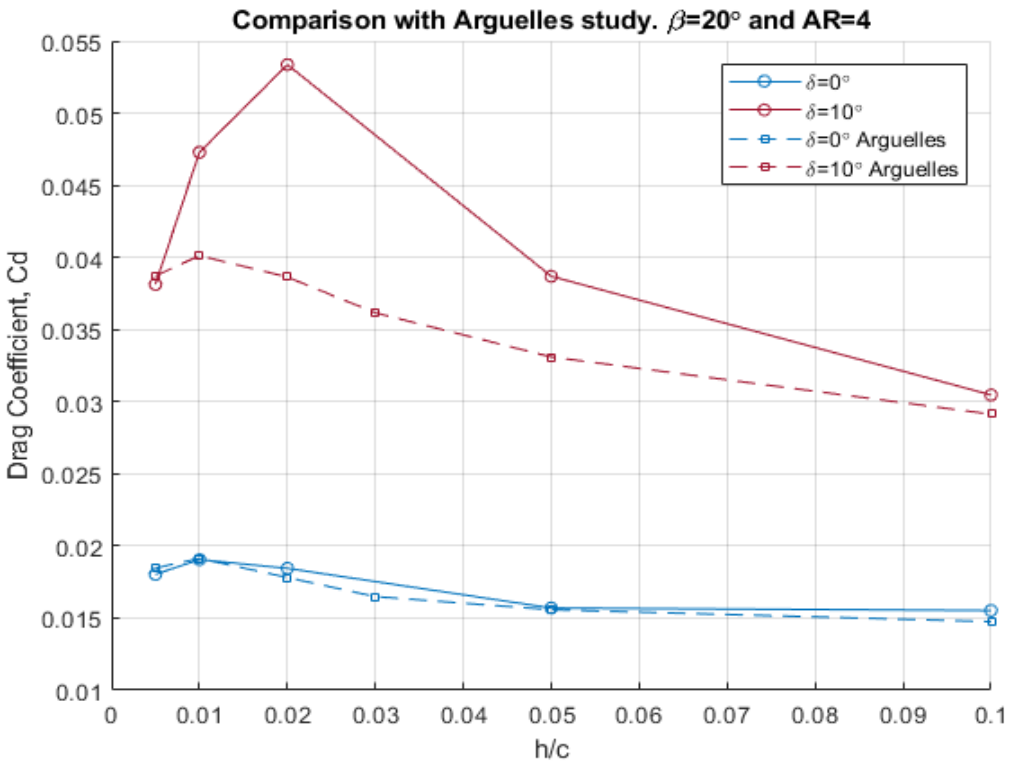

Figure 84: C_D comparison with Arguelles [6] **data for δ=10º**

Finally, the comparison between the present study and the project carried out by Arguelles [6] suggests that the use of endplates will be advantageous, in terms of aerodynamic performance, when a diffuser ramp is configured in the model. This way, a large enhancement of the downforce will be produced. However, when a completely flat plate is modelled the addition of the endplates produces almost no differences, even leading to diminish in some cases the performance of the plate, such as the increase of the aspect ratio of the VG´s

5 .CONCLUSIONS

To date many studies related to a flat plate with large-scale rectangular vortex generators in the proximity of the ground have been conducted in order to understand the effect produced by the vortices on the forces exerted on the plate. Some authors responsible for carrying out these researches are: Garcia et al. [3], Holt et al. [32], Byrne [5] and Zaproudis [4]. They consist of simple theoretical studies that can be later used as a basis for applications with more difficult and realistic aerodynamic geometries, such as the under-trays of the racecars with the aim of improving dynamic performance.

Arguelles took a step forward and designed a moveable flap in the trailing edge of the plate that will induce a remarkable change in the pressure gradient, by varying the angle of this device. Following this line, the aim of the present thesis was to conduct a fully computational study in order to assess the flow physics generated by four different shapes of VG´s and, at the same time, assess the effect of the addition of side endplates on the aerodynamic performance. Later a comparison with the same study, without endplates, carried out by Arguelles [6] was conducted.

In order to ensure that CFD simulations could accurately predict the results, a validation process was conducted. For that purpose, experimental data gathered by Arguelles [6] for the flat plate with rectangular VG´s was used. The comparison of the trend curves described by downforce and drag coefficient results was found in excellent agreement. Even the CFD data obtained by Arguelles was improved, more specifically the drag curve behaviour at distances close to the ground. Despite the fact that there is still a visible difference in the CFD data, the over prediction was reduced from 35.7% to 25%.

In terms of coefficient magnitudes, slight differences were observed. The discrepancy of the results occurred mainly at low ground clearances, where a maximum over-prediction of 24.1% was obtained for ride-height h/c=0.01 in the C_L. It was found that the experimental data was not able to capture the stall condition predicted in the simulations. Hence, one of the reasons that can cause

the differences that arise at low ground clearances could be attributed to the experimental measurement techniques used in the wind tunnel, since the initial position of the test is established at the highest distance from the ground, where the vortex can be created without the effect of the ground proximity. Despite these discrepancies, the model was quite accurate and, therefore, was used as a basis for the rest of the study.

Regarding the VG optimisation, a fixed model configuration was selected and simulated for each turning vane. The vortex generators were set to $\beta=20^{o}$ and AR=2, while the plate was configured to be a completely flat body. The comparison of the force coefficients proved that the main side area of the VG strongly influences the results. The highest downforce was produced by the rectangular VG, whereas the lowest value was attributed to the triangular VG. In other words, an increase on the area of the vane will be followed by a more negative lift coefficient and, therefore, the aerodynamic performance will be enhanced. Clearly, this effect will be produced as the model height is reduced. In addition, it was found that ogive and triangular VG´s seem to be less likely to suffer a reduction in downforce generation in the proximity of the ground, which means that they are less affected by the interaction with the ground effects. This effect is of utmost importance for motorsport applications. However, an important discovery to note entails the rectangular and gothic VG´s. At very low ground clearances (h/c=0.005) a vortex breakdown emerging from the rectangular VG was observed, which suffered a reduction of the downforce coefficient. By contrast, the gothic VG produced the highest aerodynamic load coefficient. This effect could be attributed to a flow obstruction between the rectangular VG and the ground plane due its proximity to the ground, while the smooth leading edge design of the gothic VG could avoid this situation. In short, in terms of aerodynamic performance, the rectangular VG proved to be the most efficient element for all tested riding-heights, with the exception of the shortest ground distance.

It was seen that the variation of the VG shape not only affected the pressure distribution on the plate, but also the lateral trajectories and the vorticity peak

values developed by the vortices. The comparison of the pressure peaks revealed that the early stages (x/c=0.4) of the vortex generation lead to a significant initial pressure peak followed by a progressive decay. The rectangular VG demonstrated to generate almost double the value of Cp produced by the rest of the VG´s. Following this, it was also discovered that the highest initial vorticity value was developed by the triangular VG, being able to justify that the interaction and, therefore, the fusion of the pair of vortices was delayed in comparison with the other devices. Finally, the differences observed in the lateral trajectories of the vortices were affected by the proximity to the ground and pressure peak values. It can be suggested that, the lower the value of the Cp peak generated after the VG, the path developed by the vortex would be the outer one and vice versa. This way, the differences between the extreme cases (gothic and rectangular VG, Figure 54) are explained.

A comparison of the model with and without endplates showed a remarkable improvement of the overall downforce generation for the endplates configuration, that for a standard configuration of AR=2, β=20º and δ=10º, incremented from C_L=0.35 to C_L=0.52. This effect can be associated with the strong vortex generated at the lower edge of the endplates, which will seal the low-pressure air that flows beneath the plate. This common effect was also revealed by Park et al. [37] and Galoul et al. [27].

The assessment of varying the flap for a range of angles demonstrated that as the ground height was reduced, the downforce coefficient would be increased. The main reason lies on the change in pressure distribution along the plate induced by the endplates and the flap deflection. A favourable pressure gradient was presented and, consequently, the vortex generated in the endplates was forced to flow towards the inner region of the plate. At the same time, a change in the rotational motion of the vortices was induced. While the vortices associated with the VG´s were kept clockwise, the vortex of the endplates varied from the counter clockwise direction to the clockwise direction by increasing angle of the flap. However, it was observed that maintaining δ=0º would penalise the

aerodynamic efficiency of the plate, in comparison with the same model without endplates.

The study completed by Arguelles [6] found that increasing the angle of incidence of the VG would produce a stronger vortex structure and, therefore, an enhancement of the downforce coefficient. However, the results of assembling the endplates showed a discrepancy in the statement. In this case, the vortex structure for β=20º was weaker and no improvements were obtained in the performance compared to the β=10º set up. Likewise, the increase of β angle produced the vortex breakdown in the proximity of the ground (h/c=0.02), where at lower distances than that a reduction of the downforce was observed. The fusion of the pair of vortices occurred closer to the trailing edge of the VG´s and the lateral trajectories described by the both set of vortices were also more internal.

Finally, regarding the spacing of the VG´s, the computational flow visualisation showed a separated vortex shedding as the AR was increased. This implies that the separation was large enough to avoid interaction between the pair of vortices and, therefore, contributed to the enhancement of the downforce. This increase was noted mainly in the 15-degree flap configuration, where at h/c=0.01 height an increase of 18.75% was obtained. In addition, the pressure distribution exhibited two weaker distinctive suction peaks that were smoothly diffused along the plate, while for a smaller separation distance (AR=2) the vortex fusion produced a strong initial suction peak followed by a damped development.

6 FURTHER WORK AND RECCOMENDATIONS

Once a fully computational study on the exerted forces and flow structures has been carried out and having completed the objectives set at the beginning of this project, some potential recommendations for future work have been indicated.

First, and most important, with the previously proposed tests programme or with another new programme, a moving ground wind tunnel should be used to perform a complete experimental test. Apart from measuring lift and drag forces, pitching moments and pressure gradients, a flow visualisation technique could be used in order to obtain a first sight of the real vortex development. If smoke vis, PIV or LDA measurement techniques are not available, it is proposed to use some wool tufts. The main objective should be to correlate and validate the whole set of results obtained through the computational simulations. Moreover, as previously discussed, the largest discrepancies between the experimental and CFD data arises as the moving ground was approached. Therefore, it should be also interesting to execute the experimental tests changing the starting position of the plate on the wind tunnel. For example, starting from the lowest measurement point of the plate, if possible.

In this project, rectangular shaped endplates mounted on the sides of the plate has been used. An aerodynamic study for the optimisation of the endplates design is suggested. This could not only involve new designs affecting the shape, length and width, but also try to find the optimum location of the element that maximises the aerodynamic performance of the plate.

Finally, as previously stated, the comparison performed for the four different VG shapes was undertook with a single fixed configuration. In order to evaluate more in depth the effect induced by each of the VG´s, it is proposed to vary the angle of incidence of the VG´s respect to the free flow and the spacing between them. Furthermore, it should be also involved varying the geometry of the vane. In other words, in this study a fixed length and height (150mm and 25mm respectively) of the VG was used. Hence, a reduction of the geometry of all the present VG shapes, with the exception of the rectangular VG (since it has been previously

studied), could be interesting to analyse. For that purpose, previous studies conducted by Cantore [34] and Katz et al. [19] could be helpful.

REFERENCES

[1] Zhang, X., Toet, W. and Zerihan, J. (2006) ‘Ground effect aerodynamics of racing cars’, *Applied Mechanics Reviews*, 59(1–6), pp. 33–48. doi: 10.1115/1.2110263.

[2] Katz, J. and Garcia, D. (2002) ‘Aerodynamic Effects of Indy Car Components’, *SAE International*, 2002-01-33(724), p. 9. doi: 10.4271/2002-01-3311.

[3] Garcia, D. L. and Katz, J. (2003) ‘Trapped Vortex in Ground Effect’, *AIAA Journal*, 41(4), pp. 674–678. doi: 10.2514/2.1997.

[4] Zaproudis, I. (2016) *Aerodynamic Characteristics of Controlled Longitudinal Vortices in Ground Effect*. Cranfield University.

[5] Byrne, D. (2010) *Vortex Induced Aerodynamic Forces in Ground Effect*. Cranfield University.

[6] Arguelles Pastur, M. (2017) *Vortex Induced Aerodynamic Forces on a Flat Plate in Ground Proximity*. Cranfield University.

[7] Katz, J. (1995) ‘Race Car Aerodynamics : Designing for Speed’, *Bentley Publishers*, p. 278. doi: 800-423-4595.

[8] F1 (2017) *Re-writing the F1 rule book - Part 1: from wing cars to flat bottoms*, *Formula1.com*. Available at: https://www.formula1.com/en/latest/technical/2017/2/f1-cars-rules-aerodynamics-ground-effect.html.

[9] Cui, E. and Zhang, X. (2010) ‘Ground Effect Aerodynamics’, *Encyclopedia of Aerospace Engineering*, (1927), pp. 1–12. doi: 10.1002/9780470686652.eae022.

[10] *Lotus Modell 79 wing-profile* (2017) *Wikimedia Commons*. Available at: https://commons.wikimedia.org/wiki/File:Lotus_Modell_79_wing-profile.svg.

[11] Zhang, X. and Zerihan, J. (2003) ‘Off-Surface Aerodynamic Measurements of a Wing in Ground Effect’, *Journal of Aircraft*, 40(4), pp. 716–725. doi: 10.2514/2.3150.

[12] Agathangelou, B. and Gascoyne, M. (1998) ‘Aerodynamic Design Considerations of a Formula 1 Racing Car’, *SAE International*, (724), pp. 1–4.

[13] Cooper, K. R., Bertenyi, T., Dutil, G., Syms, J. and Sovran, G. (1998) ‘The Aerodynamic Performance of Automotive Underbody Diffusers’, *SAE International*, (724), p. 980030. doi: 10.4271/980030.

[14] Katz, J. (2006) ‘Aerodynamics of Race Cars’, *Annual Review of Fluid Mechanics*, 38(1), pp. 27–63. doi: 10.1146/annurev.fluid.38.050304.092016.

[15] Senior, A. E. and Zhang, X. (2001) ‘The force and pressure of a diffuser-equipped bluff body in ground effect’, *Journal of Fluids Engineering, Transactions of the ASME*, 123(1), pp. 105–111. doi: 10.1115/1.1340637.

[16] Ruhrmann, A. and Zhang, X. (2003) ‘Influence of Diffuser Angle on a Bluff Body in Ground Effect’, *Journal of Fluids Engineering*, 125(2), p. 332. doi: 10.1115/1.1537252.

[17] Lin, J. (1999) ‘Control of turbulent boundary-layer separation using micro-vortex generators’, *30th Fluid Dynamics Conference*, (c). doi: 10.2514/6.1999-3404.

[18] Lin, J. (2002) ‘Review of Research on Low-Profile Vortex Generators to Control Boundary-Layer Separation’, *Prog. Aerosp. Sci*, 38 (4-5), pp. 389–420.

[19] Katz, J. and Morey, F. (2008) ‘Aerodynamics of Large-Scale Vortex Generator in Ground Effect’, *Journal of Fluids Engineering*, 130(7), p. 071101. doi: 10.1115/1.2948361.

[20] Escudier, M. (1988) ‘Vortex Breakdown : Observations a N D Explanations’, 25, pp. 189–229.

[21] Benjamin, T. B. (1965) ‘Significance of the Vortex Breakdown Phenomenon’, *Journal of Basic Engineering*, 87(2), p. 518. doi: 10.1115/1.3650590.

[22] Doherty, T. O. (2001) ‘Vortex breakdown : a review’, 27.

[23] Van de Wijdeven, T. and Katz, J. (2013) ‘Automotive Application of Vortex Generators in Ground Effect’, *Journal of Fluids Engineering*, 136(2), p. 021102.

doi: 10.1115/1.4025917.

[24] Chambers, J. R. (2003) ‘Concept to Reality’, pp. 209–231. doi: 10.2975/31.1.2007.23.31.

[25] Roberts, S. C. (1966) ‘An investigation of end plates to reduce the drag of plannar wings’, *USAAVLABS TECHNICAL REPORT*, pp. 65–79.

[26] SOLTANI, M. R., MASDARI, M. and TIRANDAZ, M. R. (2017) ‘Effect of an end plate on surface pressure distributions of two swept wings’, *Chinese Journal of Aeronautics*. Chinese Society of Aeronautics and Astronautics, 30(5), pp. 1631–1643. doi: 10.1016/j.cja.2017.07.008.

[27] Barber, V. G. and T. J. (2007) ‘A Study of Inverted Wings with Endplates in Ground Effect’, (December), pp. 919–924.

[28] Yao, C., Lin, J. and Allen, B. (2002) ‘Flowfield Measurement of Device-Induced Embedded Streamwise Vortex on a Flat Plate’, *1st Flow Control Conference*, (June). doi: 10.2514/6.2002-3162.

[29] Allan, B. G., Yao, C.-S. and Lin, J. C. (2002) ‘Simulation of Embedded Streamwise Vortices on a Flat Plate’, p. 19. Available at: http://hdl.handle.net/2060/20020059542.

[30] Jung, J. H., Kim, M. J., Yoon, H. S., Hung, P. A., Chun, H. H. and Park, D. W. (2012) ‘Endplate effect on aerodynamic characteristics of threedimensional wings in close free surface proximity’, *International Journal of Naval Architecture and Ocean Engineering*. Society of Naval Architects of Korea. Production and hosting by ELSEVIER B.V., 4(4), pp. 477–487. doi: 10.2478/ijnaoe-2013-0112.

[31] Ansys (2009) ‘Ansys fluent 12.0. Theory Guide’, *ANSYS Inc.*

[32] Holt, J., Garry, K. and Soares, R. F. (2016) ‘Vortex induced aerodynamic forces on a flat plate in ground proximity’, *34th AIAA Applied Aerodynamics Conference*, (June), pp. 1–14. doi: 10.2514/6.2016-4170.

[33] Forster, K. J. and White, T. R. (2014) ‘Numerical Investigation into Vortex Generators on Heavily Cambered Wings’, *AIAA Journal*, 52(5), pp. 1059–1071.

doi: 10.2514/1.J052529.

[34] Cantore, S. (2018) *Lateral Aerodynamic Control Using Asymmetric Under-Body Diffuser Flows*. Cranfield University.

[35] 'ANSYS FLUENT 12.0. User's Guide' (2009) *ANSYS Inc.*

[36] Zhang, X. and Zerihan, J. (2003) 'Aerodynamics of a Double-Element Wing in Ground Effect', *AIAA Journal*, 41(6), pp. 1007–1016. doi: 10.2514/2.2057.

[37] Park, K., Hong, C. H., Kim, K. S. and Lee, J. (2008) 'Effect of endplate shape on performance and stability of wings-in ground (WIG) craft', *World Academy of Science, Engineering and Technology*, 2(11), pp. 296–302.

APPENDICES

Appendix A : Crescent HPC

CRESCENT is the (Cranfield Educational Scientific Computing ENvironment for Teaching) HPC facility provided by Cranfield University to their Master students. The system went online in March 2018. In total, the system has 1488 cores of the Intel Xeon E5-2600 family. The maximum number of cores per node is 16 and therefore multiples of 16 are used. Each 16 cores share 128GB memory. The system runs a Red Hat Enterprise Linux Server release 7.2. All the nodes are connected with an Infiniband QDR low-latency interconnect.

Appendix B : Rotational direction of the VG´s

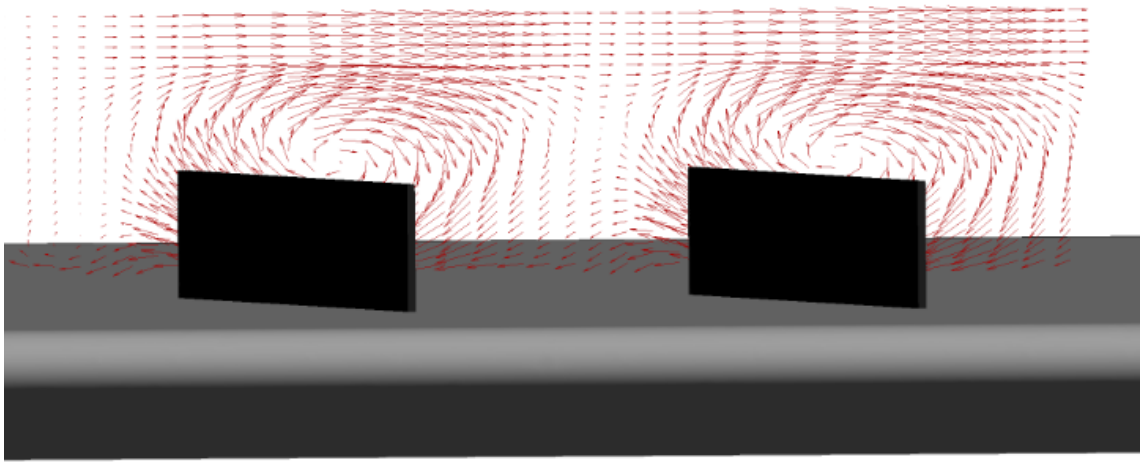

Figure B-1: Clockwise rotational direction for δ=10º

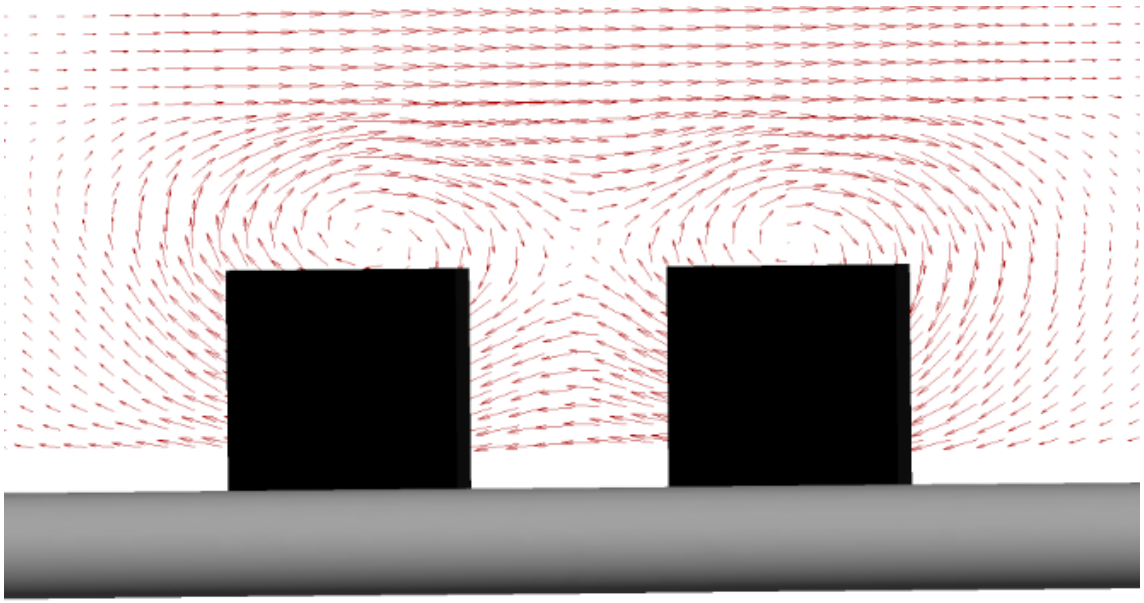

Figure B-2: Clockwise rotational direction for δ=0º

Appendix C : δ=15º

C.1 δ=15º, β=10º, AR=2

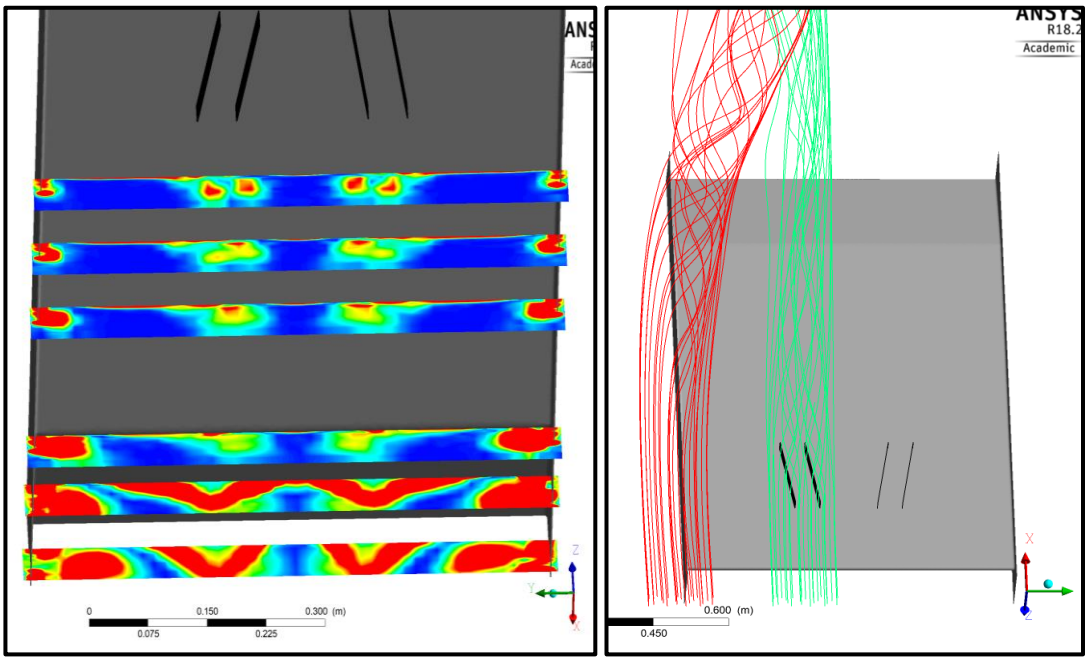

Figure C-1.1: Vorticity Contours (left) and Streamlines (right), β=10º, AR=2

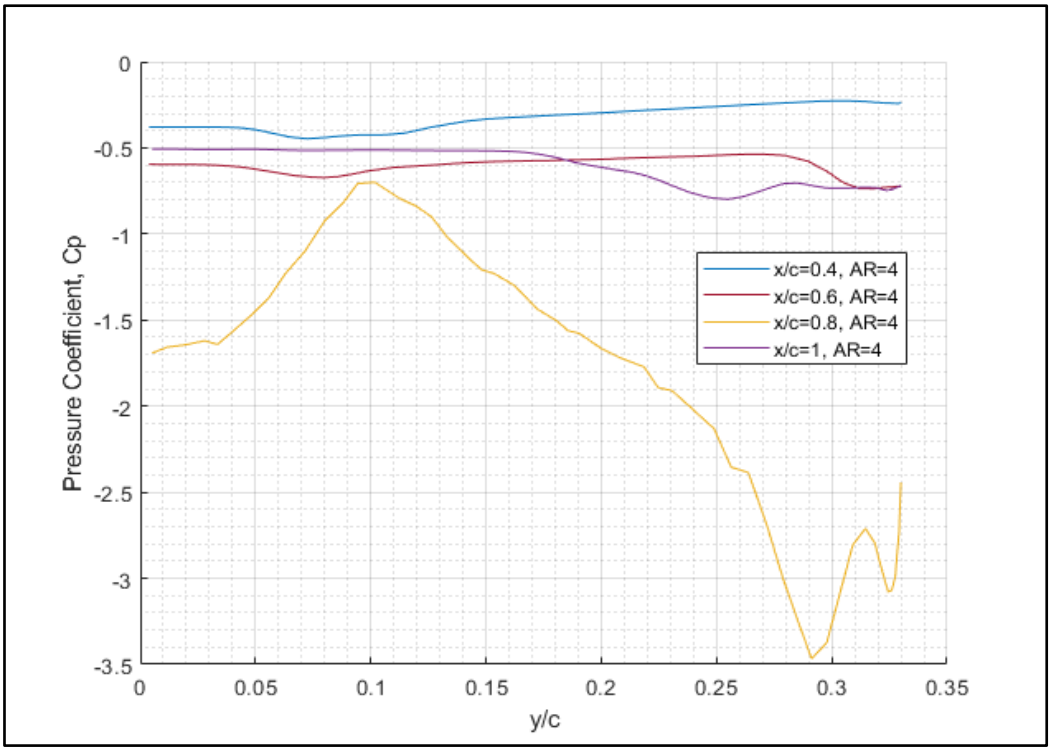

Figure C-1.2: Pressure Coefficient at different streamwise locations

C.2 δ=15º, β=20º, AR=2

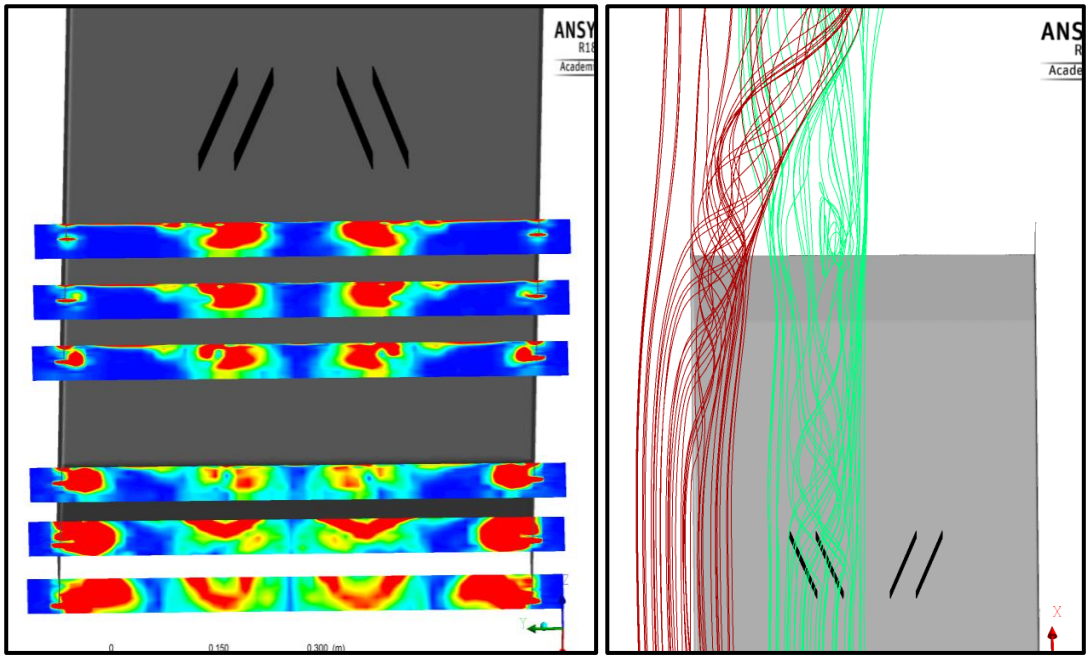

Figure C-2.1: Vorticity Contours (left) and Streamlines (right), β=20º, AR=2

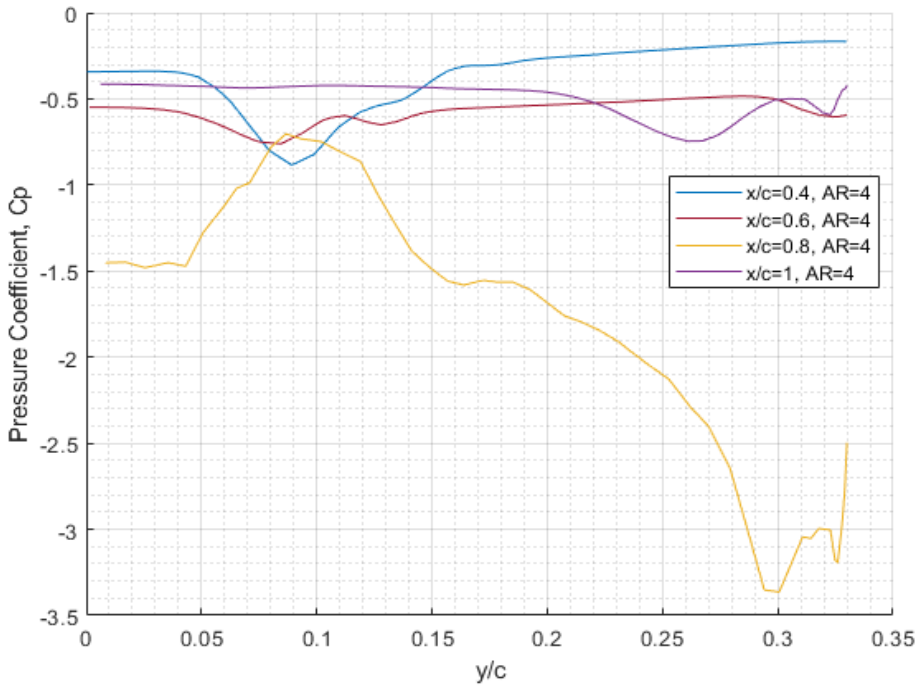

Figure C-2.2: Pressure Coefficient at different streamwise locations

Appendix D : Flat Plate Model

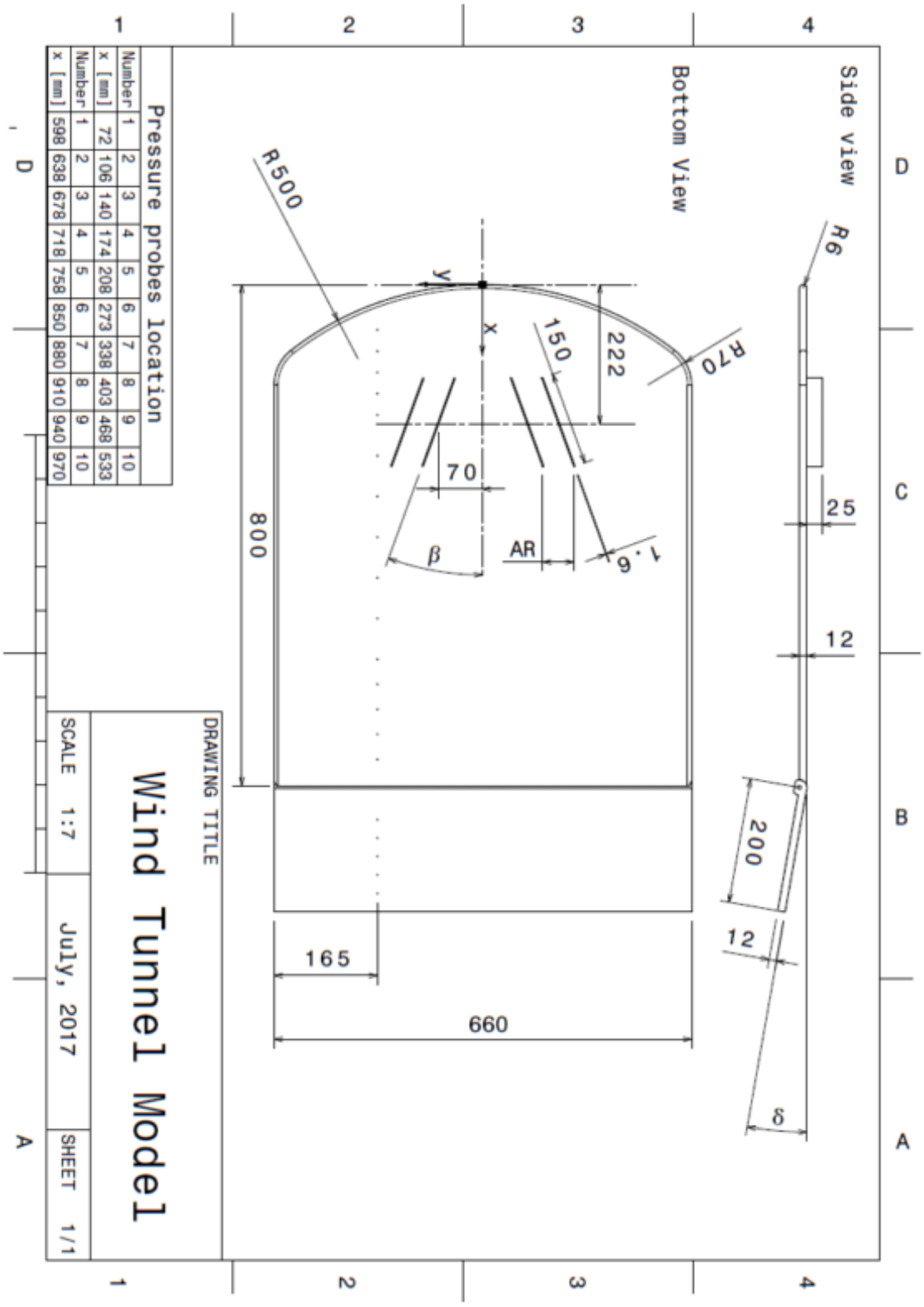

Number	1	2	3	4	5	6	7	8	9	10
x [mm]	72	106	140	174	208	273	338	403	468	533

Number	1	2	3	4	5	6	7	8	9	10
x [mm]	598	638	678	718	758	850	880	910	940	970

D.1 Endplate Model

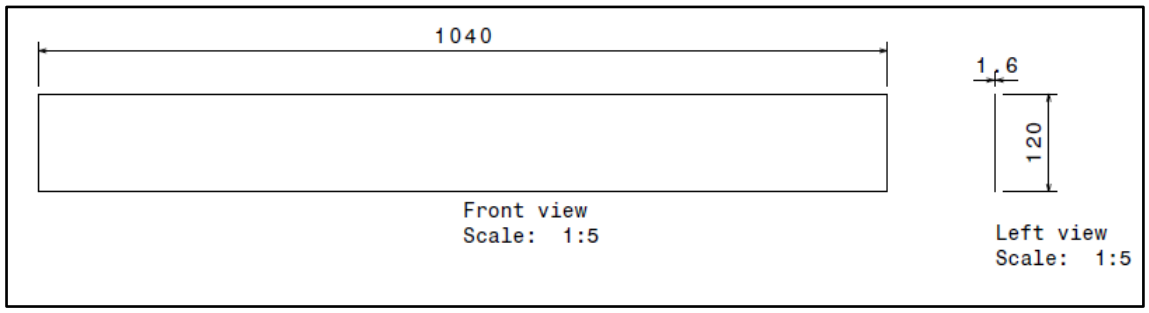

Figure D-1.1: Sketch of the endplates

D.2 Vortex Generator Designs

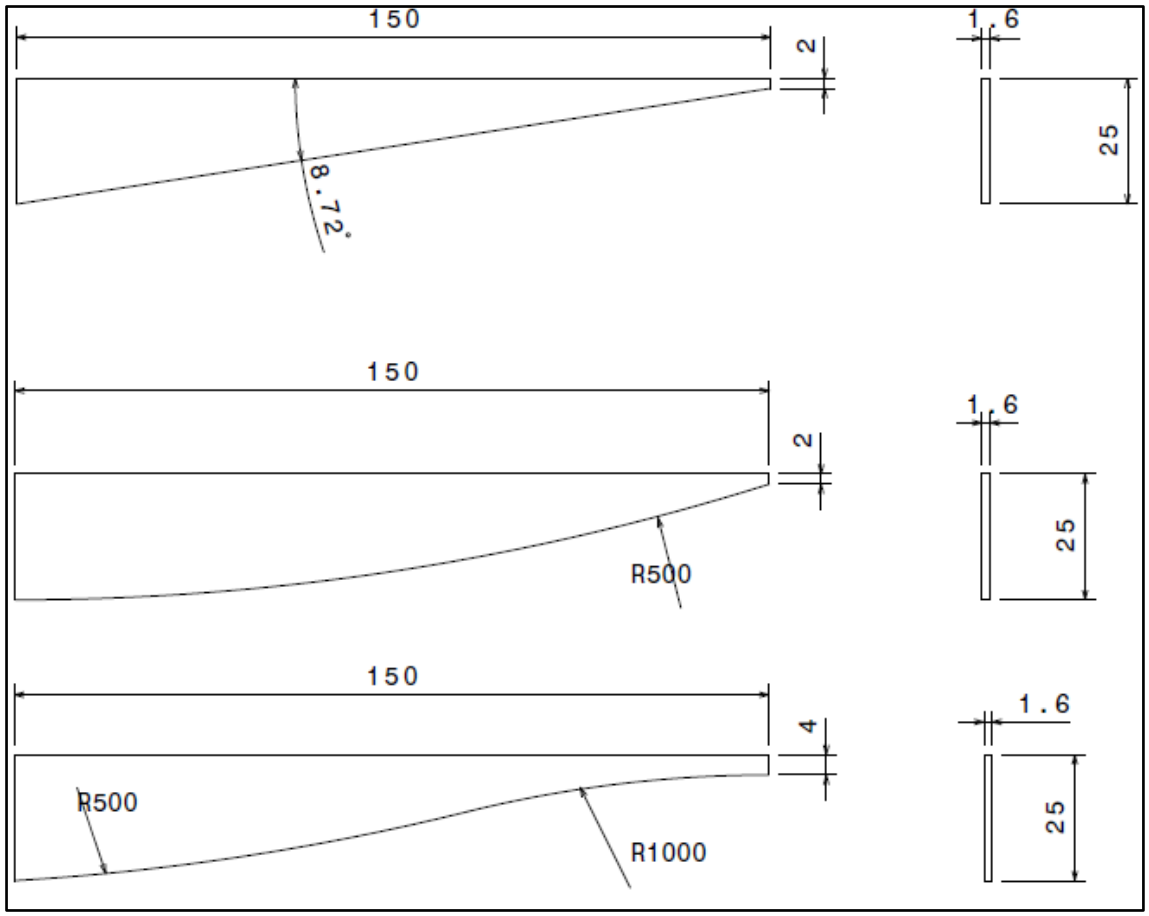

Figure D-2.1: Sketch of the Vortex Generators Geometries